Hydroxyapatite from Waste Materials for Treatment of Heavy Metals in Aqueous Medium

Shirin Akter Jahan

November 2015

Hydroxyapatite from Waste Materials for Treatment of Heavy Metals in Aqueous Medium

A Dissertation Submitted to the University of Dhaka in Partial Fulfillment for the Requirements of the Degree of Doctor of Philosophy in Chemistry

Submitted by

Shirin Akter Jahan

Registration No. 114

Session: 2010-2011

Bangladesh Concil of Scientific and Industrial Research (BCSIR)
Dr. Qudrat-I- Khuda Road
Dhanmondi
Dhaka-1205, Bangladesh

Departmentof Chemistry
Physical Chemistry Research Laboratory
University of Dhaka
Dhaka-1000, Bangladesh

November 2015

To

My caring Parents

and

my loving family

CONTENTS

Synthesis and characterization of Fe (III) doped HAP from eggshell

CHAPTER 5

Synthesis and characterization of Cu(II) doped HAP from eggshell

Acknowledgements

It is my pleasure to sincerely acknowledge the contribution of a number of people who helped me to make this journey possible. Foremost,Iwould like to express my sincere gratitude to my supervisor, **Professor Mohammad Yousuf Ali Mollah**, former Professor in the Department of Chemistry of Dhaka University, and currently a Member, University Grants Commission of Bangladesh, Dhaka, for his relentlessencouragement, constructive guidance and words of motivation throughout the duration of this research study and moreover for the inspiration he provided to ensure the completion of this work.

I would like to express my sincere gratitude and appreciation to my supervisor **Dr. Samina Ahmed**, Principal Scientific Officer, IGCRT, BCSIR, Dhaka for her valuable comments, suggestions and kind assistance for various problems at any step during this research work. Without her unwavering support, this work would never been possible.

I am also grateful to my respected supervisor **Professor Md. Abu Bin Hasan Susan**, Department of Chemistry, University of Dhaka for his continued support and willingness to share his knowledgewhenever I needed. He was always there to help me in difficult time. For this, I will remain eternally grateful to him.

I wish to express my heartfelt thanks to the Chairperson, Department of Chemistry, for her continued support and cooperation.I am highly thankfulto **Dr. M. Mominul Islam**, **Dr.Muhammed Shah Miran** and **Dr. Saika Ahmed,** Faculty members, Department of Chemistry, University of Dhaka, for their constructive advice, invaluable suggestions and noteworthy inspiration at all stages of the present work.

I am obliged to **ShahnajParveen**, Chief Scientific Officer and **NahidSharmin**,Principal Scientific Officer, BCSIR, Dhaka, for their friendly collaboration, invaluable suggestions which inspired me to continue my research work. I sincerely express my gratitude to **Sabrina Mostafa** for her sincere support throughout this work.

It was a great pleasure to work with the members of Material Chemistry Research Laboratory, Department of Chemistry, University of Dhaka. Their sincere and invaluable helps always served as a constant inspiration for me.

I would like to express my heartfelt gratitude to Md. Moniruz Zaman and Mr. BadhanSaha for their generous help providing real samples for my work. I gratefully acknowledge the support from my colleagues of IGCRT, BCSIR, Dhaka, for their encouragement and support during my research. I am also highly grateful to the authority of BCSIR for giving me necessary permission to pursue research works smoothly.

I gratefully express my sincere thanks to the Ministry of Science and Technology, Bangladesh for Bangabandhu Ph.D. Fellowship.

I am thankful to my husband**Syed RezaulHaider** for his continued moral support andencouragement throughout this research work. My two loving sons,**Spondon** and **Rhydhon**, who inspired me to complete this work even though sometimes I had very little time to look after them.I am grateful to my parents and all other family members and well-wishers for their encouragement.

(Shirin Akter Jahan)

Declaration

Experiments described in this thesis were carried out by the author in the Physical Chemistry Laboratory, Department of Chemistry, Dhaka University, Dhaka 1000 as well as in IGCRT, BCSIR, Dhaka-1205, Bangladesh. This work has neither been presented anywhere for any degree nor will be submitted elsewhere for any other degree. The results have not yet been reported in the form of publication.

Dr. Md. Abu Bin Hasan Susan
Professor
Department of Chemistry
University of Dhaka
Dhaka-1000
Bangladesh
Ph.D. Supervisor

Dr. Md. Yousuf Ali Mollah
Member
University Grants
Commission of Bangladesh
Dhaka-1000
Bangladesh
Ph.D. Supervisor

Dr. Samina Ahmed
Principal Scientific Officer
Bangladesh Council of Scientific and
Industrial Research (BCSIR)
Dhaka-1205
Bangladesh
Ph.D. Supervisor

Shirin Akter Jahan
Department of Chemistry
University of Dhaka
Dhaka-1000
Bangladesh
Author (Ph.D. Student)

Abstract

Hydroxyapatite (HAP) is an important biomaterial which could be a promising adsorbent for removal of heavy metals from aqueous medium besides its wide application in biomedical field. Flexible hexagonal structure of HAP allows incorporation of wide range of different ionic substitution which helps to make changes in HAP properties in a synergistic way for environmental remediation and biomedical applications.

This thesis was focused on synthesis and characterization of pure and doped (Fe and Cu) HAP by wet chemical precipitation method using eggshell as calcium source which was followed by investigation on their applications in treating heavy metals from aqueous system. Doping of HAP was done with various Fe(III) and Cu(II) contents and the products were calcined at different temperatures (100°, 300° and 600°C). Physical and chemical characterization of synthesized HAPs have been carried out using Fourier transform infrared spectroscopy (FT-IR), X-ray diffraction (XRD), scanning electron microscopy with energy dispersive X-ray analysis (SEM-EDX), DLS particle size analysis and BET surface area analysis. FT-IR spectra and XRD patterns of synthesized HAPs including doped and nano HAP confirmed the formation of single HAP phase in the samples. XRD patterns showed decrease in crystalline size from 34 nm to 14-16nm for Fe-HAP and 15-12 nm for Cu-HAP was observed upon doping of HAP. BET surface area of Fe and Cu doped HAP calcined at 300°C increased from 66.80 m^2g^{-1} for pure HAP to 122.29 and 153.39 m^2g^{-1} respectively. Furthermore, pure and doped HAP calcined at 300°C showed highest surface area in comparison to HAPs both oven dried at 100°C and thermally treated at 600°C.

For the first time nano HAP was synthesized from eggshell derived calcium precursor using microemulsion method. Phase purity of synthesized nano HAP was confirmed by FT-IR spectra and XRD patterns of the samples. BET surface area was measured 79.23 m^2g^{-1} for nano HAP calcined at 600°C which was 22.40 m^2g^{-1} for synthesized pure HAP calcined at same temperature. Analysis of particle size by DLS technique was found to be 12 nm for as prepared nano HAP.

After successful synthesis of HAPs from eggshell, these were applied to remove As(V), Cr(VI) and Pb(II) from aqueous system. Removal of As(V) was given priority as arsenic contamination in Bangladesh is a major concern now. Adsorption equilibrium was established at pH 9, contact time 60 min, As(V) concentration 100 μgL^{-1} and experiment was done at room temperature (30°C). Arsenic (V) removal efficiency was investigated in detail and it was observed that the efficiency of HAPincreased from 22% to 48% and 50% upon doping with Cu(II) and Fe(III) respectively keeping the equilibrium conditions same. The capacity enhanced to 59% and 74% while adsorbent dosage of copper and iron increased from 1 gL^{-1} to $10gL^{-1}$. Moreover the results show that the arsenate removal efficiency for Fe-HAP and Cu-HAP is twofold higher than that for pure HAP. Higher Cr(VI) removal efficiency of 6%Cu-HAP calcined at 300°C indicated the superiority of Copper doped HAP over pure HAP sample as a promising adsorbent. 2%Fe-HAPcalcined at 300°C showed highest Pb(II)removal efficiency which was 93.14%. Adsorption equilibrium was attained very fast at 20 and 30 mins in removing Cr(VI) and Pb(II) from aqueous system respectively.Arsenic removal efficiency of nano HAP was tested at pH 7 and 9, which shows a significant increase in arsenic removal efficiency in comparison to synthesized HAP micro particles. The equilibrium data fitted well with Langmuir model for 2 and 6% Fe doped HAP while 4%Fe-HAP followed Freundlich isotherm. However, negative values for theconstants of Langmuir, Freundlich and Temkin isotherms for As (V) adsorption for pure and copper doped HAP implied the inadequacy of the isotherm model to explain the adsorption process. First order and Pseudo second order kinetic models well describe the adsorption kinetics and probably both physical and chemical adsorptions were involved in adsorption of As (V) ion by pure and doped HAP.HAPs were further used as adsorbents in treating real waste waterandresults were found quite promising.

The potential of the pure, copper and iron doped and also nano HAP synthesized from eggshells were explored to create a new dimension in waste management system. This work will be a significant step towards environmental remediation in two ways- first, utilization of the waste eggshells for synthesis of value added products HAP and secondly these products will be applied in the removal of heavy metals from aqueous medium.

List of Abbreviations

HAP	Hydroxyapatite
CDHAP	Calcium deficient hydroxyapatite
Fe-HAP	Fe(III)-doped hydroxyapatite
Cu-HAP	Fe(III)-doped hydroxyapatite
UNICEF	United Nations Children's Fund
WHO	World Health Organization
EPA	Environmental Protection Agency
MCL	Maximum contaminant level
μgL^{-1}	Microgram per liter
mgL^{-1}	Milligram per liter
As(V)	Pentavalent arsenic
Cr(VI)	Hexavalent chromium
SEM	Scanning Electron Microscopy
EDS	Energy Dispersive X-ray Spectroscopy
XRD	X-ray diffractometer
FT-IR	Fourier Transform Infra-red Spectroscopy
DLS	Dynamic light scattering
DI	De-ionized
BET	Brunauer- Emmett-Teller

BJH	Barrett – Joyner - Halenda
HG-AAS	Hydride Generation Atomic absorption spectroscopy
FAAS	Flame Atomic absorption spectroscopy
UV	Ultra violet
DPC	1,5-diphenylcarbazide
$(NH_4)_2HPO_4$	Di ammonium hydrogenphosphate
$CaCO_3$	Calcium carbonate
HNO_3	Nitric acid
HCl	Hydrochloric acid
NH_3	Ammonia solution
$Fe(NO_3)_3.9H_2O$	Ferric nitrate nona hydrate
2%Fe-HAP1	Doping of hydroxyapatite with 2wt% ferric-salt dried at 100°C
$Cu(NO_3)_2$	Cupric nitrate
2%Cu-HAP3	Doping of hydroxyapatite with 2wt% cupric-salt dried at 300°C
β-TCP	Beta tricalcium phosphate
TX-100	TritonX-100
CH_3COOH	Acetic acid
$Ca(CH_3COO)_2$	Calcium acetate
ZPC	Zero Point Charge
JCPDS	Joint Committee on Powder Diffraction Standards

List of Symbols

q_e	adsorption capacity at equilibrium
C_i	initial concentration of adsorbate
C_f	final concentration of adsorbate
C_e	equilibrium concentration of adsorbate
V	volume of the adsorbate solution in L
M	mass of the adsorbents in g
q_{max}	theoretical maximum adsorption capacity of the adsorbent
K_L	Langmuir constant
R_L	dimensionless equilibrium parameter
K_F	Freundlich constant related to the adsorption capacity
n	Freundlich constant related to the adsorption intensity
B_1	heat of adsorption
K_T	equilibrium binding constant
R	Universal Gas Constant
T	temperature in K
R^2	correlation coefficient

List of Tables

CHAPTER 1

Introduction

In this introductory chapter an effort has been made to give a brief drescription of hydroxyapatite (HAP) along with its structural information. Synthetic routes of HAP, its derivatives and nano HAP are also described with their potential applications in various fields. This chapter also gives a portrait of environmental pollution with heavy metals in Bangladesh. Method used for removal of heavy metals from aqueous system using HAP and its derivatives is then described. In addition, the aims and objectives of this study have also been highlighted.

1.1 Hydroxyapatite

Calcium phosphate apatite with hydroxyl group attached in the structural moiety is known as hydroxyapatite (HAP). HAP is the main inorganic component of human bone. The pure HAP powder is white and is similar to the mineral component of bones and teeth. Due to its excellent biocompatibility and osteoconductivity, HAP has received a significant attention in biomedical applications. HAP is also used in water purification for removing heavy metal ions, as stationary phase in chromatographic columns for separation of proteins, albumins and low molecular weight organic acids, the polysaccharides, medicinal organic substances, hemoglobin and proteins.[1-4]

1.1.1 Structure of HAP

The chemical formula of HAP, ($Ca_{10}(PO_4)_6(OH)_2$), shows that a single unit cellcomprising 44 atoms, including 10 calcium atoms, 6 PO_4^{3-} tetrahedra, and 2 OH^- groups well organized in a hexagonal system as shown in Figure 1.1.Hydroxyapatite exhibits a hexagonal space group P63/m where $a = b \neq c$ (a = 0.943 nm and c = 0.688 nm), $\alpha = \beta = 90°$ and $\gamma = 120°$.[5-6]Depending on the crystallographic positions of the constituent atoms in the unit cell, 10 Ca atoms are classified into Ca(I) and Ca(II).The 4/10th Ca(I) atoms are situated in the 4*f* (1/3, 2/3, *Z*) position, which is coordinated to 9 O atoms in the form of a tri-capped trigonal prism[7], and these 9 coordinated O atoms are shared from 6 different PO_4 tetrahedra.[6,8]

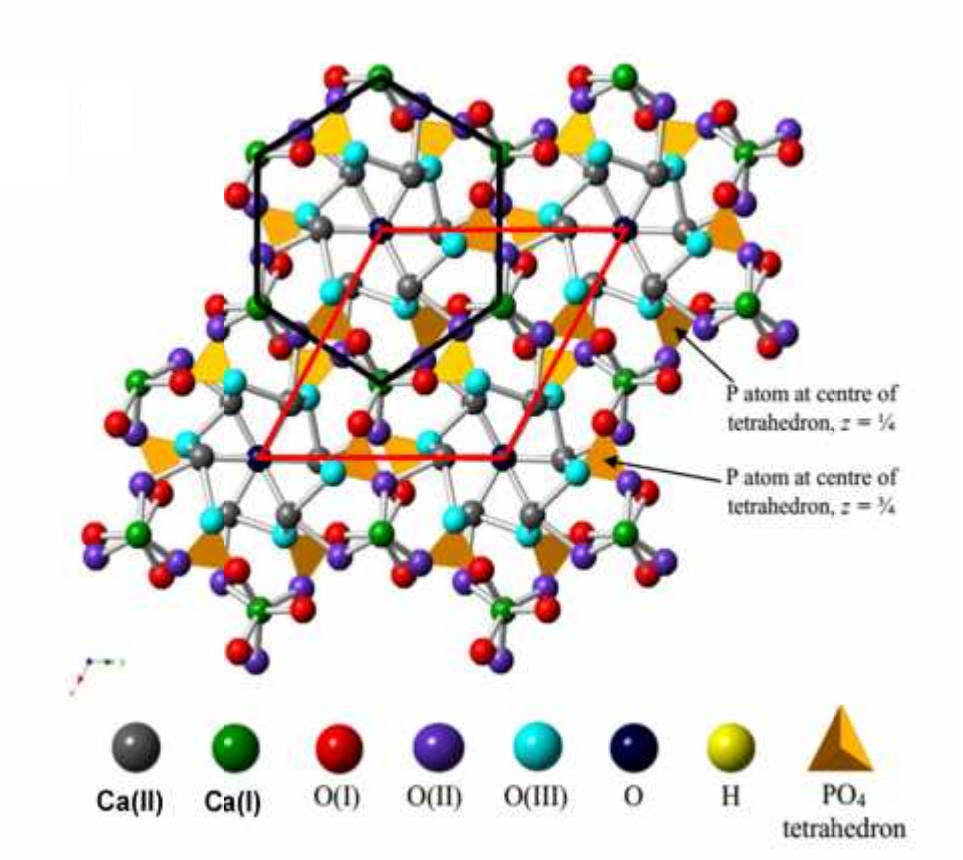

(a)

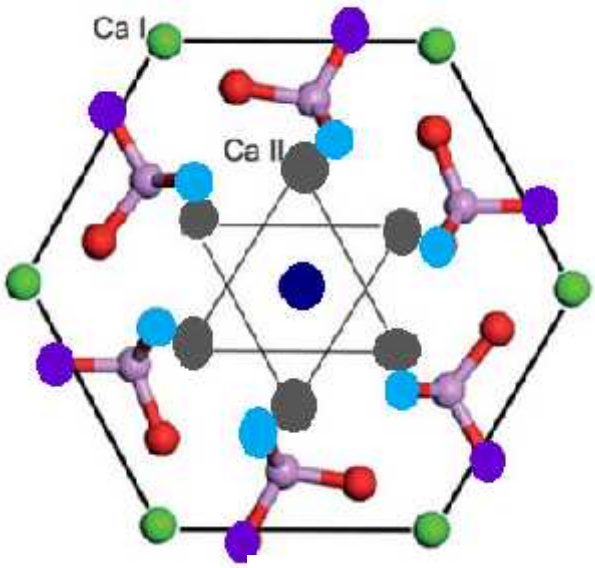

(b)

Figure 1.1Pure HAP structural model (a) unit cell highlighted by red line, (b) a view of the hexagonal unit cell of HAP when projected down *c*-axis

The remaining 6/10th Ca(II) atoms are occupied in the 6*h* special position, which are coordinated to 7 O atoms of which 6 O atoms are shared from 5 PO_4tetrahedra and one from the OH^- group.[6-8] It is revealed that 6 Ca(II) atoms are arranged into two Ca(II) triangles on the mirror planes at $z = 1/4$ and $z = 3/4$, and the successive Ca-II triangles are rotated 60° about *c*-axis.[5,9] One distinctive feature of the HAP structure are columns of OH, which are parallel to the *c*-axis at the edges of the unit cell. These columns pass through the centre of HAP channels parallel to *c*-axis. HAP has the capacity to undergo significantsubstitution without lattice distortion as it accommodates cations andanions that differ in sizes from Ca^{2+} and PO_4^{3-}, respectively.

1.1.2 HAP synthetic routes

1.1.2.1 Synthesis of pure HAP

Numerous methods are known for the synthesis of HAP and the choice of the appropriate method for the synthesis of HAP depends on the desired size andmorphology of HAP.Synthetic methods include: hydrothermal[10-13], microwave[14-18], sonochemical[19-21], sol-gel[22-24], microemulsion[25-28], surfactant based template system[29] and precipitation[30-35]. However, the present study was particularly confined with wet chemical precipitation method for the synthesis of pure and doped HAP from eggshells. In addition microemulsion method was applied to synthesize nano HAP using calcium derived from eggshells.

Wet chemical precipitation method

Wet chemical precipitation method is the most simple and common approach used for the preparation of HAP. According to this process generally an aqueous phosphate source is added in adrop wise fashion to an aqueous calcium source. In the precipitation method the pH of the reaction medium is rigidly controlled at a value higher than 9.0, otherwise, the formation of calcium deficient hydroxyapatite (CDHAP) occurred with a decrease in pH value.

1.1.2.2 Synthesis of nano HAP

Due to outstanding biocompatibility and high stability synthetic nano HAP have been considered as an excellent candidate for biomedical applications.Common methods used to synthesize nano HAP include wet chemical precipitation, hydrothermal, hydrolysis, mechanochemical and sol–gel methods.[36]More recent approach is the synthesis of nano HAP using macromolecular templates, like surfactants, polymers and also small organic compounds using as a chelating agent.[37-41]

Microemulsion method

A microemulsion is a thermodynamically stable, isotropic transparent dispersion of twoimmiscible liquids, such as water and organic, stabilized by the presence of surface activeagents (i.e.surfactants). Surfactants as amphiphilic molecules with a hydrophilic headconnected to a hydrophobic tail that can reduce the surfacetension of the immiscible liquids,resulting in a dispersed phaseconfined in nanometer regimes; the generated emulsion isthuscapable of delivering nanosized particles when the reaction is confined in the nanosized domains. In this study, for the first time, microemulsion method has been used to prepare nano HAP from calcium precursor derived from eggshell.

1.1.3 Synthesis of substituted HAP

Flexible structure of HAP allows the incorporation of wide a range of different ionic substitutions, and it leads to different degree of alterations in the original HAP structure, depending on the type of substitution and degree of the substitution .[42-44] Subsequently, it results in the changes of the characteristics of HAP, such as the degree of crystallinity, morphology, lattice parameters and stability of HAP structure.[42,45-46] As a consequence, synthesis of substituted HAP has attracted considerable interest, as substituted HAP can exhibit desirable properties and satisfy variety of needs in a wide range of applications.[42,45-46] HAP is capable of accommodating several substituents, while still maintaining its basic apatitic structure. Ca^{2+} can be substituted by various cations, such as, monovalent (Na^{+}, K^{+})[47], divalent (Mg^{2+}, Sr^{2+}, Ba^{2+}, Pb^{2+})[48]and trivalent, Y^{3+} cations[48]. Significant anionic substitutions, include the replacement of OH^{-} by CO_3^{2-}, F^{-} , Cl^{-} and

PO_4^{3-} by CO_3^{2-},[49,50] AsO_4^{3-} and VO_4^{3-} [51].Some substitutions are coupled with others to maintain the charge balance in the apatite, such as, CO_3^{2-} for PO_4^{3-} coupled with Na^+ for Ca^{2+}.[52]

In the present study Fe(III) and Cu(II) doped HAP particles were successfully synthesized from eggshell solution using wet chemical precipitation method.

1.1.3.1 Fe(III) doped HAP (Fe-HAP)

Iron (Fe) is a potential element to enhance the strength ofHAP. Fe-HAP is usually prepared bywet chemical reaction with diammonium hydrogenphosphate, calcium nitrate and ferrous nitrate solution.[53,54]Iron substitutions in HAP havealso been reported during apatite synthesis via controlled temperatureand pH following ion-exchange method.[55] Fe-HAP could be synthesized by mechanosynthesis method using high energy milling at varied milling time.[56]Mechanosynthesis is a direct mechanical method which isbased on mechanical activation created by collided balls during milling time.[57]It is a feasible and effective process to produce metal ion doped HAP composites with improved mechanicalproperties.[56] Synthesis of Fe-HAP by auto-combustion method was carried out by Pramod*et al*. with calcium nitrate, iron nitrate and diammoniumhydrogenphosphate as the Ca, Fe and P sources.[58]

1.1.3.2Cu(II) doped HAP (Cu-HAP)

Cu-HAP has also received significant attention to the researchers. In order to overcome infection problem with the bone implant material after surgery, biomedical device with good antimicrobial property is important. Copper has attracted attention of the researchers for its antimicrobial property which showed synergistic properties in Cu-HAP. The antimicrobial activity of copper substituted HAP is found tobe higher than unsubstituted HAP.[59]Copper ion co-doped with calciumphosphate synthesized by conventional high temperature solid state method is reported in the literature.[60] Kim et al. synthesized metal ion (silver, copper and zinc) doped hydroxyapatite bywet chemical method.[61] Cu-HAP could also be synthesized using co-precipitation[62] method and chelate

decomposition method[63] and the product was applied as an adsorbent for removal of heavy metals from aqueous system[64].

1.1.4 Applications of HAP and doped HAP

(a) Biomedical applications

Generally HAP is the material of choice for various biomedical applications, e.g. as a replacement for bony and periodontal defects[65,66], alveolarridge[67], middle ear implants[68], tissue engineering systems[69,70], drug delivery agent[71], dental materials[72] and bioactive coating on metallic osseous implants[73]. Though pure HAP is extensively used for recovering bones and teeth, HAP substituted with cations or anions improves bioactive properties of HAP. Substituted HAP has attracted significant interest as it can exhibits desirable properties and satisfy variety of needs in a wide range of applications. Incorporation of Mg and Sr into HAP increased efficiency of HAP in orthopaedic and dental applications[74] and also reduce the risk of vertebral fracture effectively[75]. Presence of Si and carbonate in HAP increased and promoted osteoblast-like activity[76] and osseointegration rate of HAP in their applications, such as bone grafting[77].Recently Fe(III)-HAP with paramagnetic properties has been synthesized and it can be used for hyperthermia treatment of bone tumors[78-80]and also for drug delivery system (DDS)[81]. HAP doped with metal ions (Cu, Zn and Ag) were reported to show antibacterial activity.[62]

(b) Environmental applications

Application of synthetic HAP is significant as sorbents of heavy metals from aqueous systems. Hydroxyapatite has been widely used as adsorbent for removal offluoride from water.[82]Some studies have focused on the ability of HAP to sorption of Pb,[83-85] Ni,[86] Zn,[87,88] Cd[89,90]. Simultaneous sorption of more than one heavy metals (Pb, Cu, Zn, Mn and Fe) by HAP and doped HAPfroma mixture of heavy metals in aqueous solutions has been reported.[91-93] Though HAP has a significant role in removing toxic metal cations from waste water, it is less significant in removing anions like arsenate and chromate from water.

(c) Other industrial applications

Despite biomedical and environmental application, HAP and its derivatives have also been used in numerous nonmedicalindustrial and technological applications, e.g. as a catalystfor chemical reactions such as the Michael-type addition andmethane oxidation,[94,95] host materials for lasers,[96] fluorescence materials,[97] ion conductors[98] and gas sensors[99].Synthetic HAP may also be used in column chromatography for simple and rapid fractionation of proteins and nucleic acids.[100,101]

1.2 Water pollution scenario in Bangladesh

Most of the industries in Bangladesh are established in the riverside to carry raw materials and products at a low cost. These industries in different areas of the country are discharging heavy metals (cadmium, lead, chromium, mercury, zinc, and in few cases copper and manganese) to the environment .[102] Most of the industries in Bangladesh are discharging their untreated effluents into nearby rivers, canals, lakes and lagoons, thus contaminating the water bodies. The situation in Bangladesh demands major attention in water pollution remediation. Chromium is quite often released into the environmentfrom tanneries, laboratory analysis, electroplating, metal finishing,mining, paint and dyestuff, duplicating, rubber and plastics, textile industries, oxidants and cleaning agents.[102]

Arsenic contamination of groundwater came out unexpectedly as a major health issue inBangladesh in the 1990s, arisingfrom a highly successful tube wellboring project sponsored in part by UNICEF.[103] Natural sources of arsenic mobilization include weathering of arsenic-bearing rocks, biological activity and volcanic eruption along with anthropogenic sources which include mining of metal ores (e.g., gold), combustion of fossil fuels, pesticide use, livestock feed additives, wood preservatives, and pigment production.Today, an estimated 25-40 million people in Bangladeshhave been exposed to arsenic levels above the national limit (which is still at 50 μgL^{-1}).[103] About 5.6 million are using drinking water containing arsenic which is more than 20times the WHO standard (10 μgL^{-1}).[103] At least 40,000 people in Bangladesh currently show symptoms of

arsenicosis, the actual figuremay be even higher. Above all, arsenic pollution of ground water in Bangladesh is in an alarming condition for last decade.

1.2.1 Heavy metals in water

Among thewide diversity of contaminants affecting water resources, heavy metals receive particularconcern considering their strong toxicity even at low concentrations.[104]Most heavy metal ions are non-degradable ions, persistent in the environment andtoxic to living organisms. Therefore, the elimination of heavy metal ions from water isimportant to protect public health. It is reported that industries such as plating, ceramics, glass,mining and batterymanufacturing are considered as the main sources of heavy metals in localwater streams, which can cause the contamination of groundwater with heavy metals.[105] Inaddition, heavy metals which are commonly found in highconcentrations in landfill leachatealso are a potential source of pollution for groundwater.[104]The chemistry, source and toxicity of some heavy metals are briefly mentioned below.

(a) Arsenic

Chemically, arsenic compounds are two types: inorganic and organic. Inorganic arsenic isagain divided into two types:trivalent and pentavalent. Inorganic arsenic is more toxicthan the organic ones.Arsenic can exist in several oxidation states including the +5, +3,+1, and -3 valences andrarely in the elemental form. Pe-pH diagram of arsenic species is shown and discussed in Chapter 7. In the pH range of4.0 to 10.0, the prevalent As(III) species is neutral in charge, while the As(V) species isnegatively charged.If arsenic builds up in the human body, open lesions, organdamages (such as deafness), neural disorders and organ cancer, often fatal, can develop.[106] The maximum acceptable concentration of arsenic in drinking water recommended bythe World Health Organization is 10 μgL^{-1} and this limit for Bangladesh is 50 μgL^{-1}.[107]

(b) Chromium

Chromium exist in oxidation states rangingfrom +6 to -2: however, only the hexavalent Cr(VI) and trivalent Cr(III) are commonly present in the aquatic environment. Toxicity of

chromium and also its mobility in differentgeologic environment are dependent on its oxidationstate.[108] Pe-pH diagram of chromium species (Chapter 7 Fig. 7.2) shows that under oxidizing conditions, Cr(III) is stable as Cr^{3+} at pH< 2.0 and Cr(VI) is stable at higher pH. Cr(VI) compounds are much more soluble and toxic thanCr(III) to microorganisms, plants,animals and humans. Cr(VI) exerts toxic effectson biological systems. Inhalation and retention of Cr(VI) containing materials can causeperforation of the nasal septum, asthma, bronchitis, pneumonitis, inflammation of the larynx andliver, and increased incidence of bronchogenic carcinoma along with skin diseases.[109]The maximum acceptable concentration limit in drinkingwater guideline for total chromium is $50\mu gL^{-1}$.[107]

(c) Lead

Lead contamination can occur in groundwater due to mining and smelting activities, battery plant emissions, battery reprocessing plant wastes, automotive exhaust emissions, leaded fuelspills and municipal or industrial land fill leachates.[110] The predominant form of lead in naturalwaters is a function of the ions present, their concentrations, the pH and the redox potential. Children and pregnant mothersare most susceptible to lead poisoning. The effect of lead on the central nervous system can be particularlyserious. Lead poisoning also affects development of central nervous systems of children, leading tohyperactivity, irritability, headaches, and learning and concentration difficulties. Themaximum acceptable concentration of lead in drinking water is 0.01 mgL^{-1}.[107]

1.2.2 Methods for treatment of polluted water

Due to the severe effect of heavy metals in aqueous system, a number of methods for removal of heavy metals from contaminated water are known to be in practice in order to meet regulatory standards. The conventional processes used in the removal of heavymetals from contaminated water include among others, chemical precipitation, reverse osmosis, chemical reduction, electrochemical deposition, cementation and adsorption.[111]Among these methods, adsorption is currently considered to be very suitable for wastewater treatment because of its simplicity and cost effectiveness.[112].

1.2.2.1 Adsorption

Adsorption is the most common but easy to use approach for the removal of toxic metal ions from various industrial effluents.[113] If the adsorbent (solid surface) ischosen carefully and conditions for the adsorptioncan be adjusted appropriately, adsorption-basedprocesses are capable of removing metals over a wider pH range and to much lower levelsthan processes based on other methods. Some of the widely used adsorbents for adsorption of metal ions includeactivated carbon, clay minerals, biomaterials, industrial solid wastes and zeolites.[114] Waste materials from industrial oragricultural operation could be one of the resources for low cost adsorbents.

However adsorption process is being categorized as follows:

i) Ion exchange is a process in which ions of one substance concentrate at surface of another substrate as a result of electrostatic attraction tocharged sites at thesurface.

ii) Physical adsorption occurs due to weak forces of attractionbetweenmolecules (Van -der Waals forces) which is not site specific.

iii) Chemical adsorption is being formed between themolecule ofthe solute and the adsorbent (this result in stronger bonds betweenmolecules than is thecase of physical adsorption) which makes a chemical bond.

(a) Gas adsorption isotherms

The first important information about surface and porosity obtained from physisorption experiment is the isotherm. It can reveal the kind of porosity present in unknown solid samples. The adsorption isotherms can be used to analyze the pore size distribution, surface area, pore volume, fluid-wall interaction strength, and other properties. The isotherms have different shapes which depend on pore structure of solid as well as interaction between sample surface and adsorbate gas. Figure 1.2 shows IUPAC classifications of both adsorption isotherms and adsorption hysteresis loops.[115]

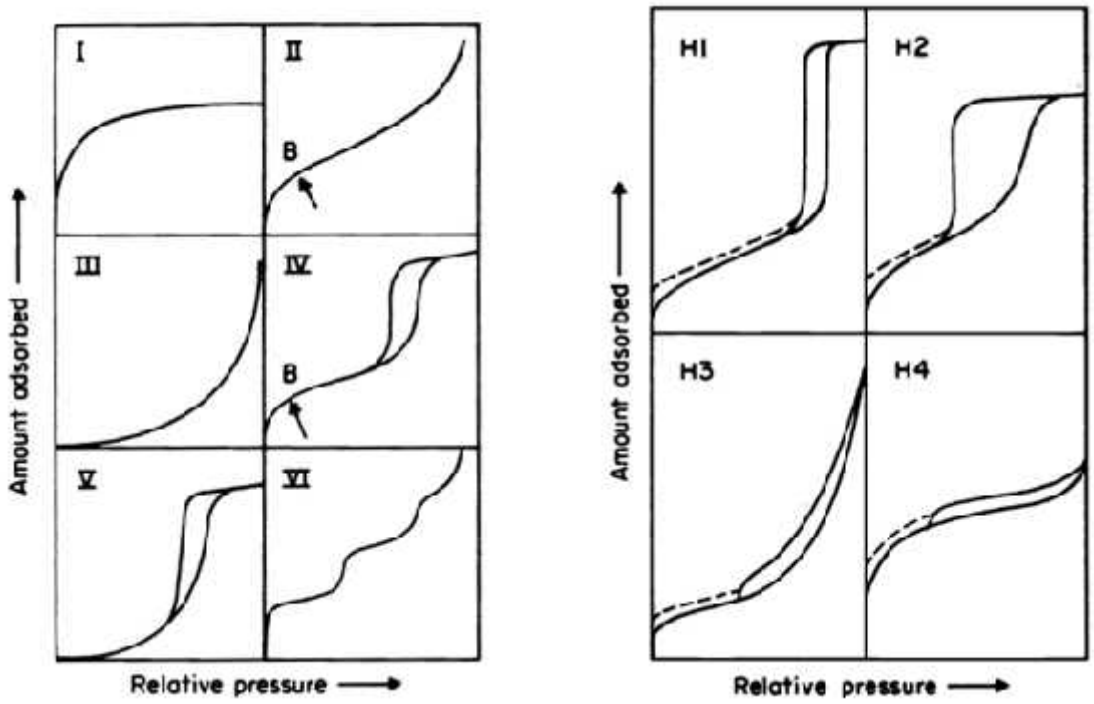

(a) (b)

Figure 1.2 IUPAC classifications of (a) adsorption isotherms, (b) Hysteresis loops

Type I isotherm is observed for microporous solids having relatively small external surfaces. The limiting uptake is governed by the accessible micropore volume rather than by the internal surface area.

Type II isotherm is the normal form obtained with a non-porous or macroporous adsorbent. This isotherm represents unrestricted monolayer-multilayer adsorption.

Type III isotherm is observed for non-porous solid. This type is not common, but there are a number of systems which exhibit isotherms with such curvature. In such cases, weak adsorbate-adsorbent interactions play an important role.

Type IV isotherm is distinguished by two characteristic features. This type of isotherm exhibits a hysteresis loop, which is associated with capillary condensation taking place in mesopores, and has a limiting uptake over a range of highrelative pressure. Type IV isotherm is characteristic of many mesoporous industrial adsorbents.

Type V isotherm is uncommon. They are related to the Type III isotherm in that the adsorbent-adsorbate interaction is weak, and they also exhibit hysteresis as in Type IV.

Type VI isotherm exhibits stepwise multilayer adsorption on a uniform non-porous surface. The step-height represents the monolayer capacity for each adsorbed layer and, remains nearly constant for two or three adsorbed layers in the simplest case.

According to the classification for hysteresis loops, **Type H1** is often associated with porous materials exhibiting a narrow distribution of relatively uniform (cylindrical-like) pores. **H2** hysteresis contains a more complex pore structure in which network effects (e.g., pore blocking/percolation) are important. **Type H3** hysteresis is usually found on solids with a very wide distribution of pore size. **H4** hysteresis loops are generally observed with complex materials containing both micropores and mesopores.

(b) **Surface area and pore size distribution**

The "specific surface area" is defined as the accessible area of solid surface per unit mass of material. It is similarly dependent on the method and experimental conditions employed. Surface area of a solid can be calculated from different plot prepared from the data of gas-adsorption measurement.

Brunauer, Emmett and Teller (BET) plot

In 1938, Brunauer, Emmett and Teller extended the Langmuir's monolayer theory to multilayer adsorption.[116]The BET equation has been utilized in determining the monolayer volume of adsorbed gas, from which we can calculate the surface area of adsorbent. It has become the most widely used standard procedure for the determination of the surface area of porous materials.It is convenient to apply the BET equation in the linear form to measure surface area of solid. The linear form of BET equation is:

$$\frac{p}{v(p_0-p)} = \frac{1}{v_m c} + \frac{c-1}{v_m}\left[\frac{p}{p_0}\right] \qquad (1.1)$$

Where, v= volume of gas adsorbed by unit mass of solid, v_m= gas volume at the monolayer coverage, c= BET constant, p= absolute pressure, p_o= saturation pressure of gas. It is evident from Equation 1.1 that a plot of $(p/v(p_o - p))$ against (p/p_o), should give a straight line, which is called the BET plot. The BET plot should give straight line to measure surface area accurately. After determining monolayer capacity(v_m) from BET plot, specific surface area(a_s) of adsorbent can be calculated from equation 1.2.

$$a_s = \frac{V_m}{22414} \times L \times \sigma \qquad (1.2)$$

Where, L= Avogadros number and σ= cross-sectional area of adsorbate molecule.

Barrett, Joyner and Halenda (BJH) plot

In 1951, Barrett, Joyner and Halenda proposed a method to evaluate pore size distribution based on Kelvin equation (Eq. 1.3).[117]Pore sizedistribution is calculated from desorption isotherm.Pore size distribution in BJH plot is expressed as percentage change of pore volume ($\Delta V_p/ \Delta r_p$) against pore radius(r_p). BJH plot is generally used to represent mesopore size distribution. It is also possible to calculate surface area and total pore volume from BJH plot.

$$\ln \frac{P}{P_0} = -\frac{2\gamma V_L}{RT} \frac{1}{r_m} \qquad (1.3)$$

where , γ is the surface tension, V_L is the molar volume, R is the gas constant,T is the absolute temperature and $r_m$is the meniscus radius.

Adsorption isotherm models

Adsorption process is usually related with the rates of adsorption and desorption which attain an equilibrium state, thus known as adsorption equilibrium. At equilibrium, no change can be observed in the concentration of the solute on the solid surface or in the bulk solution. The position of equilibrium is characteristic of the solute, adsorbent, solvent temperature and pH. The representation of the amount of solute adsorbed per unit

of adsorbent (q) as a function of the equilibrium concentration of the solute in the bulk solution (C_e) at a constant pH and temperature is called an adsorption isotherm.

A wide variety of isotherm models havebeen used for the equilibrium modeling ofadsorption systems.The most common isotherm models are Langmuir and Freundlich isotherms.

(i) Langmuir isotherm model

The Langmuir isotherm applies to monolayer adsorption on completely homogenous surfaces withnegligible interaction betweenadsorbed molecules, and assumes that the adsorption site canonly be occupied by one pollutant molecule.[118]Graphically, it is characterized by a plateau, an equilibrium saturation point where once a molecule occupies a site, no furtheradsorption can take place.[118] Moreover, Langmuir theory hasrelated rapid decrease of the intermolecular attractive forces to therise of distance. Both linear and non-linear mathematical expression ofLangmuir isothermmodels are illustrated in Chapter 7.

(ii) Freundlich isotherm model

Freundlich isotherm describes the relationship between non-ideal and reversible adsorption which is not restricted tothe formation of monolayer. This empirical model can beapplied tomultilayer adsorption, with non-uniform distribution of heat of adsorptionand affinities over the heterogeneous surface.[116] Historically,it was developed for the adsorption of animal charcoal, demonstrating that the ratio of the adsorbate onto a given mass of adsorbent tothe solute was not a constant at different solution concentrations.[114] Theslope ranging between 0 and 1 is a measure of adsorption intensity or surface heterogeneity, becoming more heterogeneous as itsvalue gets closer to zero. Whereas, a value below unity implieschemisorptions process where 1/n above one is an indicative ofcooperative adsorption.[118]Mathematical expression for both linear and non-linear equations of Freundlich isotherm model are listed in Chapter 7.

(iii) Temkin isotherm model

The isotherm contains a factor that explicitly taking into account the adsorbent–adsorbate interactions. According to the model the heat of adsorption decreases with coverage of surface of the adsorbent by the adsorbate. Therefore, Temkin adsorption isotherm model is used for evaluation of adsorption potential of the adsorbent for adsorbates. Temkin equation is excellent for predicting the gas phase equilibrium (when organizationin a tightly packed structure with identical orientation is notnecessary), conversely complex adsorption systems includingtheliquid-phase adsorption isotherms are usually not appropriate tobe represented.[118] Equations for Temkin isotherm model are given in Chapter 7.

(c) **Adsorption kinetics**

When adsorption isconcerned, thermodynamic and kinetic aspects shouldbe involved to have a detailed picture about its performance and mechanisms.[119] Except for adsorptioncapacity,kinetic performance of a given adsorbent is also ofgreat significance for the pilot application. From thekinetic analysis, the solute uptake rate, which determines the residence time required for completion ofadsorption reaction, may be established. Several widely-used batchkinetic models are mentioned here which are used to investigate adsorption kinetic in this study.

i) First-order kinetic
ii) Pseudo first-order kinetic
iii) Pseudo second-order kinetic
iv) Elovich kinetic
v) Intraparticle diffusion model

Mathematical equations of these kinetic models have been stated in Chapter 8 with brief descriptions of the models.

1.3 Motivation of this study

Water is an important natural resource for human being all along the globe. Only 1% of the total world's water resource is available for exploitation by man for domestic, agricultural and industrial purposes. Industrial wastes are contaminating the water bodies which area prime issuenow. Waste materials in excess concentration in the environment can become a critical factor for living organisms. The nature, quantity and type of waste materials vary fromcountry to country. Search for an effective way to properly manage the waste will help to protect the environment and also can improve the quality of environment. Wastes could be recycled, reused, and converted towards the valuable products for a sustainable development. This will contribute to the environment in two ways- one way is to protect the environment from pollution and on the other side to obtain value added productswhile establishing a zero waste standard.The utilization ofthe waste is a priority today in order to achieve sustainable development. Waste for waste minimization has now become a preferred area of research everywhere.

Hence an attempt has been made in the present study to remove heavy metals using value added products from eggshell under the topic "Hydroxyapatite from waste materials for treatment of heavy metals in aqueous medium". Eggshells are wastes material thrown out of kitchen and these eggshells were used to prepare pure and doped HAP and also nano HAP. These synthesized materials were applied for removal of arsenic, chromium and lead from aqueous medium. This would be a significant step in waste management system. Synthesis of the desired products and their utilization was an added benefit in two ways- one was utilization of eggshells to prepare HAPs and other one was mitigation of heavy metals from water system. Thus present work was initiated with general objective of synthesizing low cost and potential adsorbents from eggshells for the removal of heavy metals (As, Cr, Pb) from aqueous environment.

1.4 Structure of the Thesis

This thesis consists of 10 Chapters which are briefly described as follows:

Chapter 1 providesa review of previous works reporting structure of HAP, synthetic routes and applications of pure and doped HAP, water pollution and its remediation with a subsequent outline of the thesis objectives.

Chapter 2 presents a brief discussion on the instruments used for the characterization of synthesized pure and doped HAP and also treatment of waste materials used in synthesis process. This chapter also includes the instruments used to measure heavy metals in aqueous system.

Chapter 3 describes synthetic method and characterization of pure HAP from waste materials.
Synthesis of Fe-HAP and Cu-HAP are presented in **Chapter 4** and **Chapter 5** respectively along with the characterization of the respective samples.

Chapter 6 gives an outline of synthesis and characterization of nano HAP using calcium source prepared from eggshells. For the first time microemulsion method was used to synthesis nano HAP from eggshell derived calcium precursor. This chapter also includes the application of nano HAP in removing arsenate from aqueous system.

Chapter 7 describes the environmental application of pure and doped HAP which comprises removal of heavy metals specifically arsenic, chromium and lead from aqueous environment. Adsorption data for removal of arsenic used to evaluate isotherm models is also included in this chapter.

Evaluation of kinetic models for arsenic adsorption by pure and doped HAP is described in **Chapter 8**.

Application of the synthesized samples for the removal of heavy metals from tannery waste water, fish feed and a fertilizer samples are given in **Chapter 9**.

Chapter 10ispresenting final conclusions and potential future works of this research.

References

1. Andrew S. Gordon, Frank J. Millero, "Adsorption mediated decrease in the biodegradation rate of organic compounds"**,** *Microb. Ecol.*, **1985**, 11,289-298.

2. QueirozA. C.,Santos J. D., MonteiroF. J., GibsonI. R., Knowles J. C., "Adsorptionand release studies of sodium ampicillin from hydroxyapatite and glass-reinforcedhydroxyapatite composites", *Biomaterials*, **2001**, 22,1393-1400.

3. PalazzoaB., SidotiaM.C., RoveriaN., TampieribA., SandribM., BertolazzicL., GalbuseracF., DubinicG., VenacP., ControcR., "Controlleddrug delivery from porous hydroxyapatite grafts: An experimental andtheoreticalapproach", *Mater. Sci. Eng., C*,**2005**, 25, 207-213.

4. WeirM. D., XuH. H. K., "High-strength, in situ-setting calcium phosphatecomposite with protein release", *J. Biomed. Mater. Res. A*,*WileyPeriodicalsInc.*, **2007**,388-396.

5. Kay, M.I., YoungR.A., PosnerA.S., "Crystal Structure of hydroxyapatite".*Natur*e, **1964**, 204, 1050-1052.

6. Posner, A.S., PerloffA., DiorioA.F., "Refinement of the hydroxyapatite structure".*ActaCrystallogr.*,**1958**, 11,308-309.

7. HughesJ. M., RakovanJ., "The crystal structure of apatite,$Ca_5(PO_4)_3(F,OH,Cl)$," *Rev. Mineral.Geochem.,***2002**, 48, 1-12.

8. MaX., EllisD. E., "Initial stages of hydration and Zn substitution/occupationon hydroxyapatite (0001) surfaces,"*Biomaterials,* **2008**, 29, 257-265.

9. ShiD. L., WenX. J., "Bioactive ceramics: structure, synthesis, andmechanicalproperties,"*Introduction to biomaterials*, D. L. Shi, Ed.: TsinghuaUniversity Press, **2006**, 16-17.

10. Riman R.E., Suchanek W.L., Byrappa K., Chen C.W., Shuk P., Oakes C.S., "Solutionsynthesis ofhydroxyapatite designer particulates", *Solid State Ionics*., **2002,** 151, 393–402.

11. Zhang H., Darvell B.W.,"Synthesis and characterization of hydroxyapatite whiskers by hydrothermal homogeneous precipitation using acetamide", *Acta Biomater.*, **2010**, 6, 3216–3222.

12. Zhang X., Vecchio K.S.,"Hydrothermal synthesis of hydroxyapatite rods", *J. Cryst. Growth*, **2007**, 308, 133–140.

13. Zhang C., Yang J., Quan Z., Yang P., Li C., Hou Z., "Hydroxyapatite nano- and microcrystals with multiform morphologies: controllable synthesis and luminescence properties",*Cryst. GrowthDes.*,**2009**, 9, 272.

14. Siddharthan A., Sampath Kumar T.S., Seshadri S.K.,"Synthesis and characterization of nanocrystallineapatites from eggshells at different Ca/P ratios". *Biomed.Mater.,***2009,** 4, 1-9.

15. Han J.K., Song H.Y., Saito F., Lee B.T.., "Synthesis of high purity nano-sized hydroxyapatite powderby microwave-hydrothermal method", *Mater. Chem. Phys.*,**2006**, 99, 235–239.

16. Liu J., Li K., Wang H., Zhu M., Yan H.,"Rapid formation of hydroxyapatite nanostructures bymicrowave irradiation", *Chem. Phys. Lett.*, **2004**, 396, 429–432.

17. Kumar G.S., Thamizhavel A., Girija E.K., "Microwave conversion of eggshells intoflower-likehydroxyapatite nanostructure for biomedical applications", *Mater.Lett.,***2012**, 76, 198–200.

18. Sarig S., Kahana F.,"Rapid formation of nanocrystalline apatite",*J. Cryst. Growth*,**2002**, Part 1:55–59, 237–239.

19. Poinern G.E., Brundavanam R.K., Mondinos N., Jiang Z.T.,"Synthesis and charaterization ofnanohydroxyapatite using an ultrasound assisted method",

    Ultrason.Sonochem.,**2009**, 16, 469–474.

20. Brundavanam R.K., Jiang Z.T., Chapman P., Le X.T., Mondinos N., Fawcett D., "Effect of dilutegelatine on the ultrasonic thermally assisted synthesis of nano

    Hydroxyapatite",*Ultrason.Sonochem.*,**2011**, 18, 697–703.

21. Zou Z., Lin K., Chen L., Chang J.,"Ultrafast synthesis and characterization of Carbonatedhydroxyapatite nanopowders via sonochemistry-assisted microwave Process",*Ultrason.Sonochem.*,**2012**, 19, 1174–1179.

22. Haddow D.B., James P.F., Noort R.V.,"Characterization of sol-gel surfaces for biomedicalapplications", *J Mater Sci. Mater Med*., **1996**, 7, 255–260.

23. Vijayalakshmi U., Rajeswari S.,"Preparation and Characterization ofMicrocrystallineHydroxyapatite Using Sol Gel Method", *Trends Biomater. Artif. Organs*,**2006**, 19, 57–62.

24. Fathi M.H., Hanifi A.,"Evaluation and characterization of nanostructure hydroxyapatite powderprepared by simple sol–gel method", *Mater.Lett.*,**2007**, 61, 3978–3983.

25. Bose S., Saha S.K.,"Synthesis and characterization of hydroxyapatite nanopowdersby emulsion technique",*Chem. Mater*.,**2003**, 15, 4464–4469.

26. Guo G., Sun Y., Wang Z., Guo H.,"Preparation of hydroxyapatite nanoparticles by reversemicroemulsion", *Ceram. Int.*,**2005**, 31, 869–872.

27. Koumoulidis G.C., Katsoulidis A.P., Ladavos A.K., Pomonis P.J., Trapalis C.C.,SdoukosA.T., "Preparation of hydroxyapatite via microemulsion route",*J. Colloid Interf. Sci.*, **2003**, 259, 254–260.

28. Ye F., Guo H., Zhang H., He X.,"Polymeric micelle-templated synthesis of hydroxyapatite hollownanoparticles for a drug delivery system", *Acta Biomater.*, **2010**, 6, 2212–2218.

29. BoseS., SahaS. K., "Synthesis of hydroxyapatite nanopowders via sucrose-templatedsol-gel method ", *J Am. Ceram. Soc*., **2003**, 86, 1055-1059.

30. Viswanath B., Ravishankar N.,"Controlled synthesis of plate-shapedhydroxyapatite and implications for the morphology of the apatite phase in bone",*Biomaterials*, **2008**, 29, 4855–4863.

31. Bouyer E., Gitzhofer F., Boulos M.I.,"Morphological study of hydroxyapatite nanocrystal suspension",*J. Mater. Sci. Mater. Med.*, **2000**, 11, 523–531.

32. Cengiz B., Gokce Y., Yildiz N., Aktas Z., Calimli A.,"Synthesis and characterizationOf hydroxyapatitenanoparticles",*Colloid.Surf.,A,***2008**, 322, 29–33.

33. Wang P., Li C., Gong H., Jiang X., Wang H., Li K.,"Effects of synthesis conditions on the morphologyof hydroxyapatite nanoparticles produced by wet chemicalprocess", *Powder Technol.*,**2010**, 203, 315–321.

34. Swain S.K., Sarkar D.,"A comparative study: hydroxyapatite spherical nanopowdersand elongatednanorods", *Ceram. Int.*,**2011**, 37, 2927–2930.

35. Landi E., Celotti G., Logroscino G., Tampieri A.,"Carbonated hydroxyapatite as Bone substitute", *J. Eur. Ceram. Soc.*,**2003**, 23, 2931–2937.

36. SanoshK. P., Chu Min-Cheol, BalakrishnanA., KimT. N., ChoSEONG-JAI, "Preparation and characterization of nano-hydroxyapatite powderusing sol–gel

technique", *Bull. Mater. Sci*., **2009**, 32,465–470.

37. Liu Y., Hou D., Wang G., "A simple wet chemical synthesis and characterization of hydroxyapatite nanorods". *Mater. Chem. Phys.*, **2004**, 86, 69–73.

38. Zhang H.G., Zhu Q., "Surfactant-assisted preparation of fluoride-substituted hydroxyapatite nanorods". *Mater.Lett.*,**2005**, 59, 3054–3058.

39. Li C., Zhao L., Han J., Wang R., Xiong C., Xie X., "Synthesis of citrate-stabilized hydrocolloids of hydroxyapatite through a novel two-stage method: a possible ggregates-breakdown mechanism of colloid formation". *J. Colloid. Interf. Sci.*, **2011**, 360, 341–9.

40. Safronova T., Putlyaev V., Sergeeva A., Kunenkov E., Tret'yakov Y.D., "Synthesis Ofnanocrystalline calcium hydroxyapatite from calcium sacharates and ammonium hydrogen phosphate", *Dokl. Chem.*, **2009**, 426, 118–23.

41. Tan J., Chen M., Xia J., "Water-dispersible hydroxyapatite nanorods synthesized by a facile method", *Appl. Surf. Sci.*, **2009**, 255, 8774–9.

42. LiM. O., XiaoX., LiuR., ChenC., HuangL., "Structural characterization of zinc-substituted hydroxyapatite prepared by hydrothermal method," *J. Mater. Sci. Mater. Med.,***2008**,19, 797-803.

43. FadeevI. V., ShvornevaL. I., BarinovS. M., OrlovskiiV. P., "Synthesis and structure of magnesium-substituted hydroxyapatite,"*Inorg. Mater.,***2003**, 39,947-950.

44. O'DonnellM. D., FredholmY., RouffignacA.de, HillR. G., "Structuralanalysis of a series of strontium-substituted apatites,"*Acta Biomater.,* **2008**, 4,1455-1464.

45. GasquèresG., BonhommeC., MaquetJ., BabonneauF., HayakawaS.,KanayaT., OsakaA., "Revisiting silicate substituted hydroxyapatite by solid-stateNMR," *Magn. Reson. Chem.,* **2008**, 46, 342-346.

46. YanbaoL., DongxuL., WenjianW.,"Preparation of nano carbonate-substituted hydroxyapatite from an amorphous precursor," *Int. J. Appl. Ceram. Technol.,* **2008**,5, 442-448.

47. LeGeros, R. Z. et al., "Trace elements: incorporation of monovalent cations,Na^+, K^+,Li^{+l}", *J. Dent. Res.*, **1981**, 60, 452–458.

48. Suzuki T. et al., "Synthetic hydroxyapatites employed as inorganic cation-exchangers", *J. Chem. Soc., Faraday Trans.*, **1981**, 77,1059-1062.

49. LeGeros R.Z. et al., "The effect of fluoride on the stability of synthetic and biological (bone) mineral apatites", *Osteoporosis*, New York: Wiley, **1982**, 327 – 341.

50. Kreidler E.R. et al., "The crystal chemistry of apatite: structure fields of fluor and chloroapatite", *Am. Mineral.*,**1970**, 55, 171–184.

51. Azimov S.Y. et al., "Synthetic silicophosphate, silicovanadate and silicoarsenatewith the apatite structure", *Inorg.Mater.*,**1981**, 17, 1384–1387.

52. Sharon K., "Optimisation of hydroxyapatite (HAP) for orthopaedic application via the chemical precipitation technique", *Ph D Thesis*, September **2008**, Dublin City University.

53. MorrisseyR., Rodriguez-LorenzoL. M., GrossK. A., "Influence offerrous iron incorporation on the structure of hydroxyapatite", *J. Mater. Sci. Mater. Med.*, **2005**, 16, 387-392.

54. PengF., VeilleuxE.,SchmidtM., WeiM., "Synthesis ofhydroxyapatite nanoparticles with tailorable morphologies andcarbonate substitutions using a wet precipitation method", *J. Nanosci.Nanotechnol.*,**2012**, 12, 2774-2778.

55. Erica R. Kramer, Aimee M. Morey, Margo Staruch, Steven L. Suib, Menka Jain, Joseph I. Budnick, Mei Wei, "Synthesis and characterization of iron-substituted HAP via a simple ion-exchange procedure", *J. Mater. Sci.*, **2013**, 48, 665–673.

56. Nordin J.A., Prajitno D.H., Saidin S., Nur H.,Hermawan H., "Structure–property relationships of iron–hydroxyapatite ceramic matrix nanocomposite fabricated using mechanosynthesis method", *Mater. Sci. Eng. C,* **2015**, 51, 294–299.

57. SuryanarayanaC., "Mechanical alloying and milling", Marel Dekker, CRC Press, New York, **2001**, 1–184.

58. Pramod N. Jagadalea, Pramod P. Jagtapb, Sambhaji R. Bamane, "Synthesis, characterization and *in vitro* drug delivery ofnanostructured Fe-doped hydroxyapatitebioceramics", *Der Chemica Sinica*, **2015**, 6, 28-36.

59. StanicV., DimitrijevicS., StankovicJ.A., MitricM., JokicB., PlecasI.B.,RaicevicS.,"Synthesis, characterization and antimicrobial activity ofcopper and zinc-doped hydroxyapatite nanopowders", *Appl. Surf. Sci*., **2010**, 256, 6083–6089.

60. MatsumotoN., SatoK., YoshidaK., HashimotoK., TodaY., "Preparationand characterization of beta-tricalcium phosphate co-doped with monovalent and divalentantibacterial metal ions", *Acta Biomater*., **2009**, 5, 3157–3164.

61. KimT.N., FengQ.L., KimJ.O., WuJ., WangH., ChenG.C., CuiF.Z., "Antimicrobial effects of metal ions (Ag^{+}, Cu^{2+}, Zn^{2+}) in hydroxyapatite", *J. Mater. Sci.Mater. Med*., **1998**, 9, 129–134.

62. Sumathi S., Buvaneswari G., "Copper substituted hydroxyapatite andfluorapatite:Synthesis,characterization and antimicrobial properties", *Ceram. Int.*, **2014**, 40, 15655–15662.

63. Roeder R., Converse G., Leng H., Yue W.,"Kinetic effects onhydroxyapatite whisker synthesized by the chelate 23ehavior23tion method", *J. Am. Ceram. Soc.,* **2006**, *89*, 2096–2104.

64. Guojing Liu, Jeffrey W Talley, Chongzheng Na, Steve L.Larson ,Lawrence G. Wolfe,"Copper doping improves hydroxyapatite sorption for arsenatein simulated groundwaters ", *Environ. Sci. Technol., 2***010**, 44, 1366-72.

65. Furukawa T, Matsusue Y, Yasunaga T, Nakagawa Y, Okada Y, Shikinami Y, "Histomorphometric study on high-strength hydroxyapatite/poly(Llactide) compositerods for internal fixation of bone fractures",*J. Biomed. Mater. Res.*,**2000**, 50, 410–419.

66. Trombelli L., Simonelli A., Pramstraller M., Wikesjö U.M.E., Farina R., "Single flapapproach with and without guided tissue regeneration and a hydroxyapatite biomaterial in the management of intraosseous periodontal defects", *J. Periodontol.*, **2010**, 81, 1256–63.

67. Strietzel F.P., Reichart P.A., Graf H.L.,"Lateral alveolar ridge augmentation using asynthetic nano-crystalline hydroxyapatite bone substitution material(Ostim)", *Clin. Oral Implants Res.*,**2007**, 18, 743–751.

68. Ye Q., Ohsaki K., Li K., Li D.J., Zhu C.S., Ogawa T., "Histological reactionto hydroxyapatite in the middle ear of rats",*Auris Nasus Larynx*,**2001**, 28, 131–6.

69. Seol Y.J., Kim J.Y., Park E.K., Kim S.Y., Cho D.W., "Fabrication of a hydroxyapatite scaffold for bone tissue regeneration using microstereolithography andmoldingtechnology", *Microelectron. Eng*.,**2009**, 86, 1443–1446.

70. Lv Q., Nair L., Laurencin C.T., "Fabrication, characterization, and in vitroevaluationof poly(lactic acid glycolic acid)/nano-hydroxyapatite compositemicrosphere-based scaffolds for bone tissue engineering in rotatingbioreactors", *J. Biomed. Mater. Res.*, **2009**, 91, 679–91.

71. Itokazu M., Yang W., Aoki T., Ohara A., Kato N., "Synthesis of antibiotic-loaded interporous hydroxyapatite blocks by vacuum method and in vitro drugrelease testing", *Biomaterials*,**1998**, 19, 817–9.

72. Sadat-Shojai M., Atai M., Nodehi A.,"Method for production of biocompatible nanoparticles containing dental adhesive",*US Patent* 8,357,732; **2013** ht.

73. Blackwood D., Seah K., "Electrochemical cathodic deposition of hydroxyapatite: improvements in adhesion and crystallinity", *Mater. Sci. Eng. C*, **2009**, 29, 1233–1238.

74. SuchanekW. L., ByrappaK., ShukP., RimanR. E., JanasV. F.,TenHuisenK. S., "Preparation of magnesium-substituted hydroxyapatite powders by the mechanochemical-hydrothermal method,"*Biomaterials,* **2004**, 25, 4647-4657.

75. MeunierP., RouxC., SeemanE., OrtolaniS., BadurskiJ.E., SpectorT.D.,CannataJ., BaloghA., LemmelE.M., Pors-NielsenS., RizzoliR., GenantH.K., ReginsterJ.Y., "The effects of strontium ranelate on the risk of vertebral fracture inwomen withpostmenopausal osteoporosis,"*N. Engl. J. Med.,***2004**, 350, 459-468.

76. ThianE.S., HuangJ., BestS.M., BarberZ.H., BonfieldW., "Silicon-substituted hydroxyapatite: the next generation of bioactive coatings," *Mater. Sci. Eng., C,*

2007, 27, 251-256.

77. GibsonI. R., BonfieldW., "Novel synthesis and characterization of an AB-type carbonate-substituted hydroxyapatite,"*J. Biomed. Mater. Res.,***2002***,* 59, 697-708.

78. KudaO., PinchukN., IvanchenkoL., ParkhomeyO., SychO., LeonowiczM., WroblewskiR., SowkaE., "Effect of Fe_3O_4, Fe and Cudoping on magneticprope - rties and behavior in physiologicalsolution of biological hydroxyapatite/glasscomposites", *J. Mater. Process. Technol.*, **2009**, 209, 1960-1964.

79. LiY., NamC.T., OoiC.P.,"Iron (III) and manganese (II) substitutedhydroxyapatite nanoparticles: characterization and cytotoxicityanalysis", *J. Phys. Confer. Series*,**2009**, 187, 1-8.

80. MiresteanC., MocutaH.,TurcuR.V.F., BorodiG., SimonS.,"Nanostructurated materials for hyperthermia treatment of bonetumors", *J. Optoelec. Adv. Mater.*, **2007**, 9, 764-767.

81. NakahiraA., NakamuraS., HorimotoM., "Synthesis of modifiedhydroxyapatite (HAP) substituted with fe ion for DDS application",*IEEE Trans. Magnatics*,**2007**, 43, 2465-2467.

82. Jimenez-ReyesM., Solache-RiosM., "Sorption behavior of fluoride ions from aqueous solutions by hydroxyapatite," *J. Hazard.Mater*.,**2010**, 180, 297-302.

83. Baillez S., Nzihou A., Bernache-Assolant D., Champion E., Sharrock P., "Removal of aqueous lead ions by hydroxyapatites: equilibria and kineticprocesses",*J. Hazard. Mater. A*, **2007**, 139, 443-446.

84. Hashimoto Y., Sato T., "Removal of aqueous lead by poorly-crystalline hydroxyapatites, *Chemosphere*, **2007**, 69, 1775-1782.

85. Xu H.Y., Yang L., Wang P., Liu Y.,"Kinetic research on the sorption ofaqueous lead by synthetic carbonate hydroxyapatite",*J. Environ. Manage.*,**2008**, 86, 319-328.

86. Mobasherpour I., Salahi E., Pazouki M., "Removal of nickel(II) from aqueous solutions by using nano-crystalline calcium hydroxyapatite", *J. SaudiChem. Soc.*,

2011, 15, 105-112.

87. Meski S., Ziani S., Khireddine H., Boudboub S., Zaidi S.,"Factorial designanalysis for sorption of zinc on hydroxyapatite", *J. Hazard.Mater*.,**2011**, 186,1007-1017.

88. Sheha R. R., "Sorption of Zn(II) ions on synthesized hydroxyapatites", *J. Colloid. Interf. Sci.*, **2007**, 310,18-26.

89. Lusvardi G., Mamavasi G., Menabue L., Saladini M., "Removal of cadmium ionbymeans of synthetic hydroxyapatite", *Waste manage.*, **2002**, 22, 853-857.

90. McGrellis S., Serafini J.N., JeanJean J., Pastol J.L., Fedoroff M., "Influence ofthe sorption protocol on the uptake of cadmium ions in calciumhydroxyapatite",*Sep. Purif. Technol.*, **2001**, 24, 129-138.

91. Corami A., Mignardi S., Rerrini V.,"Copper and zinc decontamination from single-and binary-metal solutions using hydroxyapatite", *J. Hazard.Mater.*,**2007**, 146, 164-170.

92. Oliva J., De Pablo J., Cortina J.L., Cama J., Ayora C., "The use of Apatite IITMto remove divalent metal ions zinc(II), lead(II), manganese(II) andiron(II) from waterin passive treatment systems: Column experiments", *J. Hazard.Mater*.,**2010**, 184, 364-374.

93. Takeuchi Y., Suzuki T., Arai H.,"A study of equilibrium and mass transfer in processes for removal of heavy-metal ions by hydroxyapatites", *J. Chem. Eng. Japan*, **1988**, 21, 98-100.

94. Zahouily M, Abrouki Y, Bahlaouan B, Rayadh A, Sebti S.,"Hydroxyapatite: new efficient catalyst for the Michael addition", *Catal.Commun.*,**2003**, 4, 521–524.

95. Sugiyama S., Minami T., Hayashi H., Tanaka M., Shigemoto N., Moffat J.B.,"Partialoxidation of methane to carbon oxides and hydrogen on hydroxyapatite:enhanced selectivity to carbon monoxide with tetrachloromethane", *Energ.Fuel.*,**1996**, 10, 828–30.

96. DeLoach L.D.,Payne S.A., Chase L.,Smith L.K., Kway W.L., Krupke W.F., "Evaluation ofabsorption and emission properties of Yb^{3+} doped crystals for laser applications", *IEEE J. Quantum Elect.*, **1993**, 29, 1179–91.

97. Li L., Liu Y., Tao J., Zhang M., Pan H., Xu X., "Surface modification of hydroxyl -apatite nanocrystallite by a small amount of terbium provides abiocompatiblefluorescent probe",*J. Phys. Chem. C*,**2008**, 112, 12219–24.

98. Bouhaouss A., Bensaoud A., Laghzizil A., Ferhat M.,"Effect of chemical treatments on the ionic conductivity of carbonate apatite", *Int. J. Inorg.Mater.*,**2001**, 3, 437–41.

99. Mahabole M., Aiyer R., Ramakrishna C., Sreedhar B., Khairnar R.,"Synthesis, characterization and gas sensing property of hydroxyapatite ceramic", *Bull. Mater. Sci.*, **2005**, 28, 535–45.

100. Jungbauer A., Hahn R., Deinhofer K., Luo P.,"Performance and characterization ofa nanophased porous hydroxyapatite for protein chromatography", *Biotechnol. Bioeng.*,**2004**, 87, 364–75.

101. Purdy K., Embley T., Takii S., Nedwell D.,"Rapid extraction of DNA and rRNA from sediments by a novel hydroxyapatite spin-column method*", Appl. Environ. Microbiol.*,**1996**, 62, 3905–3907.

102. MondolM. N., ChamonA. S., FaizB., ElahiS. F., "Chromium in urban soil-plant-water ecosystems", *J. Bangladesh Acad. Sci.,*2013, 37,173-187.

103. "Arseniccontamination in groundwater", UNICEF Position Paper, No.2, April**2013.**

104. Marcovecchio J.E., BotteS.E., FreijeR.H., "Heavy metals, major metals, trace elements. In: handbook of water analysis", NolletL.M., (Ed.). 2nd Edn. London, CRC Press, **2007**, 275-311.

105. Momodu M.A., Anyakora C.A. "Heavy metal contamination of ground water: the adsorptive removal of heavy metals from groundwater by iron oxide based adsorbentssurulere case study",*Res. J. Environ. Earth Sci.,***2010**, 2, 39-43.

106. Pal B.N., "Granular ferric hydroxide for elimination of arsenic from drinking water",*BUET-UNU International workshop on Technology for arsenic removal*

Fromdrinking water, 5-7 May, **2001**, 59-68.

107. WHO, Guidelines for Drinking water quality: Health Criteria and other supporting information. *World health organization*, Geneva, Switzerland 2nd edition, **2011**, 2.

108. Rai D, Eary LE, Zachara JM,"Environmental chemistry of chromium",*Sci. Total Environ.*,**1989**, 86, 15-23.

109. Kotas J, Stasicka Z,"Chromium occurrence in the environment and methods of its Speciation",*Environ.Pollut.*,**2000**, 107, 263-283.

110. James R.O., Ramamoorthy S., "Heavy metals in natural waters: applied monitoringand impact assessment, **1984**, New York, USA.

111. Barakat M.A., "New trends in removing heavy metals fromindustrial wastewater",*Arab. J. Chem*., **2011**, 4, 361–377.

112. Kwon J.S., Yun S.T., Lee J.H., Kim S.O., Jo H.Y., "Removal of divalent heavymetals (Cd, Cu, Pb, and Zn) and arsenic (III) from aqueous solutions using scoria: kinetics and equilibrium of sorption, *J. Hazard. Mater.*,**2010**, 174,307–313.

113. Gottipati R., Mishra S., "Application of response surfacemethodology for optimization of Cr(III) and Cr(VI) adsorption on commercial activated carbons", *Res. J. Chem. Sci.,***2012**,2, 40-48.

114. Lakherwal D., "Adsorption of heavy metals: areview", *Int. J. Environ. Res. Develop.*, **2014**, 4, 41-48.

115. Kenneth S.W., Sing Ruth, Williams T., "Physisorption hysteresis loops and the characterization of nanoporous materials", *Adsorpt. Sci. Technol.*, **2004**, 22, 773-782.

116. Brunauer S., Emmett P.H., Teller E., "Adsorption of gases in multimolecular layers", *J. Amer. Chem. Soc.* **1938**,60, 309-319.

117. Barrett E.P., Joyner L.G., Halenda P.P., "The determination of pore volume and area distributions in poroussubstances, I, computations from nitrogen isotherms", *J. Am. Chem. Soc*., **1951**, 73, 373–380.

118. FooK.Y., HameedB.H., "Review insights into the modeling of adsorption isotherm systems", *Chem. Eng. J.*, **2010**, 156, 2–10.

119. Hui QIU, Lu LV, Bing-cai PAN, Qing-jian ZHANG, Wei-ming ZHANG, Quan-xing ZHANG, "Review: Critical review in adsorption kinetic models", *J. Zhejiang Univ. Sci. A,* **2009**, 10, 716-724.

CHAPTER 2

Materials and Methods

This chapter describes the instruments and materials used throughout the study. In addition to this, treatment and characterization of waste materials (eggshell and prawn shell) have also been covered.

2.1 Instruments

A number of instruments were used for characterization and adsorption study. Brief discussion on the instruments and methods used is presented in the following sections.

2.1.1 Instruments for characterization

Instruments used for characterization of raw materials, pristine and doped HAP are discussed here in brief.

- **SEM-EDS analysis**

A Hitachi, S-3400N Scanning Electron Microscope coupled with Energy Dispersive Spectroscopy (EDS) was used. In Scanning Electron Microscopyapplications, data is collected over a selected area of the surface of the sample and a two-dimensional image is generated that displays spatial variations in properties including chemical characterization, texture and orientation of materials. Energy Dispersive X-ray Spectroscopyis used to analyze the energy spectrum in order to determine the abundance of specific elements. A typical EDS spectrum is portrayed as a plot of X-ray counts vs. energy (in keV). Energy peaks correspond to the various elements in the sample.

Pure and doped HAP samples were characterized in powder form. Morphological and micro-structural changes were determined before and after calcinationof the samples. Synthesized samples were oven dried and calcined at 100°C, 300°C and 600°C and

powder samples were dispersed on a black carbon tape in order to carry out the experiment.

- **X-ray diffraction (XRD)**

PANalytical X-ray diffractometer (X'Pert PRO XRD PW3040) was used to investigate the phase purity of the synthesized pure and doped HAP. This technique was also used to examine the phase purity of synthesized nano HAP and the thermally treated HAP samples. The intensity data were collected in 0.02°steps following the scanning range of 2θ=5°-75°using CuK_α (γ= 1.54178OA) radiation. The phases appeared in the samples were compared and confirmed using standard JCPDS files. The average crystallite size was calculated using the Scherrer equation as given in equation 2.1.

$$D = \frac{K\lambda}{\beta \cos\theta} \qquad (2.1)$$

Where D = crystallite size in angstrom (Å), K= Scherrer constant (≈0.95), λ = X-ray wavelength (CuKα=1.54056Å), β= peak width (FWHM in degree), and θ = Bragg angle. Thevalues of lattice parameters (a, c) for hexagonal system were calculated using equation 2.2. The unit cell volume of the samples was calculated using equation 2.3.

$$\frac{1}{d^2} = \frac{4}{3}\left[\frac{(h^2 + hk + k^2)}{a^2}\right] + \frac{l^2}{c^2} \qquad (2.2)$$

Where $d$is the interplanar spacing, hkl are miller's indicesand $a$and$c$are latticeparameters.

$$V = \frac{\sqrt{3}}{2}\, a^2.c \qquad (2.3)$$

Where $V$is the unit cell volume, $a$and$c$are latticeparameters.

- **Fourier Transform Infra-red Spectroscopy (FT-IR)**

FT-IR spectroscopy is an important toolfor molecular characterization of organic and inorganic compounds. Prestige 21 Shimadzu FT-IR spectrophotometer was used in this study. FT-IR spectra were recorded in the range of 400-4000 cm^{-1} with 4 cm^{-1} resolution and averaging 30 scans. The experiment was conducted preparing a pellet of KBr in which the sample to KBr ratio was always maintained at 1:100.

- **Analysis of particle size by dynamic light scattering (DLS)**

Particle size of the synthesized HAP was measured by DLS technique using Zetasizer Nano ZS90 (ZEN3690, Malvern Instruments Ltd, UK). A He–Ne laser of 632.8 nm wavelength was used as light source and the measurements were made at a fixed scattering angle of 90°. The scattering intensity data were analyzed to obtain the hydrodynamic diameter (D_h). A cell of 10 mm diameter was used. 0.002 g HAP powder was added to 50 mL of DI water and ultrasonicated for 20 min to minimize the degree of agglomeration. The particle sizes were automatically determined from the translational diffusion coefficient using the Stokes–Einstein equation,

$$d\,(\mathrm{H}) = \frac{kT}{3D\pi\,\eta} \qquad (2.4)$$

Where d (H) is the hydrodynamic diameter, k is the Boltzmann constant, T is the absolute temperature, D is the translational diffusion coefficient, and η is the viscosity of the liquid in which the particles were suspended.

- **Brunauer, Emmett and Teller (BET) surface area analysis**

The BET theory is the most useful model used to determine surface area. Pristine and doped HAP samples were pretreated by purging N_2 gas for 4 h at the heating temperature of 120°C to remove moisture and organic impurities from the surface of the particles.

Pretreatment of the HAP samples were done by BELPREP-flowII (BEL Japan, Inc.) and the measurements were carried out by BEL sorp mini II (BEL Japan, Inc.) equipment.

2.1.2 Instruments for investigation of adsorption of metal ions

Part of this study was focused on removal of heavy metals from aqueous system using synthesized pure and doped HAP. Heavy metal ions in aqueous system before and after adsorption treatment were determined using spectrophotometer following standard procedure.

- **Hydride Generation Atomic absorption spectroscopy (HG-AAS)**

Atomic absorption spectroscopy (HG-AAS, NOVAA 350, Analytik Jena, Germany) instrument was used to determine concentration of As(V) in aqueous solution. Preparation of As(V) standards solution was carried out according to the standard procedure (SOP) reported by HG-AAS, NOVAA 350, Analytik Jena, Germany.

AAS equipped with Hydride Generation and Hollow Cathode Lamp operated at 10mA was used for determination of arsenic. A spectral band width of 0.5 nm was selected to isolate the 193.7 nm As line. Calibration standards (2, 5, 10 and 20 μgL^{-1}) were prepared from the As(V) stock solution by appropriate dilution of the standard solutions. A calibration curve of As(V) standard solutions is presented in Figure 2.1 which was used to calculate concentrations of As(V).

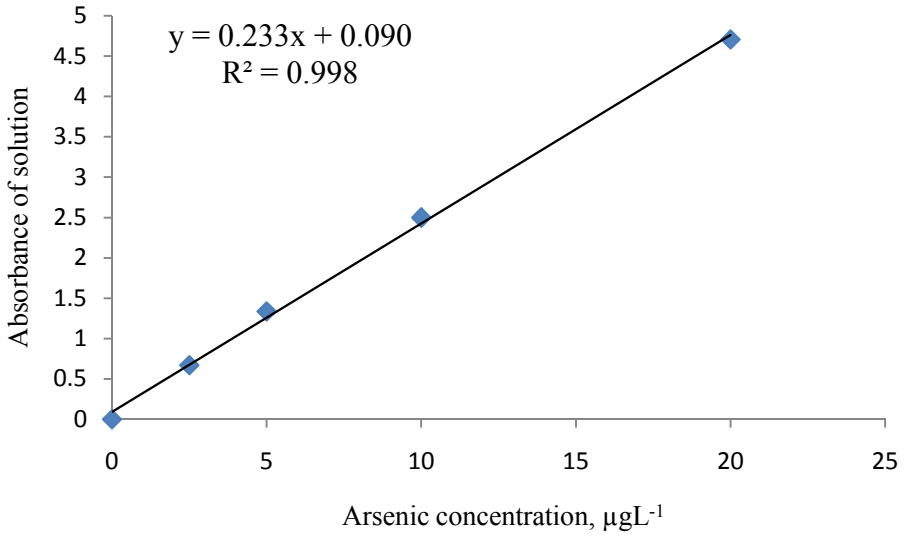

Figure 2.1 A calibration curve of As(V) standards solution by HG-AAS

- **UV–Visible spectrophotometer**

A double-beam UV–visible spectrophotometer (UV-2910, Hitachi, Japan) with a quartz cell of 1cm width was used for absorbance measurements. The reaction of Cr(VI) with 1,5-diphenylcarbazide (DPC) in acidic medium form a red-violet color complex which exhibits a characteristic absorbance at 542 nm wavelength. Cr(VI) solution was prepared by appropriately diluting a standard stock solution. The pH of the solution was then adjusted (pH=1.5) in acid medium (with 1:1 Phosphoric acid) along with 2mL of diphenylcarbazide in a 100 mL volumetric flask. Calibration standards (0.2, 0.5, 0.8, 1.0 and 1.5 mgL^{-1}) were prepared and the calibration curve of Cr(VI) standard solutions is presented in Figure 2.2. The amount of Cr(VI) present in the sample was deduced from the standard calibration curve.

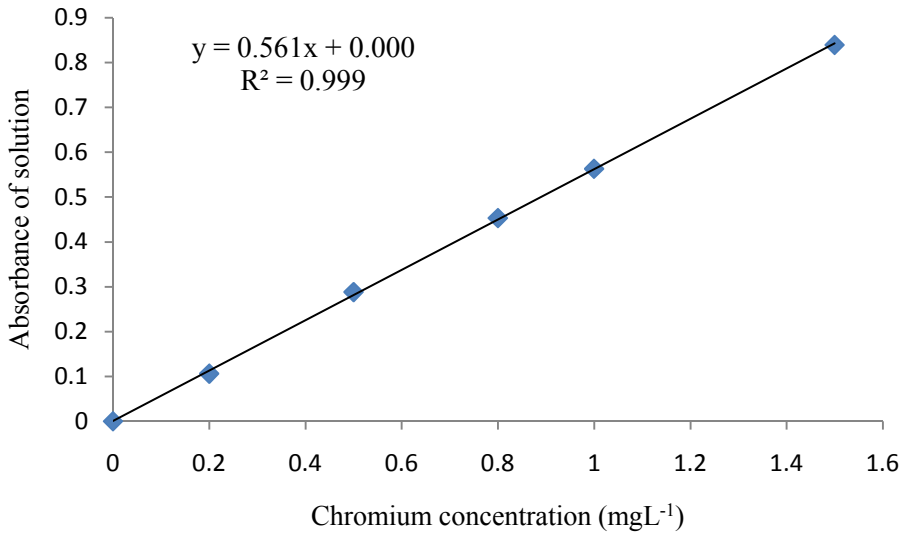

Figure 2.2 A calibration curve of Cr(VI) standards solution by UV-Visible Spectrophotometer

- **Flame atomic absorption spectroscopy (FAAS)**

Flame atomic absorption spectroscopy is one of the most common instrumental methods for analyzing metal ions. In this study a flame atomic absorption spectrometer, FAAS, model: NOVAA 350, (Analytik Jena, Germany) was used. Calibration was done by preparing standard solutions of Pb(II) from standard stock solution by appropriate dilution. Details preparation procedure of Pb(II) standards solution has been done by following manual of NOVAA 350. Calibration curve (Figure 2.3) was used to determine Pb(II) concentrations in the samples.

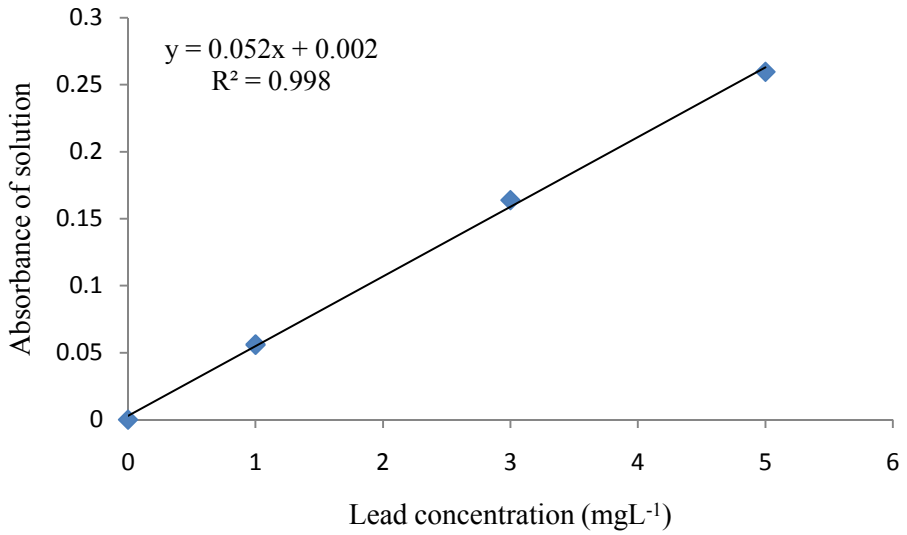

Figure 2.3 A calibration curve of Pb(II) standard solution by Flame AAS

2.2 Materials

Waste materials, for instances, eggshells and prawn shells were used as raw materials for the synthesis of pure and doped HAPs. Both of the waste materials were collected from the local restaurants nearby the laboratory. Calcium acetate was synthesized from eggshells and its purity was compared with the commercial calcium acetate. All solutions were prepared using either de-ionized water or distilled water. All the chemicals used for this work were purchased from local market and are listed in Table 2.1. The sources and purity of the chemicals are also mentioned.

Table 2.1: List of chemicals used in this study

Chemicals	Grade and purity	Origin
Nitric acid	65%	Sigma-Aldrich, Germany
Hydrochloric acid	37%	Merck, Germany
Sulphuric acid	95-97%	Merck, Germany
Acetic acid	AR, 100%	Merck, Germany
Sodium hydroxide	98%	Merck, Germany
Aqueous ammonia	25%	Merck, Germany
Cyclohexane	89%	BDH, England
1-pentanol	AR	BDH, England
Acetone	Analar, 99%	Merck, Germany
Ethanol	Analar,99.8%	Merck, Germany
Diammonium hydrogen phosphate	99%	BDH, England
Copper nitrate	Analar	Merck, Germany
Ferric nitrate nona hydrate	98%	Merck, Germany
Cetyltrimethyl ammonium bromide	99%	Merck, Germany
Sodium dodecyl sulphate	85%	Merck, Germany
Triton X-100		Packard Co. Inc., USA
Potassium dichromate	Analar, 99.9%	Merck, Germany
Sodium arsenate seven hydrate		BDH, England
Phenolphthalein indicator	Analar	Merck, Germany
1,5-diphenyl carbazide		Merck, Germany
Sodium borohydride		Lancaster, England
Potassium iodide		Merck, Germany
Buffer solution pH 4.0		Sigma-Aldrich, Germany
Buffer solution pH 7.0		Sigma-Aldrich, Germany
Buffer solution pH 10.0		Sigma-Aldrich, Germany
Standard solution of As(V), Cr(VI), Pb(II)		Sigma-Aldrich, Switzerland

Treatment and characterization of waste materials

Waste materials (eggshell and prawn shell) were treated and characterized prior to their use as a precursor to calcium for the synthesis of hydroxyapatites.

2.3.1 Treatment of waste materials

- **Treatment of eggshells**

Raw eggshells were washed thoroughly with water and the inner membranes were removed. The shells were boiled in water for 30 min. Then cleaned eggshells were dried at 110°C and ground to fine powder using a grinder (Rotsch, Type:RM 100, 250V, Germany). At this stage half of the eggshell powder was calcined at 950°C for an hour and the temperature of the furnace was raised at a rate of 5°C/min. The calcination resulted the formation of CaO ($CaCO_3 \longrightarrow CaO + CO_2$) while all organic substances were burnt off. The calcined eggshell powder was kept in a container and marked as 'A'. Other half of the eggshell powder was kept as uncalcined and marked as 'B'. Both 'A' and 'B' were used to synthesize HAP according to the following procedure. Percentage of $CaCO_3$ in eggshell was determined by a titremetric method, while XRD and FT-IR were used for the characterization.

- **Treatment of prawn shell**

Prawn shells were collected and washed thoroughly with tap water and then boiled with distilled water for 1 h. Cleaned prawn shells were then suspended in NaOH solution (1M) for 24 h at room temperature maintaining the ratio of prawn shell and NaOH solution as 1:16. This treatment is known as de-proteinization and then the shell was rinsed with distilled water to remove excess NaOH and proteins. In the next step demineralization was carried out with 4% HCl solution and again the shells were suspended in the acid solution for 24 h at room temperature. At this stage formation of CO_2 bubbles in the

solution was observed due to the conversion of calcium carbonate to calcium chloride according to the following reaction:

$$CaCO_3(s) + HCl\ (aq.) \longrightarrow CaCl_2(aq) + CO_2(g) + H_2O(l) \qquad (2.5)$$

The insoluble organic materials were removed from the solution by filtration. The filtrate was collected and used as source of Ca^{2+} ions. The concentration of Ca^{2+} ion was determined by FAAS using calcium specific hollow cathode lamp (wavelength 422.7 nm) for which the instrument has a detection limit of 0.10 mgL^{-1}.

2.3.2 Characterization of waste materials

Eggshell and prawn shellwerecharacterized using FT-IR, XRD and SEM techniques. Prior to that, the concentrations of $CaCO_3$ in eggshells and prawnshells were determined by chemical analyses.

A. Eggshell

Determination of percentage of $CaCO_3$ in eggshell

A known amount of eggshell powder was taken into a cleaned 250 mL conical flask. Few drops of ethanol were added to it to wet the sample. Eggshell powder was slowly dissolved by addition of 10 mL HCl (1.0 M). The solution was heated very carefully on a hotplate until it just began to boil and then it was allowed to cool to room temperature. The walls of the flask were rinsed with distilled water followed by addition of phenolphthalein indicator. 0.1 M NaOH solution was used for the titration.

The quantity of $CaCO_3$ present in eggshell wasdetermined following titration method (Table 2.2) and calculated using Equation 2.8. The percentage of $CaCO_3$was calculated approximately 93%, which is comparable with literature data.[1]

Table 2.2 Titration data to calculate percentage of $CaCO_3$ in eggshell

No. of reading	Amount of eggshell taken, g	Volume of NaOH required , mL (0.1046 M)	Volume of HCl added, mL (0.9648 M)
1.	0.4549	12.0	
2.	0.4511	11.8	10
3.	0.4553	11.9	

The percentage of $CaCO_3$ present in eggshell was calculated using the equations 2.6- 2.10.

Moles HCl added (initial moles) = $V_{HCl} M_{HCl}$ (2.6)

Moles HCl left = $V_{NaOH} M_{NaOH}$ (2.7)

Moles HCl reacted = $V_{HCl}M_{HCl}$ - $V_{NaOH}M_{NaOH}$ (2.8)

Moles $CaCO_3$ = (Moles HCl reacted) (1 mole $CaCO_3$ / 2 moles HCl) (2.9)

$$\%CaCO_3 = \frac{(\text{moles of } CaCO_3) \times (100.1 \text{ g/mole } CaCO_3)}{\text{grams of sample}} \times 100 \qquad (2.10)$$

$\%CaCO_3$ in eggshell = 93%

B. Prawn shell

Percentage of calcium carbonate in prawn shell was calculated using equation (2.11) and (2.12). Calcium carbonate content in prawn shell is approximately 28.52%.

$$\text{Ca in mgg}^{-1} = \frac{(C)\,(V)\,(\text{d.f})}{(W)} \qquad (2.11)$$

$$\% \, CaCO_3 = (\text{Ca in mgg}^{-1}) \left[\frac{\text{Molecular mass of } CaCO_3}{\text{Atomic mass of Ca}} \right] (0.0001) \qquad (2.12)$$

Where C is the concentration of calcium in the sample solution inmgL^{-1},V is the volume of the undiluted sample solution in mL,W is thesample weight in grams; and *d.f.* is thedilution factor, if used, asdescribed below:

$$d.f. = \frac{\text{Volue of diluted sample solution in mL}}{\text{Volue of aliquot taken for dilution in mL}}$$

65.6840 g of prawn shell was taken to prepare 1375 mL of undiluted solution containing Ca^{2+} ion.

% $CaCO_3$ in prawn shell = 28.52%

- **FT-IR analysis**

FT-IR analysis was performed to identify carbonate group in the eggshell powder. Both oven dried (100°C) and calcined (900°C) eggshell powder were analyzed and spectra are shown in Figure 2.4. Oven dried eggshell powder shows the presence of carbonate with the appearance of vibration bands at 2356, 1427, 875 and 710 cm^{-1}. Similar FT-IR spectrum of natural calcite confirms the presence of calcium carbonate in oven dried eggshell powder.[1,2] Vibration band at 1427 cm^{-1} represents the asymmetric stretching of CO_3^{2-} group whereas bands for bending mode of carbonate group appeared at 875 and 710 cm^{-1}.[2] Thus FT-IR analysis suggests the presence of $CaCO_3$ in oven dried eggshell powder. Furthermore, a sharp peak at 875 cm^{-1}confirmed that the $CaCO_3$powder obtained from oven dried eggshell is calcite.[3]

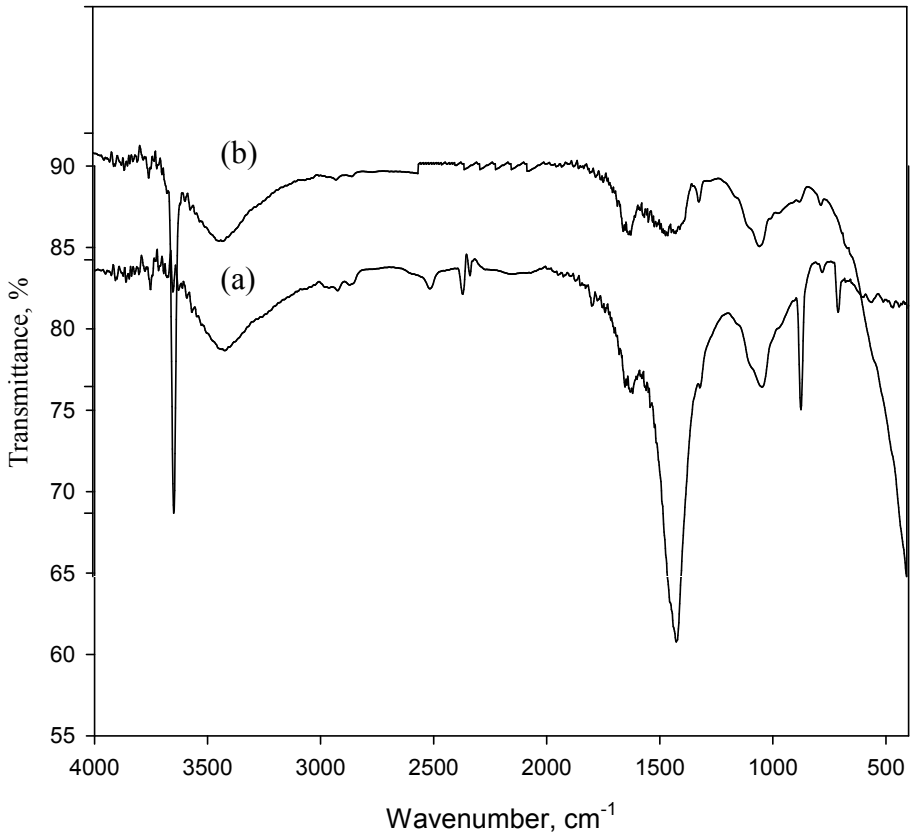

Figure 2.4 FT-IR spectra of eggshell (a) dried at 100°C and (b) calcined at 900°C

FT-IR spectrum ofeggshell calcined at 900°Cfor 1 h showsstrong band at 3641 cm^{-1}corresponds to the O─H bonds from the remaining hydroxide.[4] The wide and strong band at around 400cm^{-1}corresponds to theCa─O bonds.[4] Disappearance of vibration band at 2356 cm^{-1} in Figure 2.4(b) indicates the elimination of carbonate from eggshell caicined at 900°C.

- **XRD analysis**

The data obtained from the X-ray diffraction patterns (Figures 2.5) demonstrate the crystalline nature and phase composition of oven dried and calcined eggshell powder. The XRD pattern of the oven dried (100°C) eggshell in Figures 2.5 (a) exhibits characteristics peak at 2θ position~29.45° which confirm the presence of calcite phase in

eggshell powder. XRD pattern of oven dried eggshell powder shows the presence of peaks at ~43.19° for (202) plane, at ~39.45° for (113) plane and alsohighest intensity peak at 2θ position~29.45° for (104) plane. This is in excellent agreement with JCPDS File for rhombohedral calcite (File # 5-0586) as reported in the literature.[5]FT-IR spectrum of oven dried eggshell powder also support the presence of calcite in the sample. Again XRD pattern for eggshell powder calcined at 900°C in Figure 2.5 (b) shows the presence of calcium oxide with its characteristic peak at2θ position ~34.16°. This is consistent with JCPDS No. 01-077-2010 for CaO.[6]Presence of CaO in calcined eggshell indicates complete removal of CO_2 from the sample after thermal treatment.The thermal processing used for elimination the organic component of eggshells at 900°C produce the conversion of calcite into calcium oxide.

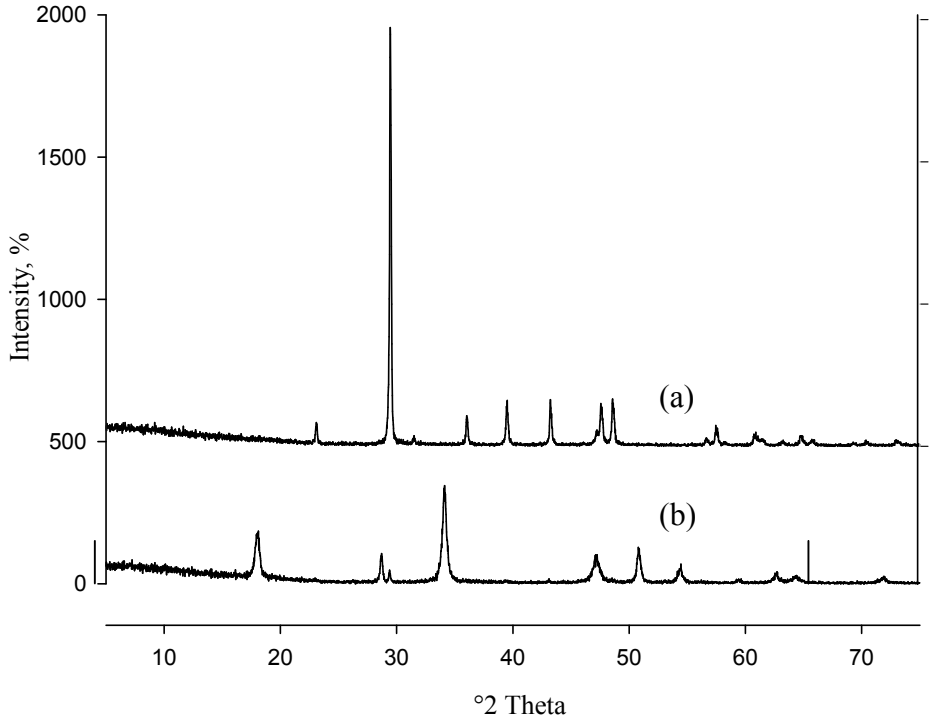

Figure 2.5 XRD patterns of eggshell powder (a) dried at 100°C (b) calcined at 900°C

- **SEM analysis**

The morphology of the eggshell powder was studied using SEM. Figure 2.6(a) shows SEM micrograph of eggshell powder. It is observed from the micrograph that eggshell powder is agglomerated, though SEM micrograph of the inner part of eggshell in Figure 2.6(b) shows the fibre-like morphology with similar pore size on the surface.

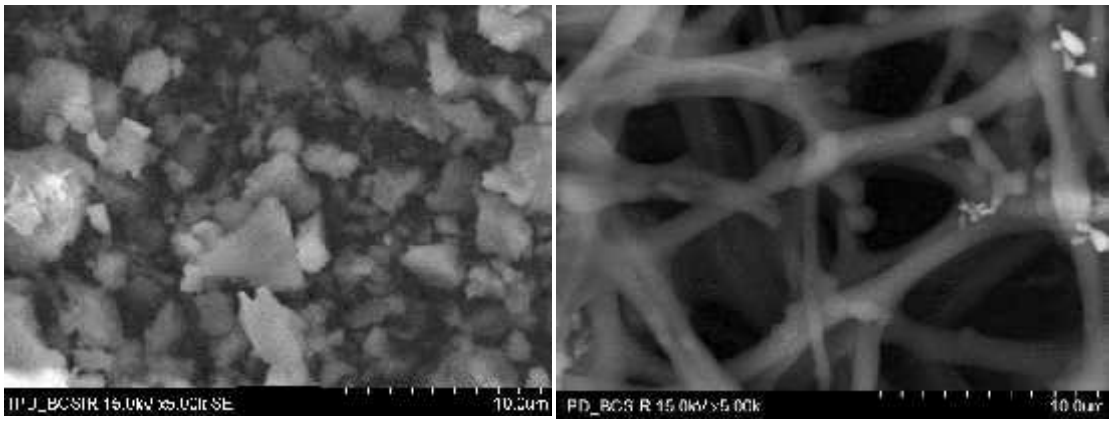

(a) **(b)**

Figure 2.6SEM micrograph of (a) eggshell powder (b) inner part of eggshell

2.3.3 Waste management by utilization of waste materials

Raw eggshell with rhombohedral form is completely converted into aface-centered cubic CaO after calcination at900°C. The percentage of $CaCO_3$ in eggshell and prawnshell are 93% and 28.52% respectively. Hence, both eggshell and prawnshell can be used as a source of calcium in the synthesis of pure and doped HAP. Eggshell contains higher percentage of calcium carbonate than that of prawnshell. Hence eggshell was preferably used for the synthesis of pure and doped HAP in this study. This will enhance the waste management by utilization of waste materials.

References

1. AhmedS., AhsanM., "Synthesis of Ca-hydroxyapatite bioceramicfrom eggshell and itsCharacterization", *Bangladesh J. Sci. Ind. Res.*, **2008**, 43,501-512.

2. Baird T., Solomon S.E.,"Calcite and aragonite in the egg shell of *Chelonia mydas* L.", *J. Exp. Marine Biol. Ecol.*, **1979**, 36, 295-303.

3. HariharanM., VargheseN., Benny CherianA., SreenivasanP.V., PaulJenish, AntonyAsmy, "Synthesis and characterisation ofCaCO3 (calcite) nano particles from cockle shells using chitosan as precursor", *Int. J. Sci. Res. Pub.*, **2014,**4, 1-5.

4. Park J., Min D., Song H., "Structural investigation of $CaO–Al_2O_3$ and $CaO–Al_2O_3–CaF_2$slags viaFourier Transform Infrared spectra", *ISIJ Int.*,**2002**, 42, 38–43.

5. RiveraE.M., AraizaM., BrostowW., CastanoV.M., Diaz-WstradaJ.R., HemandezR., RudriguezJ.R., "Synthesis of hydroxyapatite fromeggshell", *Mater.Lett.*,**1999**, 41, 128-134.

6. TangboriboonN.,, KunanuruksapongR., SirivatA., "Preparation and properties of calcium oxide from eggshellsvia calcinations", *Mater. Sci. Poland*, **2012**, 30,313-322.

CHAPTER 3

Synthesis of pure HAP from waste materials and its characterization

3.1 Introduction

Hydroxyapatite (HAP), $Ca_{10}(PO_4)_6(OH)_2$is the major mineralogical component of bones and teeth. Being highly bioactive and biocompatible, it is capable to form bonds between bone tissues and implant. Despite the application as implant material, HAP has great importance for bothenvironmental processes and various industrialpurposes due to its great sorptionproperties. Applications of HAP includes waterpurification, degradation of pollutants andfabrication of biocompatible ceramics.[1] It is reported that a wide variety of metals e.g. Cr, Cu, Pb, Ni, As, Co, Sb and U have been stabilized using HAP.[2-4]

Calcium is one of the main componentsof synthetic HAP and hard tissues of all living bodies. So hard tissues of living bodies can be used as calcium source in synthesis of HAP and doped HAP. This will also minimize the chances of finding impurities in the synthesized materials.Eggshells are one of the richest sources of calcium.The eggshellsconstitute 11% of the total weight of the egg and are composed by calcium carbonate (94%),calcium phosphate (1%),organic matter (4%) and magnesium carbonate (1%).[5]A huge amountof eggshells are produced daily which are basically of no use causing environmental pollution.So an attempt has been made to utilize waste materials for the synthesis of HAP. Coral, seashell, prawn shell also can also be used as a source of calcium in the synthesis process.

A number of synthetic procedures have usually been used for the preparation of calcium hydroxyapatites. The most commonly used technique for the preparation of HAP is wet chemical precipitation method which was followed in this study.

3.2 Materials and Methods

Pure HAP was prepared by wet chemical precipitation method. In a typical synthetic method, a requisite amount of eggshell powder was dissolved in concentrated nitric acid with 60 mL of distilled water and this solution was filtered to obtain a clear solution. Finally the eggshell solution in nitric acid was prepared in such a way that the concentration of Ca^{2+} was maintained to achieve a specific molar concentration. This solution was named as '***Solution I'***. ***'Solution II'*** was prepared by dissolving requisite amount of $(NH_4)_2HPO_4$ in distilled water to keep the concentration of the solution specific to maintain the Ca/P ratio 1.67 in the synthesized HAP. ***Solution I*** was transferred into a container and the pH of the solution was maintained at 10 by using aqueous NH_3. The phosphate precursor ***Solution II*** was then slowly added to the ***Solution I*** with continuous stirring of the reaction mixture at room temperature (30°C). A gelatinous precipitate was formed and in order to obtain the expected product, the precipitate was kept for 24 h in mother solution. The precipitate was then filtered and washed with double distilled water up to 10 times. Finally the product was dried at 100°C for 8 h and it was ground to powder for further characterization. The synthesized product was also calcined at different temperatures at 300°C and 600°C and the calcined products were collected for characterization. The calcination temperatures were achieved by maintaining rising of temperature at the rate of $3°Cmin^{-1}$ with 1 h soaking time. The reaction is shown in equation 3.1.

$$10\ Ca(NO_3)_2 + 6\ (NH_4)_2HPO_4 \longrightarrow Ca_{10}(PO_4)_6(OH)_2 \qquad (3.1)$$

Schematic diagram of the synthesis of hydroxyapatite from eggshell and prawn shell is given in Figure 3.1.

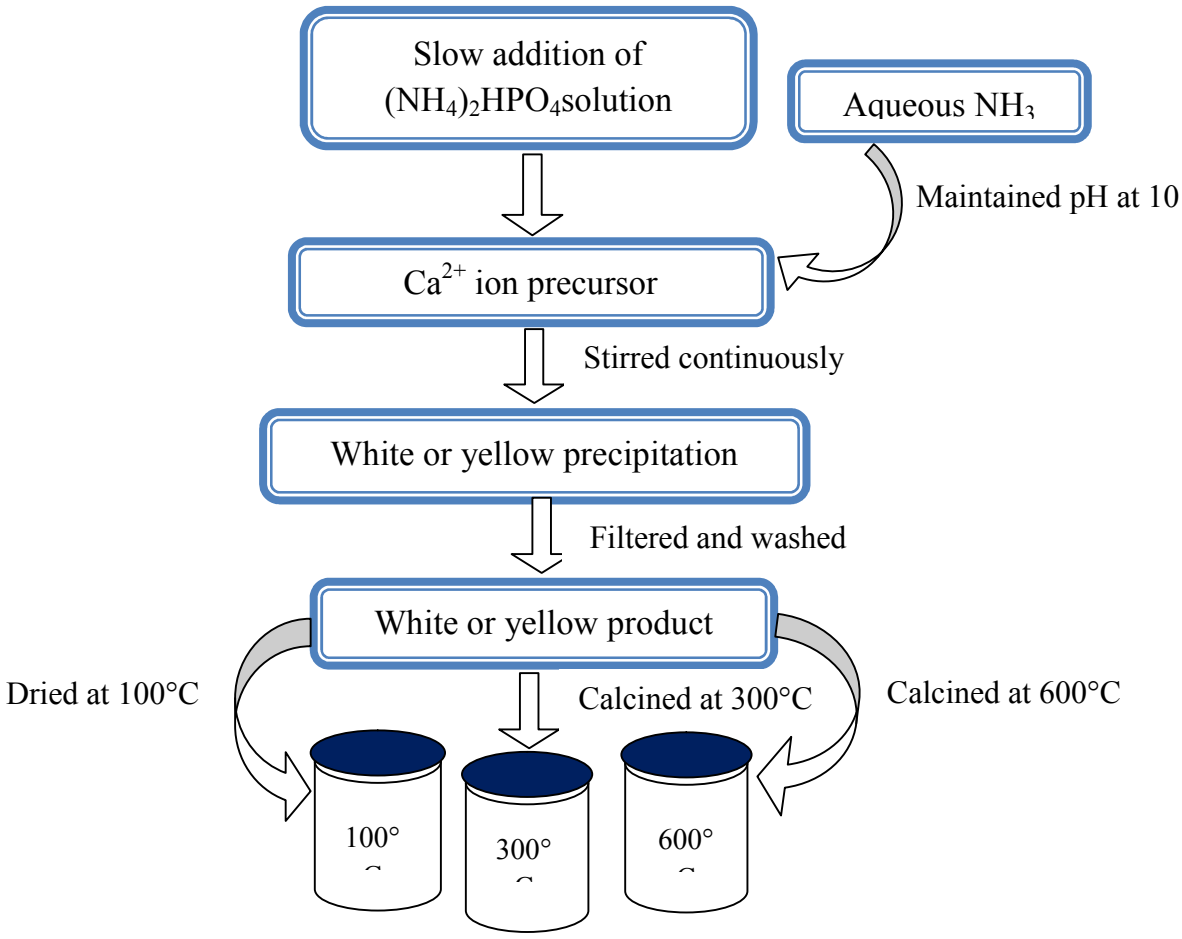

Figure 3.1 Schematic diagramfor synthesis of pure HAP from eggshell or prawnshell

Prawnshell and both the raw and calcined eggshell powders were used to prepare the Ca^{2+} ion precursor solution. HCl and HNO_3 were used for the preparation of prawn shell and eggshell solutions. Eggshell contains higher amount of $CaCO_3$ than that of prawnshell. Eggshell was therefore preferentially used for synthesis of pure and doped HAP in this study.

3.3 Characterization of pure HAP

Synthesized pure HAP was characterized using EDS, XRD, FT-IR, SEM, DLS particle size analyzer, BET surface area analyzer techniques.

3.3.1 Elemental analysis

Synthesized products were analyzed using EDS for chemical characterizationEDS spectrum of pure HAP from eggshell is shown in Figure 3.2(a). It shows the presence Ca, P, C and O in the product. Calculated Ca/P ratio of the pure HAP from eggshell is 1.44. Figure 3.2(b) shows EDS spectrum of pure HAP from prawn shell. Spectrum shows the presence of Ca, P, Mg and O in the product. Ca/P ratio of the pure HAP from prawnshell is calculated as 1.53.

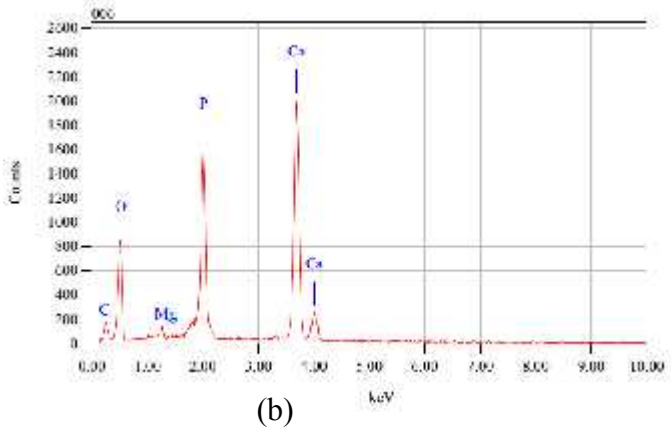

(b)

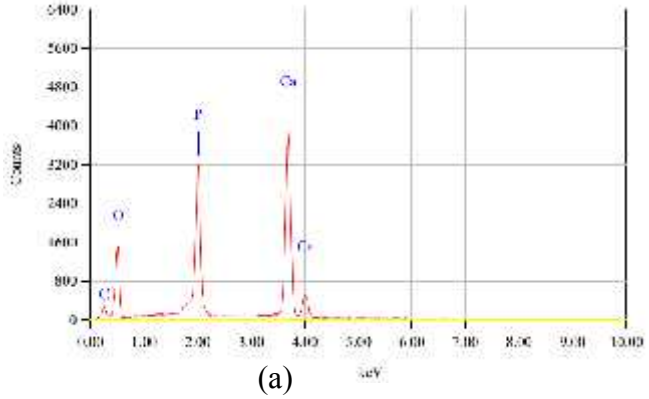

(a)

Figure 3.2 EDS spectra ofpure HAP from (a) eggshell (b) prawnshell

The Ca/P ratio of the human bone was calculated 1.67,[6]which indicates that the synthesized HAP products are non-stoichiometric or calcium deficient. One of the main reasons of non-stoichiometry is inclusion of impurities in the crystal lattice. Presence of carbon and magnesium in the spectra also support this observation. Phosphate group in HAP may be partially substituted by carbonate group which decreases Ca/P ratio in the product. Presence of carbon in pure HAP is introduced from environmental CO_2 and magnesium appears in pure HAP from prawn shell.[7] FT-IR spectra of pure HAP also support the presence of carbon in the product.

3.3.2 FT-IR analysis

The FT-IR spectra of eggshell and prawn shell derived pure HAP (both oven dried and thermally treated) are shown in Figure 3.3. The IR spectra of HAP samples exhibited well defined absorption bands in the range of 870-1045 cm^{-1} and 570-630cm^{-1}, characteristic of a well crystallized apatite phase.[8]Presence of phosphate group in pure HAP from eggshell and prawnshell (Figure 3.3) can be attributed by double bands at 567 and 601 cm^{-1}which refer to asymmetric and symmetric deformation modes $\nu_4$of phosphate group. Intensive absorption band in the range of 1033-1090 cm^{-1} corresponds to a bandcharacteristic of asymmetric stretching mode ν_3 of PO_4^{3-} group. Thebroad band in the range 3421–3441 cm^{-1}can beattributed to traces of water incorporated into HAP structure,together with the weak, band around 1627-1637 cm^{-1} due to H–O–H bending mode.[9]Shoulders are observed at 3564 $cm^{-1}$and 3568 cm^{-1} after calcining synthesized HAP at 300°C and 600°C respectively. This implies the presence of structural OH group in the product which was masked by the broad H_2O absorption band in the spectra for oven dried HAP from eggshell and prawnshell (Figure 3.3 a and b).

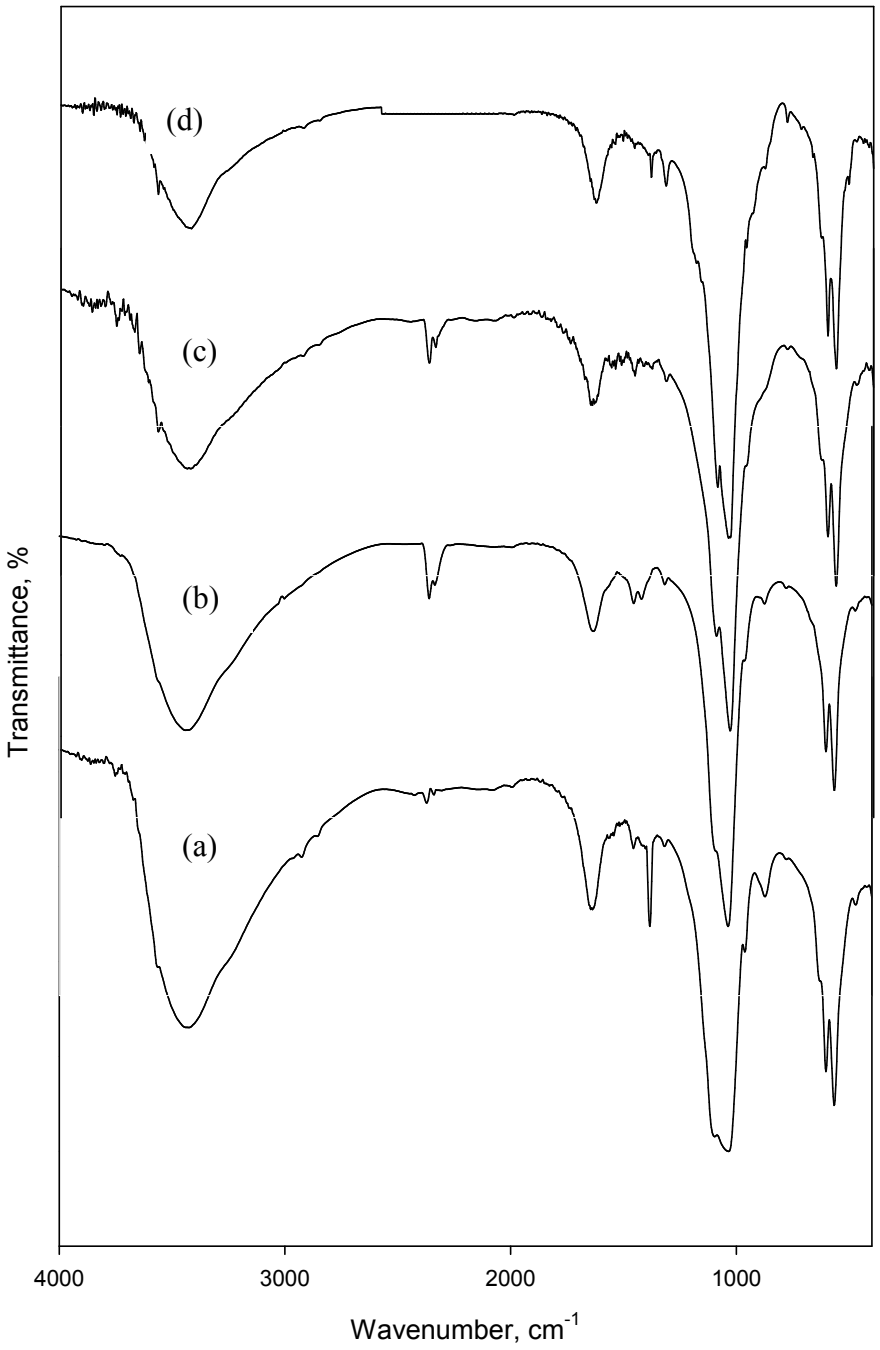

Figure 3.3 FT-IR spectra of synthesized (a) pure HAP from prawn shell dried at 100°C, pure HAP from eggshell,(b)dried at 100°C, fired at (c) 300°Cand (d) 600°C

Band appearing at ~2360 cm^{-1} corresponds to the presence of CO_3^{2-} incorporated in HAP from eggshell. A very weak band at ~1382 cm^{-1}assigned to ν_3 asymmetric stretch

vibration of CO_3^{2-}indicates substitution in pure HAP.[10] Figure 3.3(a) indicates the absence of carbonate group in HAP from prawnshell. Removal of carbonate from HAP calcined at 600°C appears from the disappearance of bands at 2360 and 1384 cm^{-1} in Figure 3.3(d). The band positions and their respective assignments are given in Table 3.2.

Table 3.1 FT-IR band positions and their corresponding assignments of synthesized pure and thermally treated HAP

Observed band position, cm^{-1}				
HAP at 100°C	HAP(eggshell) treated at			Corresponding assignments
(Prawn shell)	100°C	300°C	600°C	
563	567	567	565	PO_4^{3-} bending
601	603	601	601	
1035	1035	1037	1033	PO_4^{3-} stretching
_	1382	1384	_	CO_3^{2-} stretching
1635	1637	1629	1627	Adsorbed H_2O
_	2358	2360	_	CO_3^{2-} stretching
3441	3425	3442	3421	Structural $OH^-$and adsorbed H_2O
_	_	3564	3568	Structural OH^-

Incorporation of carbonate in HAP may be attributed to the atmospheric CO_2 during the wet chemical synthesis with long maturing time.[11]Decrease in intensity of bands at 3425-3442 and 1629-1637 cm^{-1} with increase in calcination temperature of the product can also be observed in Figure 3.3. This indicates the partial removal of adsorbed H_2O from HAP

surface. FT-IR spectra of synthesized pure HAP illustrate the presence of single HAP phase in the products.

3.3.3 XRD analysis

Phase composition of synthesized pure HAP was determined using X-ray powder diffractometer and Figure 3.4 shows the XRD patterns of the products from eggshell. Broad and merged peaks in Figure 3.4 indicate the amorphous nature i.e. low crystallinity of the synthesized HAP. All HAP samples exhibit XRD patterns that are in good agreement with the XRD pattern for single phase HAP reported by other researchers.[12] The crystallinity of the HAP samples increases with the increase in the calcination temperature of HAP samples and amorphous nature is gradually changed to a well defined crystalline HAP phase (Figure 3.4 a, b, c). XRD pattern of the HAP samples show the typical diffraction peaks with major *d*-spacing values in good agreement with the JCPDS Standard Data (Card no. 09-6439). Strong diffraction peaks at 2θ position 31.68 for reflection plane (211) along with other two peaks at ~32 (112 plane) and at ~33 (300 plane) are of almost equal intensities which confirms the formation of well-crystalline pure HAP.[13]

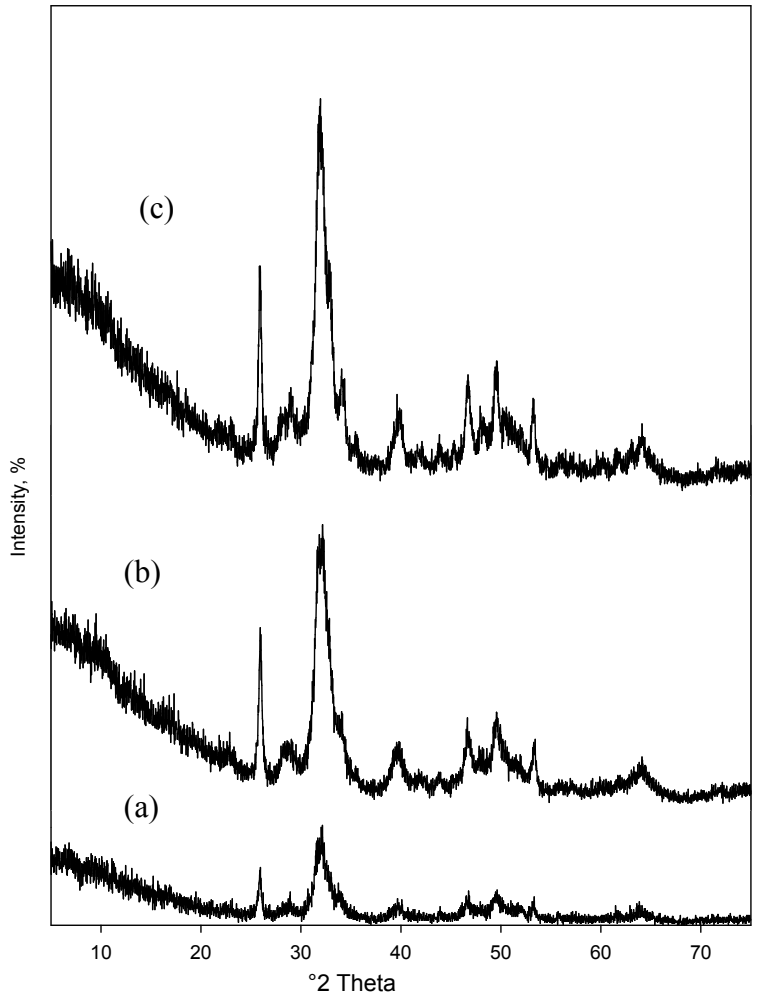

Figure 3.4 XRD patterns of synthesized pure HAP from eggshell (a) dried at 100°C, fired at (b) 300°C and (c) 600°C

The crystallographic parameters of the synthesizedpure HAP were calculated using Equations 2.1-2.3 (Chapter 2). Table 3.3 summarizes the comparison of *d*-spacing values and the corresponding plane with crystallite sizes of the synthesized HAPs and the JCPDS Standard Data. The calculated cell parameters of the HAP samples are also provided in Table 3.3. The Bragg reflectionat (002), (211), (112) and (300) planes of HAPare consideredto calculate the crystallite size. The sizes ofthe crystallites for

ynthesized oven dried and thermally treated pure HAP are in the range of 17-42 nm.Calculated lattice parameters of synthesized pure HAP arecompared with the JCPDS Standard Data in Table 3.3.

Table 3.2 Comparison of *d*-spacing values and the corresponding plane with crystallite sizes and unit cell volume of the synthesized HAPs and the JCPDS Standard Data.

Sample	*d*-spacing (Å)	Intnsity (%)	(h k l)	Crystallite size, nm	Cell parameter, Å	Unit cell volume, $(Å)^3$
JCPDS	4.0777	6.40	2 0 0	-	a = b= 9.42	528.71
	3.4399	35.50	0 0 2		c = 6.88	
	3.0861	14.15	2 1 0			
	2.8131	100	2 1 1			
	2.7776	47.60	1 1 2			
	2.7185	64.20	3 0 0			
	2.6293	21.90	2 0 2			
	2.5282	4.00	3 0 1			
	1.7200	13.70	0 0 4			
HAP at 100°C	3.4368	74.93	0 0 2	17-34	a = b= 9.46	533.21
	3.1613	5.58	2 1 0		c = 6.88	
	2.8253	87.81	2 1 1			
	2.7780	100	1 1 2			
	2.6279	11.05	2 0 2			
	1.7166	16.21	0 0 4			
HAP at 300°C	3.4384	83.70	0 0 2	17-42	a = b= 9.41	527.59
	2.7838	100	2 1 1		c = 6.88	
	1.7203	22.24	0 0 4			
HAP at 600°C	3.4401	65.60	0 0 2	19-42	a = b= 9.42	528.71
	3.0714	9.27	2 1 0		c = 6.88	
	2.8162	100	2 1 1			
	2.7197	44.45	3 0 0			
	2.6178	13.80	2 0 2			
	1.7169	17.45	0 0 4			

3.3.4 SEM analysis

SEM micrographs (Figure 3.5) show the morphology and micro structural features of synthesized pure HAP. Image of HAP dried at 100°C in Figure 3.5(a) shows elongated spheroid shape with particle size 80-120 nm. Presence of large agglomerates of particles is observed for calcined HAP in the Figure 3.5. It is observed from the surface morphology that the particle size as well as agglomeration increases with increase in calcination temperatures of the samples. Effect of temperature on particle size is also observed in the calculated crystallite size from XRD data. Hence tendency of particles to agglomerate at high temperatures and also tendency to increase crystallinity of the sample with increase in temperature is observed in HAP in agreement with literature.[14-15]

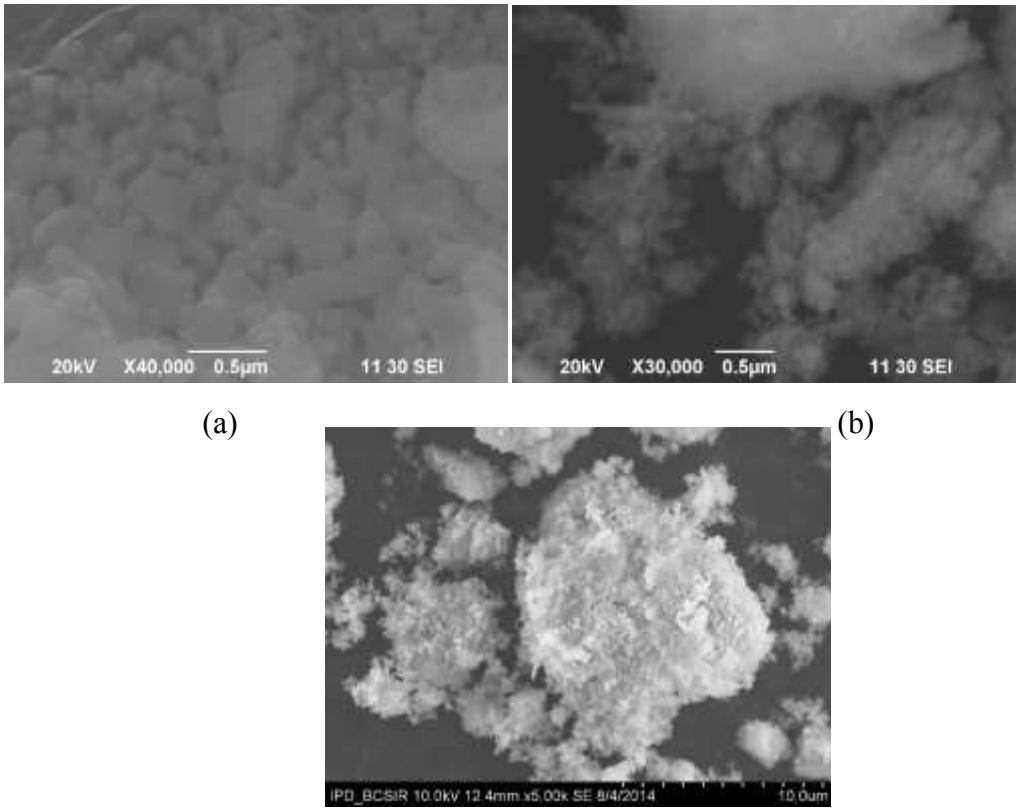

(a) (b)

(c)

Figure 3.5 SEM micrographs of synthesized pure HAP (a) dried at 100°C, fired at (b) 300°C and (c) 600°C

3.3.5 Analysis of surface area

Surface area is an important parameter that determines many physical and chemical properties of solid materials. Specific surface area of a material is an important property for the study of adsorption capacity and for describing pore type of the porous media. Gas adsorption techniques are widely used to characterize the pore structures and surface areas of various materials.

Analysis of nitrogen adsorption behavior of pure HAP

N_2 gas (at 77K) is mostcommonly used for surface area and mesopore characterization. The shape of the isotherm and its hysteresis pattern provide useful information about thephysisorption mechanism, the solid and gas interactions, and can be used to qualitativelypredict the types of pores present in the adsorbent.IUPAC classifiedthe adsorption isotherms into six types (Type I to VI), along with four hysteresis patterntypes (H1 to H4).[16]The different hysteresis patterns H1 to H4 are characteristic of the shapes of different mesopore. A detailed description of the IUPAC isotherm classification is presented in **Chapter1**.

N_2 gas adsorption/desorption isotherms for thermally treated pure HAP are shown in Figure 3.6 (a) and (b). According toIUPACclassification of adsorption isotherms, type IVisotherms typically have a hysteresis loop associated with capillary condensation inmesopores.TheisothermofHAPcalcined at 300°C resembled type IV,suggesting the existence of mesopores.[17] Type V isotherm is observed for HAP calcined at 600°C which also have hysteresis loop indicating the existence of mesopores and micropores. This is also supported by the data obtained from the analysis of BET and BJH plots (Table 3.4). A vertical hysteresis loop in the isotherms for HAP calcined at 300°C and 600°C (Figure 3.4 a and b) in the narrow range of P/P_0(0.90 to 0.99)indicatesthe presence of limited mesopore volumes in the samples, and suggests the presence of cylindricaltype pores.[17]

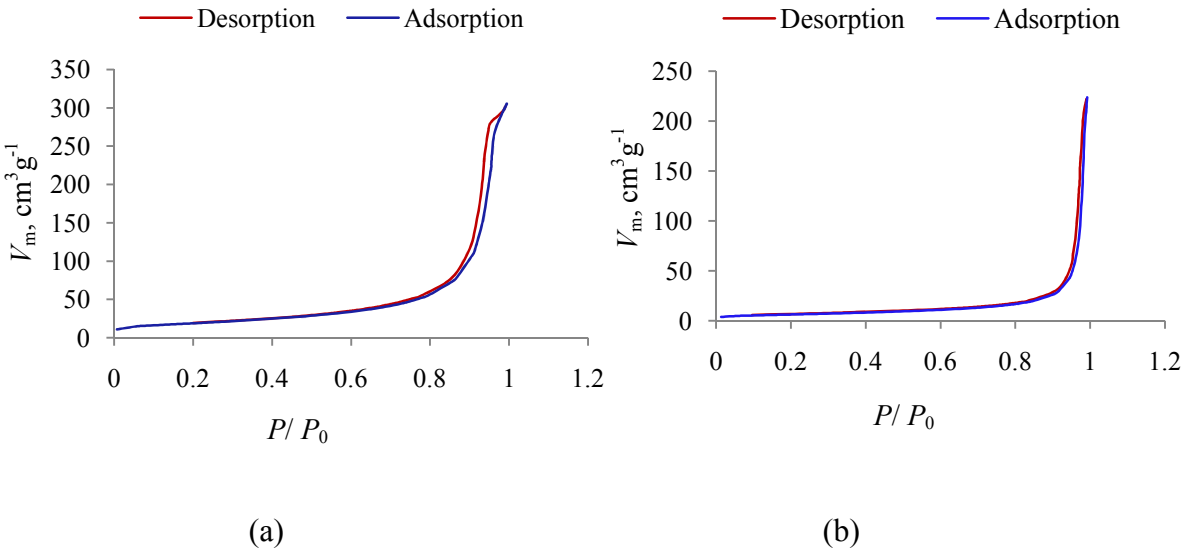

Figure 3.6 Adsorption/ desorption isotherm of pure HAP fired at (a) 300°C and (b) 600°C

Analysis of adsorption data for pure HAP by BET isotherm

Extension of Langmuir's monolayer theory of adsorption to multilayer adsorption theory by Brunauer, Emmett and Teller is known as BET theory. BET analysis of pure HAP was made after thermal treatment of HAP samples and results obtained from the analysis are presented in Table 3.4. Surface area of pure HAP decreases from 66.80 m^2g^{-1} to 22.40 m^2g^{-1} with the increase in calcinations temperature from 300°C to 600°C. This remarkable decrease in surface area may be due to the fact that at 600°C crystals of HAP begins to grow which is also observed in XRD pattern of HAP.

Table 3.3 Data obtained from analysis of BET isotherms and BJH plot for thermally treated pure HAP

Synthesized pure HAP calcined at	BET surface area	BJH total pore volume	BET mean pore diameter	BJH pore radius, nm	BET mean particle size
	m^2g^{-1}	cm^3g^{-1}	nm		nm
300°C	66.80	0.4713	27.85	16.29	28.15
600°C	22.40	0.3436	59.21	29.5	83.97

Moreover, the pore volume decreases from 0.4713 to 0.3436 cm^3g^{-1}while calcination temperatureincreases from 300°C to 600°C, which implies that the shrinkage of HAP occurred during sinteringprocess. Pore size distribution is also an important parameter influencing the adsorption property of HAP. The distributions of pore size at different calcination temperature are shown in Figure 3.7 (a) and (b).

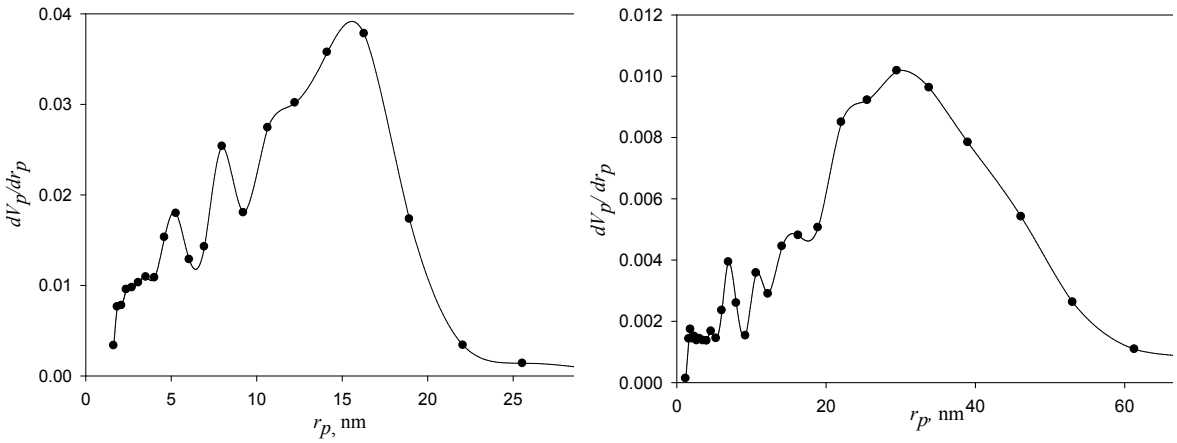

(a) (b)

Figure 3.7 Differential curves of BJH plot of a N_2 adsorption isotherm of pure HAP calcined at (a) 300°C and (b) 600°C

During increase in calcination temperature, agglomeration of HAP is observed in SEM micrographs which can be justified by the determination of particle diameters and pore volumes. Calcination affects the chemical bonds between HAP particles which lead to the formation of agglomeration. Due to increase in temperature voids betweenthe particles become more filled which justifies the decreaseof pore volume of calcined HAP also.[18]

3.3.6 Particle size and its distribution

Dynamiclight scattering(DLS) is an important tool forcharacterizing the size ofparticles inasolution. The hydrodynamic size of the particles and agglomeration of particle can be determined by DLS measurements. If the particles are agglomerated, the DLS measurement can have a high polydispersity index (large variability in the particle size).Particle size distribution of pure HAP is plotted in Figure 3.8 and it is inthe range of 3 to 6μm withaverage particle size 4.15 μm. Agglomeration of the particles may be the reason for obtaining larger particle size and this is also supported by the SEM micrograph of synthesized pure HAP. Moreover DLS measures the hydrodynamic size of the particle, so particle size of HAP may be smaller than that measured by DLS technique.

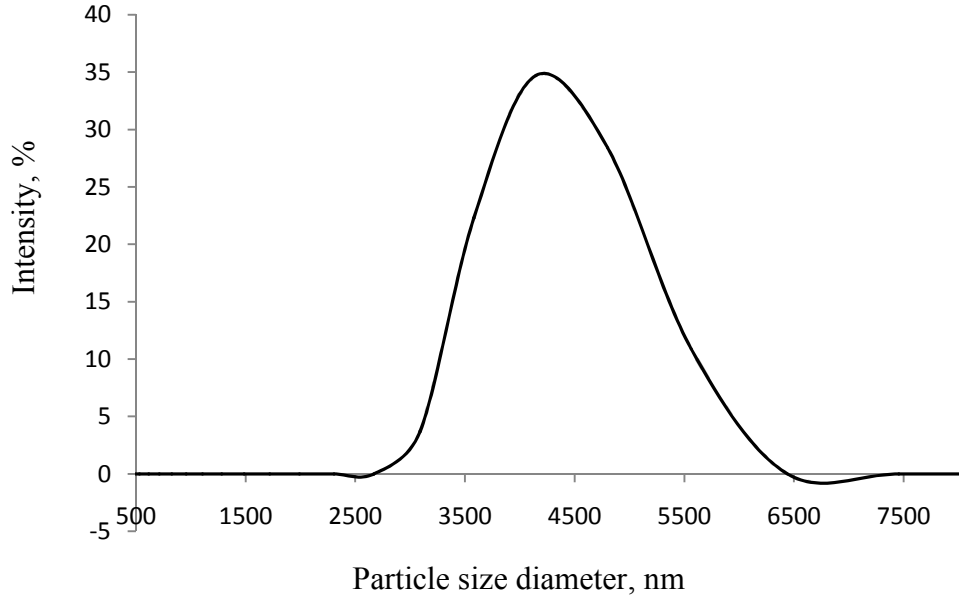

Figure 3.8 Particle size distribution of pure HAP6

3.4 Conclusions

Various methods are available for the synthesis of pure HAP from different calcium and phosphorous sources, of which, wet chemical method is the mostly used technique because it is simple, cheap and easy to apply in the industrial production. In this study, hydroxyapatite could be synthesized by wet chemical reaction using waste materials e.g. eggshells and prawn shells as a calcium source. As prawn shells contain lower percentage of calcium than eggshells, utilization of eggshells was the main concern in the present study. Analysis of the HAP indicates successful synthesis of pure HAP from eggshells.

Crystallinity of the products increases with increase in calcined temperatures and pure HAP calcined at 300°C exhibits higher surface area measured from BET isotherm. XRD pattern also confirm the amorphous phase of the product which also indicates the higher surface area of HAP at 300°C.

It is important that waste material was used to produce a useful value added product with great potential for the removal of heavy metals from aqueous media. Additionally, synthesis of pure HAP from eggshells will create a new dimension in waste management system by both using and reducing the environmental pollution.

References

1. KanedaK., MoriK., HaraT., MizugakiT., EbitaniK., "Design of hydroxyapatite-boundtransition metal catalysts for environmentally-benign organic syntheses", *Cat. Surv. Asia*, **2004**, 8, 231–239.

2. Omar W., Al-Itawi H.,"Removal of Pb^{+2}ions from aqueous solutions by adsorptionon kaolinite clay", *A. J. Appl. Sci*.,**2003**, 7, 498-502.

3. Ramesh S.T., Rameshbabu N., Gandhimathi R., Nidheesh P.V., SrikanthKumar M., "Kinetics and equilibrium studies for the removal of heavy metals in both single andbinarysystems using hydroxyapatite', *Appl. Water Sci*., **2012**, 2, 187-197.

4. Vega E.D., Pedregosa J.C., NardaG.E.,"Interaction of oxovanadium(IV) with crystalline calcium hydroxyapatite: surfacemechanism with no structural modification", *J. Phys. Chem. Solids*., **1999**, 60, 759-766.

5. Krithiga G., Sastry T.P., "Preparation and characterization of anovel bone graft compositecontaining bone ash and egg shell powder",*Bull.Mater.Sci*.,**2011**, 34, 177–181.

6. Trommer R.M., Santos L.A., Bergmann C.P.," Alternative technique for hydroxyapatite coatings", *Surf. Coat. Technol.*, **2007**, 201, 9587-9593.

7. SuchanekW. L., ByrappaK., ShukP., RimanR. E., JanasV. F., TenHuisenK. S., "Preparation of magnesium-substituted hydroxyapatitepowders by the mechanochemical-hydrothermal method," *Biomaterials*,**2004**, 25, 4647-4657.

8. XuG., AksayI. A.,. GrovesJ. T, "Continuous crystalline carbonate apatite thin films.abiomimetic approach," *J. Am. Chem. Soc.,* **2001**,123, 2196-2203.

9. PrabakaranK., RajeswariS., "Development of hydroxyapatite from natural fish bone through heat treatment", *Trends Biomater.Artif. Organ*, **2006**, 20, 20-23.

10. FleetM.E., "Infrared spectra of carbonate apatites:ν_2-region bands",*Biomaterials*, **2009**, 30, 1473–1481.

11. Luna-ZaragozaD., Romero-GuzmanE.T., Reyes-GutierrezL.R., "Surface and physicochemical characterization of phosphates vivianite, $Fe_2(PO_4)_3$ and hydroxyapatite, $Ca_5(PO_4)_3OH$", *J. Miner. Mater.Charact.Eng*., **2009**, 8, 591-609.

12. KoutsopoulosS., "Synthesis and characterization ofhydroxyapatitecrystals: a review study on the analytical methods," *J. Biomed. Mater. Res.*, **2002**, 62, 600-612.

13. Ahmed, S., Ahsan, M., "Synthesis of Ca-hydroxyapatite bioceramic from eggshell and itscharacterization", *Bangladesh J. Sci. Ind. Res.,***2008**, 43, 497-508.

14. Barakat N., Khil M., Omran A., Sheikh F., Kim H.,"Extraction of pure natural hydroxyapatitefrom the bovine bones bio waste by three different methods", *J. Mater. Process. Tech.*,**2009**, 209,3408-3415.

15. Han Y. Li S., Wang X., Jia L., He J.,"Preparation of hydroxyapatite rod-likecrystals by proteinprecursor method",*Mater. Res. Bull.*,**2007**, 42, 1169-1177.

16. SingK., Everett D., Haul R., Moscou L., Peirotti R., Rouquerol J., "IUPAC commission on colloid and surface chemistry including catalysis",*Pure Appl. Chem.*,**1985**, 57,603–619.

17. Ki-Joong Kim, Ho-GeunAhn, "The effect of pore structure of zeolite on the adsorption of VOCs and their desorption properties by microwave heating", *Microporous Mesoporous Mater.,* **2012**,152, 78-83.

18. Khal H.E., Batis N.H., "Effects of temperature on the preparation and characteristics of hydroxyapatite and itsadsorptive properties toward lead", *New J.Chem.*, **2015**, **39**, 3597-3607.

CHAPTER 4

Synthesis and characterization of Fe(III) doped HAPfrom eggshell

4.1 Introduction

Most attractiveproperty for environmental application that HAP possesses is its ability of adsorption of complex organic materials and thecapacity of removal of heavy metals.[1,2]Due to cost effectiveness, HAP has been widely used as the adsorbent for the adsorption of many cationic heavy metals in water andsoils.[3,4] However, doping of HAP increases surface area and porosity of the material which consequently increases the adsorption capacity. Higher adsorption capacity oftheFe-enrichedmaterials was reported due to the strong affinity between heavy metals and iron specifically with arsenic.[5]Keeping this view in mind, this research work is focused on increasing the metal adsorption efficiency of pure HAP by doping with iron.

4.2 Materials and Methods

Eggshell powder (both oven dried and calcined) was used to prepare Ca^{2+} ion precursor solution using HNO_3. Fe(III) doped HAP was synthesized following synthesis procedure of HAP as described in Chapter 3. But in this case, Fe^{3+} ion solution was added to the Ca^{2+} ionsolution prior to the addition of PO_4^{3-} ion precursor. Table 4.1summarizes the quantity of the doping salt used in the synthesis. Schematic diagram of the synthetic process is shown in Chapter 3 (Figure 3.1).

Table 4.1Quantity of Fe(III)-salt used in synthesis of Fe-HAP and sample identification

Sample	Wt % $Fe(NO_3)_3.9H_2O$	Firing temperature, °C	Identification of samples
Pure HAP	0.0	-	-
2%Fe-HAP	2.0	100	2%Fe-HAP1
		300	2%Fe-HAP3
		600	2%Fe-HAP6
4%Fe-HAP	4.0	100	4%Fe-HAP1
		300	4%Fe-HAP3
		600	4%Fe-HAP6
6%Fe-HAP	6.0	100	6%Fe-HAP1
		300	6%Fe-HAP3
		600	6%Fe-HAP6

Fe-HAP was a brownish yellow solid. These were then oven dried at 100°C and calcined at 300°C and 600°C. For each calcination 30 min soaking time was maintained while heating rate was 3°Cmin^{-1}. Synthesized products are named according to wt% of Fe(III) used in the process. Thermally treated Fe-HAP samples are labeled on the basis of the temperature selected for calcination as the affix of the temperatures in hundred (Table 4.1).

4.3 Characterization of Fe-HAP

Thermally treated Fe-HAPs were characterized using EDS, XRD, FT-IR, SEM, DLS particle size analyzer, BET surface area analyzer techniques.

4.3.1Elemental analysis

EDS was used for the elemental analysis of synthesized Fe-HAP. The presence of Fe along with Ca, P and O is clearly evident in the EDS spectrum in Figure 4.1. This indicates possible doping of Fe in the HAP as expected.The(Ca+Fe)/Pratio of the sample is calculated as 1.67 which is similar to that ratio in human bones.[6] Stoichiometry of Ca/P ratio of the sample implies possible substitution of Ca by Fe in HAP structure.

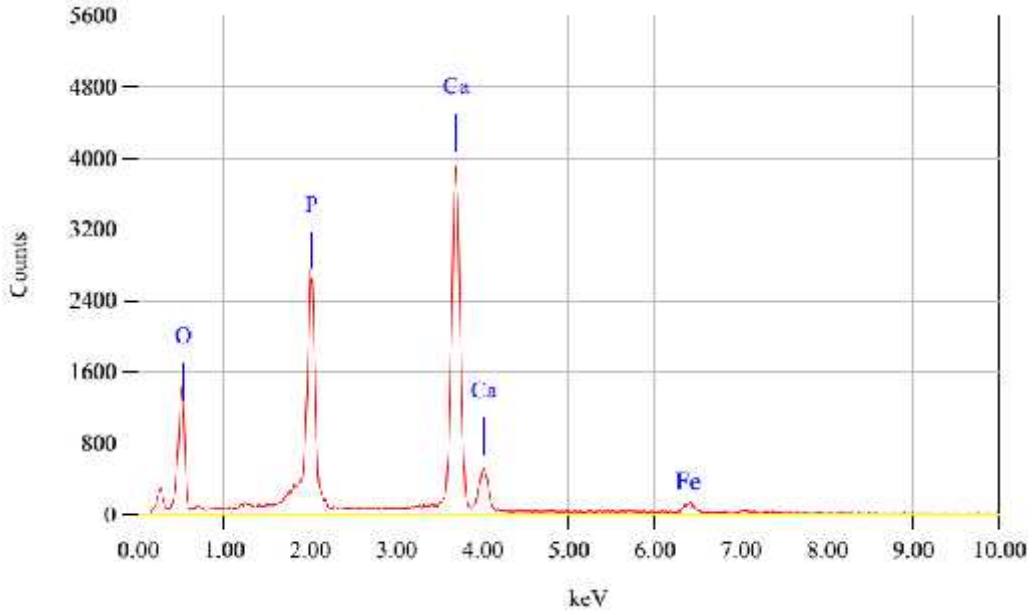

Figure 4.1 EDS spectrum of Fe-HAP from eggshell

4.3.2 FT-IR analysis

FT-IR analysis provides the nature of chemical bonds present in the material under analysis, i.e. functional groups are determined. Fe-HAP samples (oven dried and thermally treated) containing different wt% of Fe(III) were characterized by FT-IR technique. Corresponding spectra are shown in Figures4.2 and 4.3. For clarity, the scales selected in spectra maintained identical. The presence of doublet at around 603and ~560 $cm^{-1}$are attributed to the O-P-O bending mode $v_4$of phosphate group (PO_4^{3-}) andasymmetric stretching mode v_3 of PO_4^{3-} group characterized by a strong, complex band in 1000–1150 cm^{-1}regionwhich are clearly shown in both Figures4.2 and 4.3.[7-10] The broad vibration band in the range 3000-3650 cm^{-1} and small peak at 1630 cm^{-1} are

observed due to the presence of O-H and absorbed water on the Fe-HAP surface. Stretching vibration for structural OH group is mostly masked by the broad H_2O absorptionandis observed as ashoulder at 3570 cm^{-1}.[11] Band appearing at ~2360 cm^{-1} corresponds to the presence of CO_3^{2-} incorporated from the atmospheric CO_2 which was introduced during the prolonged wet chemical synthesis for precipitation of HAP.[12]

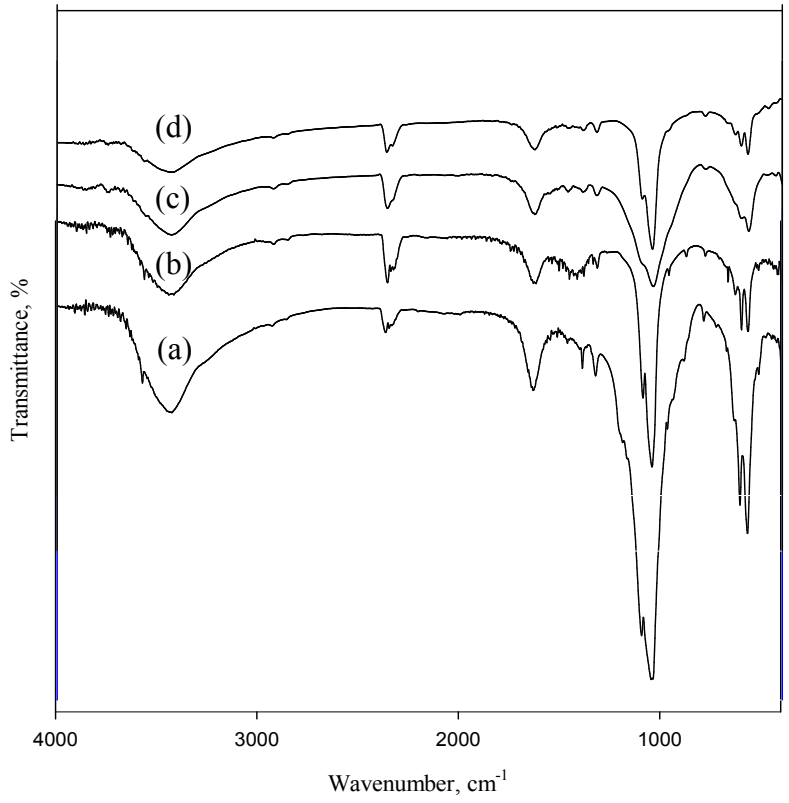

Figure 4.2 FT-IR spectra of Fe-HAP from eggshell containing (a) 0, (b) 2, (c) 4 and (d) 6 wt% Fe

A very weak doublet at about ~1500 and ~1450 cm^{-1} and a singlet at ~876cm^{-1} are assigned to ν_3 asymmetric stretch vibration and ν_2 out-of-plane bendvibration of B-type CO_3^{2-} substitution in pure HAP.[13]This is clearly shown in Figure 4.4 in which spectra are presented for finger print region (400-1500 cm^{-1}) only.

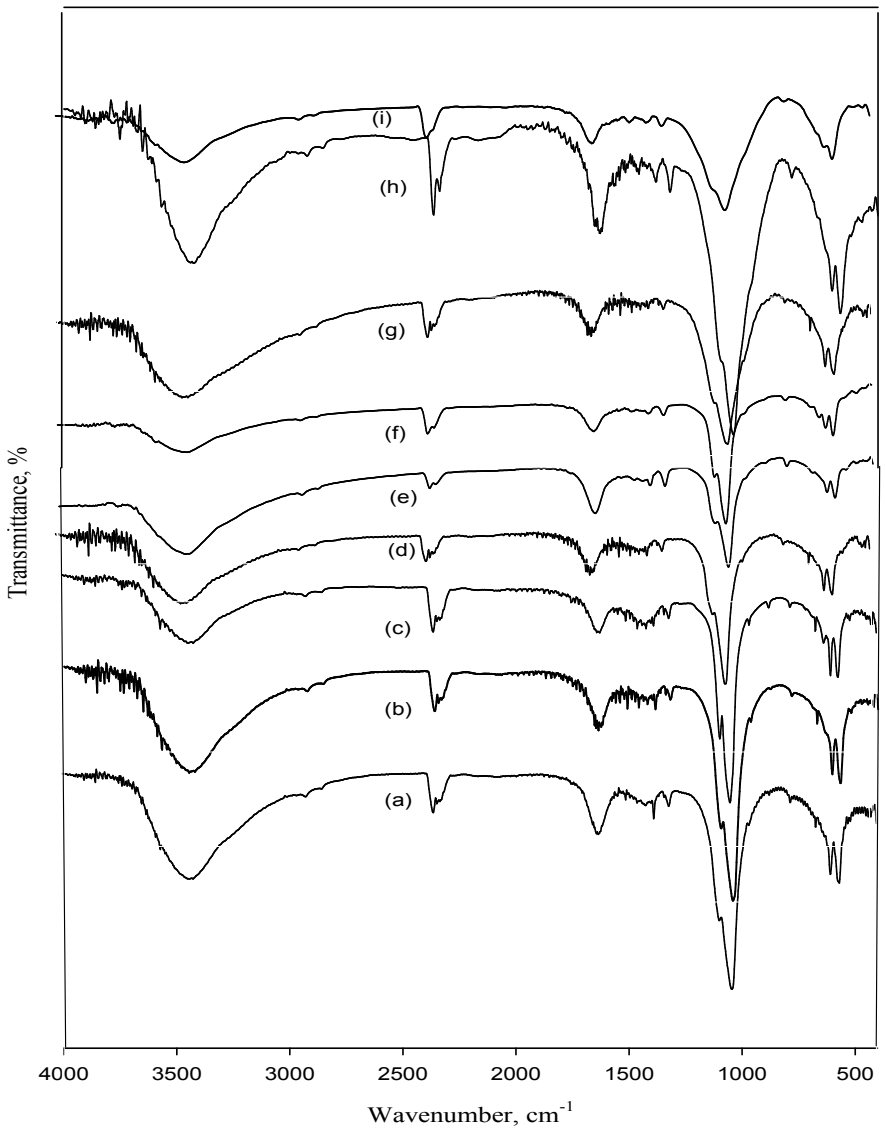

Figure 4.3 FT-IR spectra of 2%Fe-HAP treated at (a) 100°C, (b) 300°C (c) 600°C, 4%Fe-HAP treated at (d)100°C,(e) 300°C, (f) 600°C, 6%Fe-HAP treated at g) 100°C, (h) 300°C and (i) 600°C

Presence of the smaller shoulder at ~670 cm^{-1} in all the spectra is due to the substitution of hydroxyl ions by carbonate ions. Presence of carbonate ions is responsible to promote incorporation of the cation in the doped HAP.[14]

The intensity of bending and stretching vibration bands at 1630 and ~3440 cm^{-1} (Figures 4.2 and 4.3) for theH–O–H,decreases with increase in calcination temperature. However positions of vibration bands characteristics for phosphate group in HAP structure remain unchanged in Fe-HAP. This can be attributed to the fact that thermal treatment of Fe-HAP does not make any change to the HAP phase in the samples. The width of the broadband assigned forasymmetric stretching mode v_3 of PO_4^{3-} groupin the range 1150-950 cm^{-1} increases with increase of iron content in Fe-Hap. This can be explained by the structural deformation of Fe-HAP with increase in Fe content in the samples. XRD patterns of the samples also support this feature. The main absorption band positions and their assignments for Fe-HAP are summarized in Table 4.2.

Table 4 .2 Major absorption band positions and their assignments of different wt% of Fe-HAP treated at different temperatures

Observed band position, cm^{-1}									Corresponding assignments
2 wt%Fe-HAP			4 wt%Fe-HAP			6 wt%Fe-HAP			
100 °C	300 °C	600 °C	100 °C	300 °C	600 °C	100 °C	300 °C	600 °C	
569	569	570	565	567	565	560	564	565	
603	603	603	603	602	603	601	602	602	PO_4^{3-} bending
–	–	630	–	–	632	–	–	–	Structural OH
1039	1041	1047	1038	1040	1045	1033	1039	1040	PO_4^{3-} stretching
1384	1386	1392	1382	1419	1390	1382	1382	1463	CO_3^{2-} stretching
1631	1627	1627	1637	1628	1622	1620	1622	1625	H_2O adsorbed
2362	2362	2362	2360	2361	2360	2360	2366	2358	CO_3^{2-}stretching
3435	3425	3441	3440	3439	3430	3420	3440	3431	H_2O adsorbed
–	–	3558	–	–	3565	–	–	3560	Structural OH^-

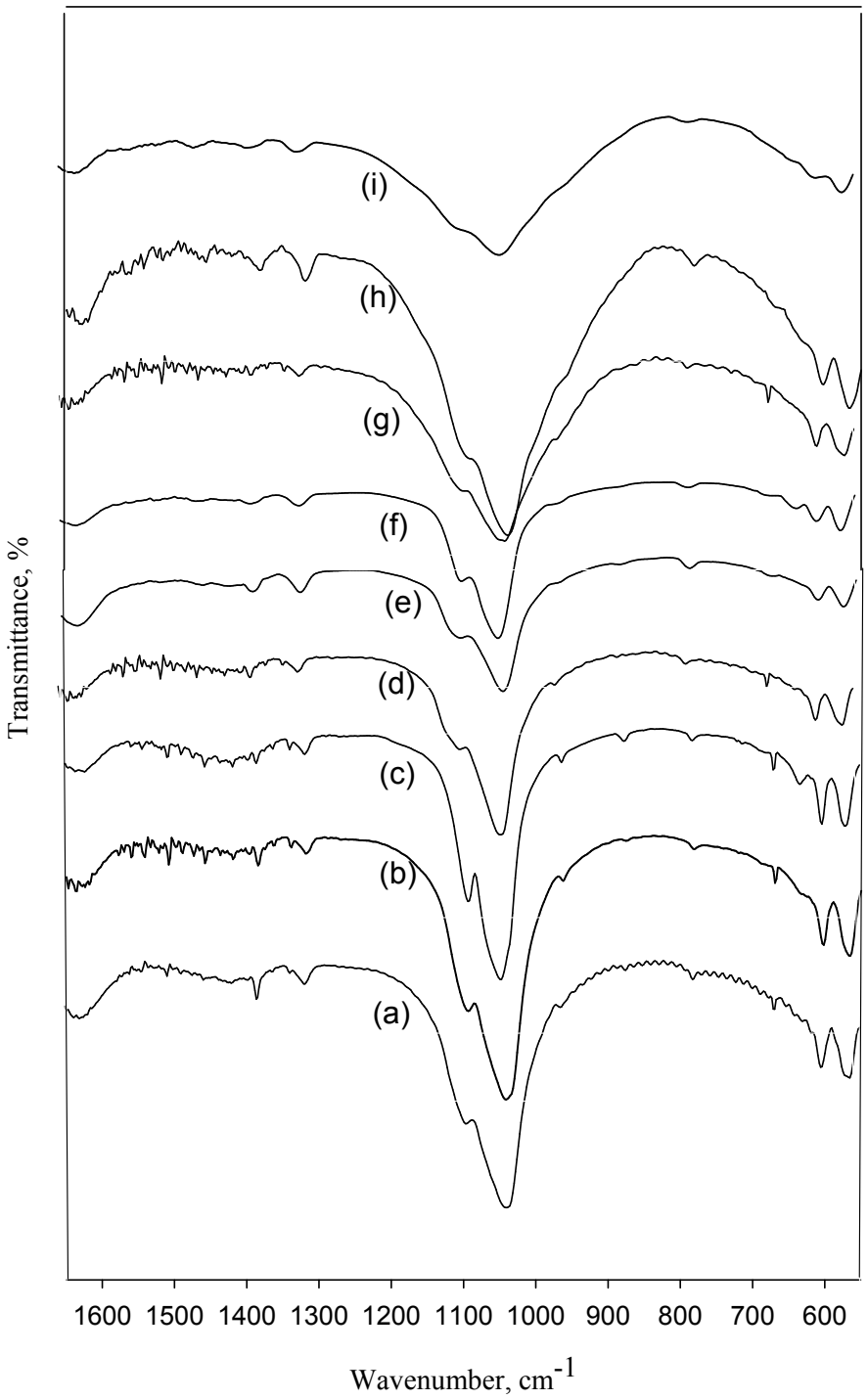

Figure 4.4 Finger print region FT-IR spectra of 2%Fe-HAP treated at (a) 100°C, (b) 300°C (c) 600°C, 4%Fe-HAP treated at (d)100°C, (e) 300°C, (f) 600°C, 6%Fe-HAP treated at (g) 100°C, (h) 300°C and (i) 600°C

As Fe^{3+} ion substitutes both the calcium sites, the vibration peaks for PO_4^{3-} group in the finger print region are gradually merged into a broadpeak with the increase in Fe^{3+} ion content in Fe-HAP. Broadening of vibration band for phosphate group indicates substitution of Ca-I by Fe^{3+} ion.[15]Much broader vibration band in the range 1150-950 $cm^{-1}$for 6% Fe-HAP calcined at 600° C (Figure 4.4i) indicates the structural distortion in the HAP phase. Simultaneous decrease in band intensity at 3435 cm^{-1} and gradual diminishing of band for structural OH at 3558 cm^{-1} indicates substitution of Ca-II site by Fe^{3+} ion.[16]This feature is also supported by the XRD patterns of the samples.

4.3.3 XRD analysis

XRD method was used for the phase identification of samples under investigation and Figures 4.5 and 4.6 show the XRD patterns of synthesized pure and Fe-HAP. Strong diffraction peaks at 2θ position 31.92 for reflection plane (211) along with other two peaks at 2θ positions ~32.34 (112 plane) and at ~32.84 (300 plane) are of almost equal intensities which confirm the formation of well-crystalline Fe-HAP.[17]The peaks are in good agreement with ICSD File No. 26204 which correspond to hexagonal HAP and all of the patterns showedin the Figure 4.6reveal single phase inFe-HAP structure. Figure 4.6 does not show any significant change in peak positions, but intensity of peaks decreases with the increase of Fe content in Fe-HAP. As a result, amorphous nature of Fe-HAP increases with increase of Fe content in the samples. This justifies that ionic radius of Fe(III) (0.64 Å) is smaller than that of Ca(II) (0.99 Å) which induces strain on HAP crystal lattice, thus the crystallinity of the samples are decreased.[18]The crystallographic parameters of the synthesizedpure HAP are calculated using Equations 2.1-2.3 (Chapter 2). Lattice parameters along with major peak positions of HAP phase calculated from XRD data are summarized in Table 4.3. The Bragg reflectionat (002), (211), (112) and (300) planes of Fe-HAPare consideredto calculate the crystallite size using Scherrer equation (Eq.2.1). The sizes ofthe crystallites for oven dried and thermally treated Fe-HAP are in the range of 14-19 nm. Crystallite size of Fe-HAP is much smaller than that of pure HAP, which demonstrates similar effect for Fe doping in HAP structure as mentioned in literature.[19]

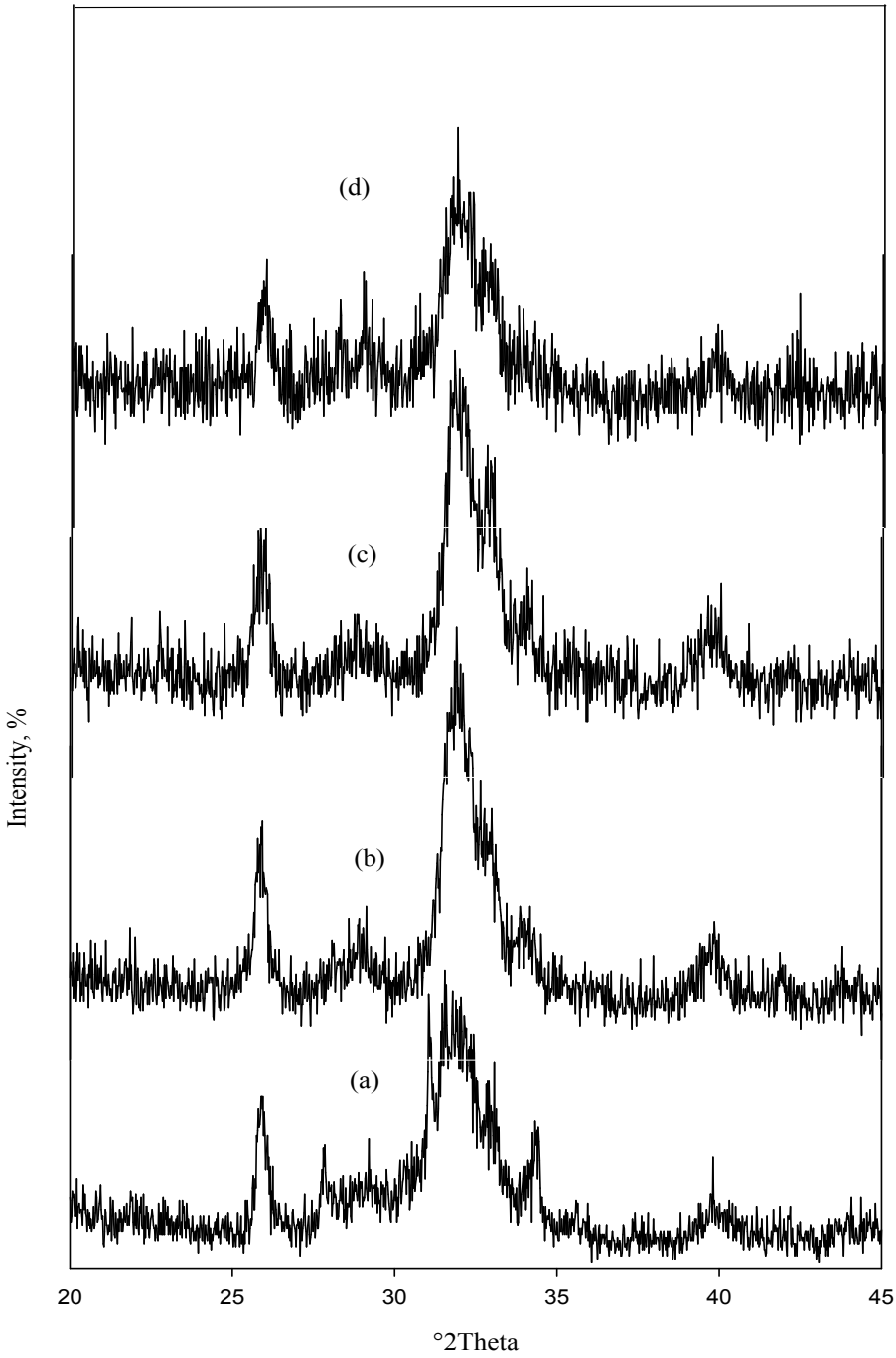

Figure 4.5 XRD patterns of synthesized Fe-HAP calcined at 600°C containing (a) 0%, (b) 2%, (c) 4% and (d) 6% Fe.

Table 4.3 Comparison of *d*-spacing values and the corresponding plane with crystallite sizes and unit cell volume of the synthesized Fe-HAPs and the JCPDS Standard Data.

Sample		*d*-spacing (Å)	Position (2θ)	(h k l)	Crystallite size, nm	Cell parameter, Å	Unit cell volume, $(Å)^3$
JCPDS		3.4399 2.8131 2.7776 2.7185 1.7200		0 0 2 2 1 1 1 1 2 3 0 0 0 0 4	-	a= b= 9.42 c = 6.88	528.71
2%Fe-HAP at	100°C	3.4354 2.8258	25.87 31.92	0 0 2 2 1 1	14.02	a=b=9.47 c =6.87	535.82
	300°C	3.4359 2.7809	25.93 32.19	0 0 2 2 1 1	14.65	a = b=9.40 c = 6.87	525.71
	600°C	3.4445 2.8027 2.7126	25.87 31.93 33.02	0 0 2 2 1 1 3 0 0	18.55	a= b= 9.39 c = 6.89	526.12
4%Fe-HAP at	100°C	3.4355 2.7967 1.7197	25.94 32.00 53.27	0 0 2 2 1 1 0 0 4	16.05	a= b= 9.45 c = 6.87	531.31
	300°C	3.4341 2.2707	25.95 39.69	0 0 2 1 3 0	17.55	a= b= 9.45 c = 6.87	531.31
	600°C	3.4433 2.8126 2.7252	25.88 31.82 32.87	0 0 2 2 1 1 3 0 0	15.95	a= b= 9.39 c = 6.89	526.12
6%Fe-HAP at	100°C	3.4330 2.8067	25.95 31.89	0 0 2 2 1 1	16.62	a= b= 9.47 c = 6.87	533.56
	300°C	3.4326 2.7913	25.96 32.07	0 0 2 2 1 1	13.40	a= b= 9.47 c = 6.87	533.56
	600°C	3.4435 2.8035	25.87 31.92	0 0 2 2 1 1	18.23	a=b= 9.42 c = 6.89	531.73

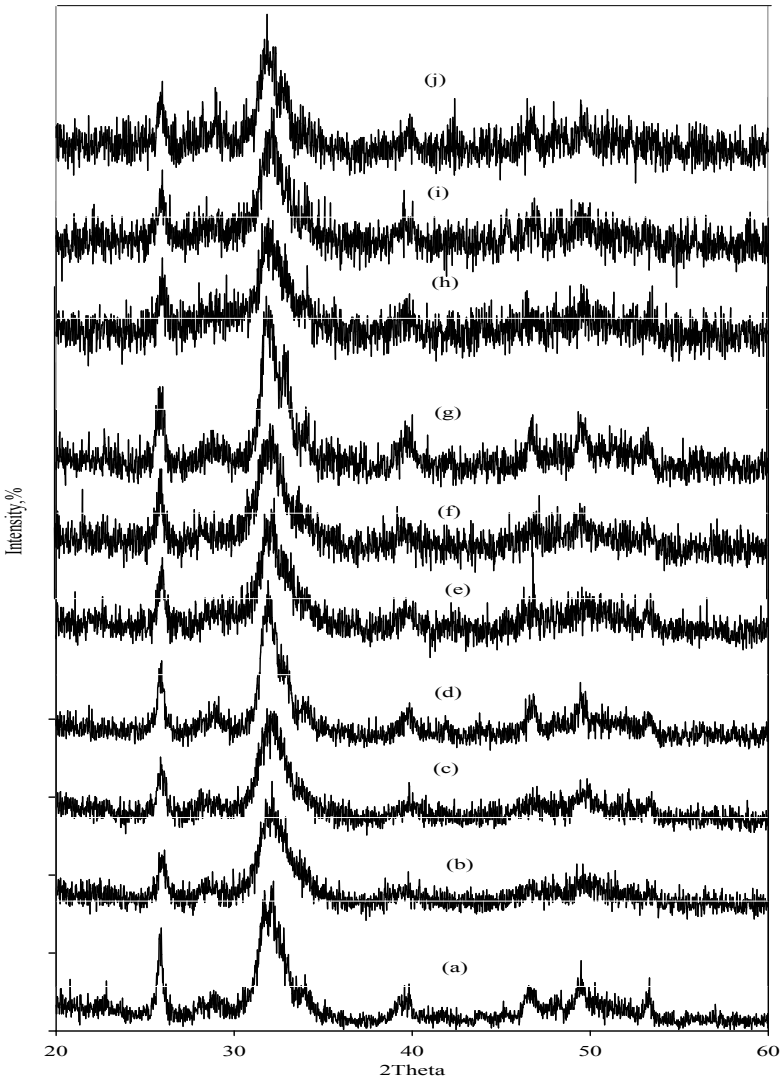

Figure 4.6 XRD patterns of synthesized of (a) pure HAP treated at 100°C; 2%Fe-HAP treated at (b) 100°C, (c) 300°C, (d) 600°C; 4%Fe-HAP treated at (e) 100°C, (f) 300°C, (g) 600°C; 6%Fe-HAP treated at (h) 100°C, (i) 300°C, (j) 600°C

Effects of Fe content and calcination temperatures on Fe-HAP are summarized in Table 4.3. In the unit cell of HAP crystal there are ten sites occupied by calcium ions; four of them denoted as Ca-I, form channelsparallel to the c-axis(Site I), and the remaining six, named Ca-II (Site II), arelocated around hydroxyl channels and form calcium triangles. Cations larger than Ca^{2+} ion couldoccupy calcium type (II) sites in the apatite lattice,

whereas smaller cations preferred calcium type (I) sites.[20,21] Though Fe^{3+}(0.64 Å) is smaller than Ca^{2+} (0.99 Å),Ca-II site is the preferred location forFe^{3+}ion at low concentration, moreover, there ispartial substitution into Ca-I site when concentration of Fe^{3+} ion is higher.[22]Incorporation of ferric (Fe^{3+}) iron into HAP requires insertion of counter ions, usually incorporation of carbonate ions from environmental CO_2 is observed.It is established that incorporation of CO_3^{2-} ions in the hexagonal channel of apatite structure (A-type) causes an expansion along *a*-axis and a contraction along *c*-axis in HAP crystal, whereas the condition is reverse in case of a partial substitution of PO_4^{3-} by smaller CO_3^{2-} ions (B-type).[23] In case of mixed AB-type substitution, part of the CO_3^{2-} ions are placed in the channels, while part ofthe CO_3^{2-}ions replace PO_4^{3-}ions and hence cell parameters also change in both directions, but the changes in parameter *c* are much less than in parameter *a*.[24] For oven dried Fe-HAP cell parameter *a* increases and *c* decreases, which indicates A type substitution in HAP structure. While thermally treated Fe-HAP show decrease in both parameter *a* and*c* for 2%Fe-HAP that indicates both A and B type substitution. Again both cell parameters *a* and*c* increase for calcined 4% and 6%Fe-HAP, this fluctuation also indicates A and B type substitution. So in case of Fe-HAP forboth oven dried and calcined samples, substitution can occur in both the calcium type I and II sites, which is evident by the fluctuation in cell parameter values. Structural distortion in HAP phase in 6%Fe-HAP can be explained by decrease in intensity of peak for (0 0 2) plane which is due to saturation of HAP lattice with Fe^{3+} ions. This is also observed in FT-IR spectrum of 6%Fe-HAP in Figure 4.4 (i). Cell parameter and unit cell volume for both 2% and 4%Fe-HAP are similar which indicates substitution of Ca^{2+} by Fe^{3+} is similar in these samples. This fact is also confirmed by specific surface areaof the samples measured by BET analysis (*Vide infra*).

4.3.4 SEM analysis

SEM technique was used to study the microstructure of Fe-HAP. The micrographs of thermally treated pure HAP and Fe-HAP are shown in Figure 4.7. From the micrographs, agglomeration of the particles is clearly observed which is attributed to the fact that thermal treatment of the samples resulted in an agglomeration of the smaller particles of Fe-HAP.

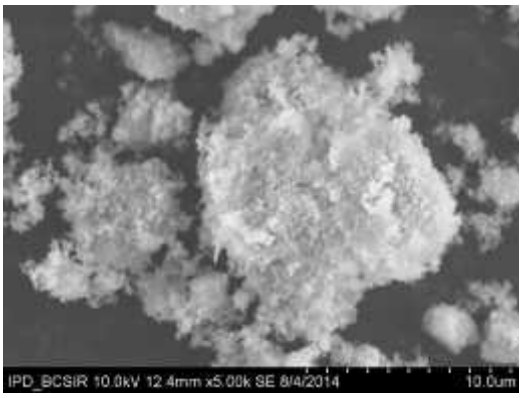

(a)

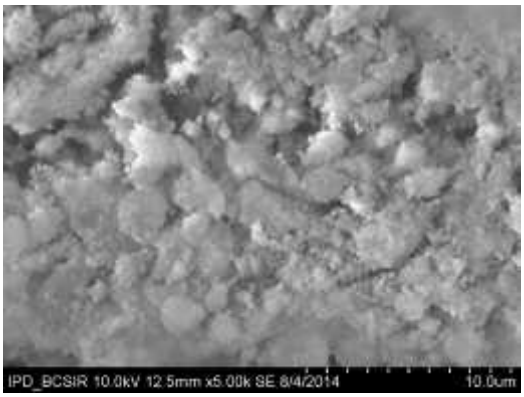

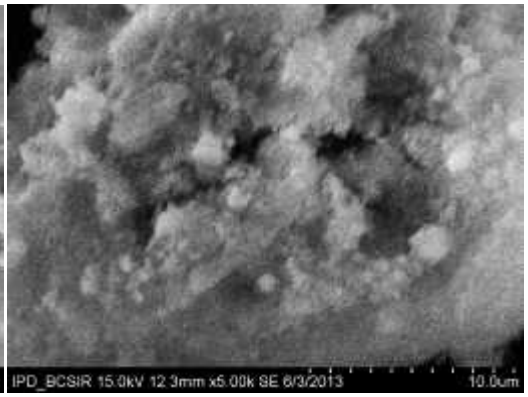

(b) **(c)**

Figure 4.7 SEM micrographs of synthesized Fe(III)-HAP calcined at 600°C containing (a) 0 wt% , (b) 2 wt% and(c) 4 wt% Fe(III)

4.3.5 Analysis of surface area

Specific surface area is one of the most important physical property which controls the adsorption efficiency of a material. Hence it was necessary to determine surface area of all the synthesized samples prior to their application as adsorbent. Gas adsorption technique was used to characterize pore structures and specific surface areas of synthesized Fe-HAP samples.

Analysis of nitrogen adsorption behavior of Fe-HAP

For determination of surface area and total pore volume of Cu-HAP N_2 gas (at 77K) is usually used in the experiment. Type of the isotherm and its hysteresis patterns are discussed in Chapter 1.

Figure 4.8 shows N_2 gas adsorption/desorption isotherms for thermally treated Fe-HAPsamples.As shown in Figure 4.8, type IV isotherm is observed with a hysteresis loop for 2% Fe-HAP calcined at 300°C and type V isotherms with hysteresis are observed for 4%Fe-HAP calcined at 300°C and also for 6%Fe-HAP calcined at 300°C and 600°C. Hysteresis loops in the isotherms indicate that the adsorption and desorption isotherms do not coincideover a certain region of external pressures.Type IV isotherm is associated with capillary condensation and evaporation taking place in mesopores. At lower relative pressure ($P/P_0 <$ 0.4) the isotherm profile is similar to Type II isotherm which indicatesformation of an adsorbate monolayer on the pore surface and then followed by multilayer formation.Generally, hysteresis loops of type H2 are believed as a consequence of interconnectivity of the pores, where both, pore blocking and percolation phenomena may contribute to the observed asymmetry of the hysteresis loop.[25] Figure 4.8(a) for 2%Fe-HAP3 exhibits H2-type hysteresis and indicate interconnected pore structure with narrow pore openings.Type V isothermsare observed in Figure 4.8(b),(c) and (d) for 4% and 6% Fe-HAPcalcined at 300°C and 600°C which also have hysteresis loop and indicate the existence of mesopores and micropores.Verticalhysteresisloops of H1 type in Figure 4.8 (b), (c) and (d) indicate a narrow distribution of cylindrical or tubular pores.

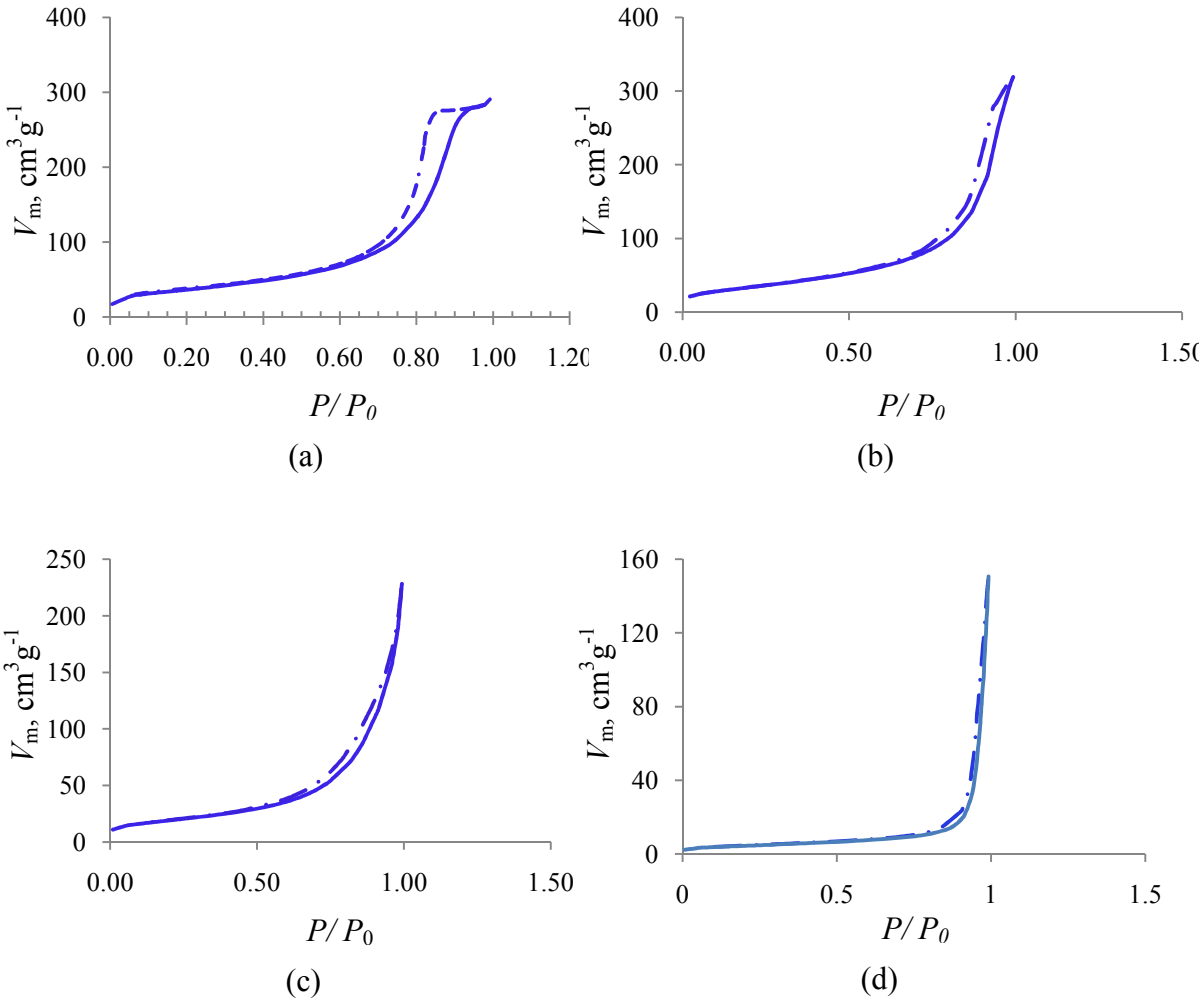

Figure 4.8 Adsorption/ desorption isotherm of (a) 2% (b) 4% (c) 6% Fe-HAP calcined at 300°C and (d) 6%Fe-HAP calcined at 600°C

Analysis of adsorption data for Fe-HAP by BET isotherm

The data obtained for specific surface areaby BET method, pore diameter and pore volume of thermally treated Fe-HAP are given in Table 4.4. All the parameters are strongly influenced by doping quantity and calcination temperatures. Specific surface area of Fe-HAP treated at 600°C decreases with decrease in total pore volume which is also observed in BJH plot in Figure 4.9.

Doping of 2wt% Fe(III) in pure HAP raises surface area significantly when it is calcined at 300°C and surface area decreases with increase in Fe content from 4% to 6%

(Table4.4). Effect of doping of Fe(III) is also observed in particle size of the samples analyzed by BET isotherm (Table 4.4). This implies that substitution of Ca^{2+} ion with Fe^{3+} ion in Fe-HAP is significant for 2% and 4%Fe-HAP. However, internal surface area and pore volume of Fe-HAP are occupied with Fe^{3+} ions as iron content increases from 2 wt% to 6 wt%, which cause reduction in surface area and total pore volume of the products. This fact is also supported by BJH plot (Figure 4.9) of the samples.

Table 4.4 Data obtained from analysis of BET isotherms and BJH plot for Fe-HAP

Sample		BET surface area m^2g^{-1}	BJH total pore volume cm^3g^{-1}	BET mean pore diameter nm	BJH pore radius, nm	BET mean particle size nm
HAP calcined at 300°C		66.80	0.4713	27.85	16.29	28.15
Fe-HAP Calcined at 300°C	2%	122.09	0.4519	14.67	6.06	15.55
	4%	122.29	0.4771	16.01	6.04	15.53
	6%	68.25	0.3473	19.74	4.03	27.82
6% Fe-HAP calcined at 600°C		16.00	0.2304	56.10	18.94	118.68

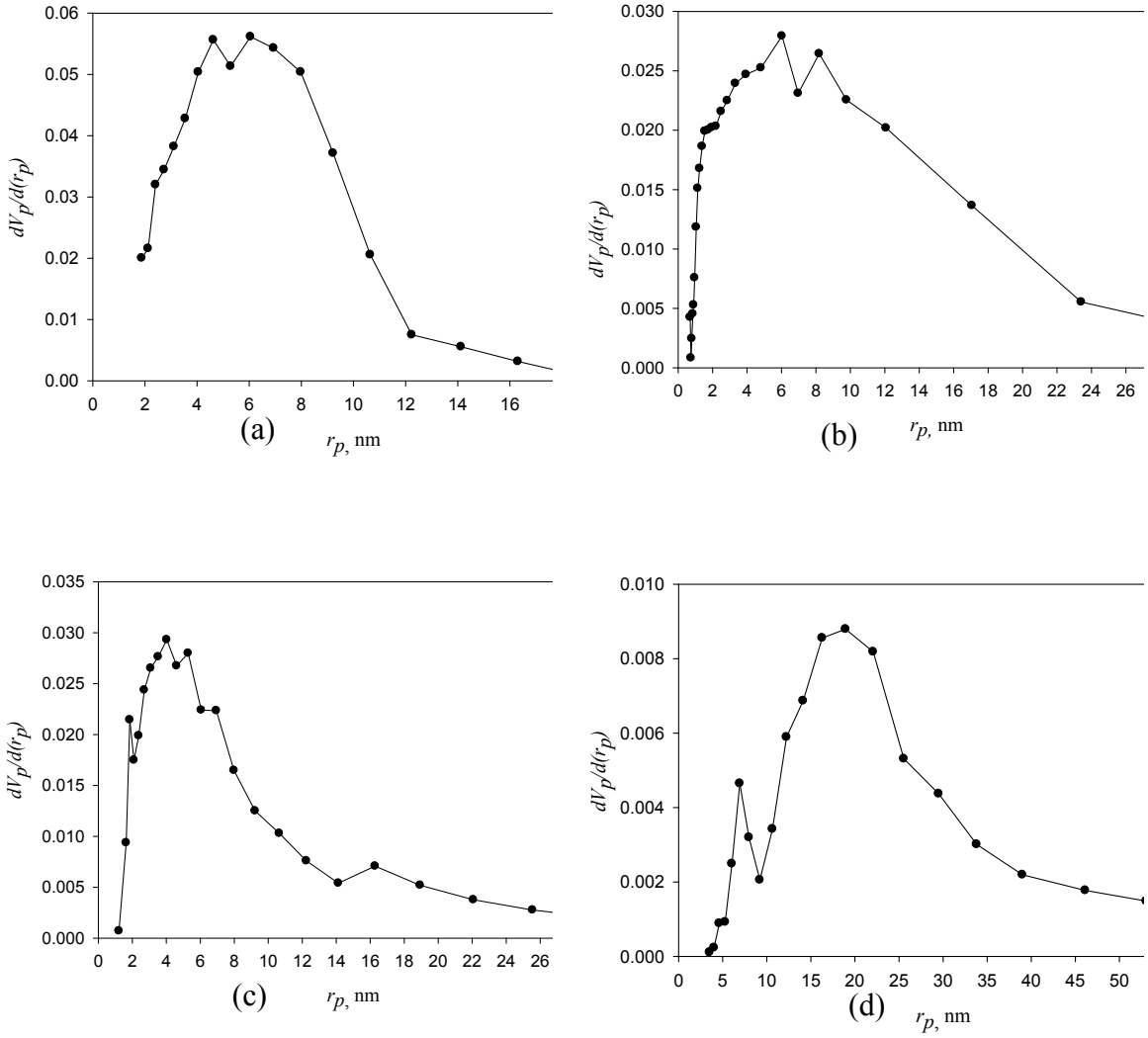

Figure 4.9 Differential curves of BJH plot of a N_2 adsorption isotherm of Fe-HAP samplescalcined at 300°C containing (a) 2%, (b) 4%, (c) 6%Fe and(d) 6%Fe-HAP calcined at 600°C

It is remarkable that total pore volume and specific surface area for Fe-HAP samples decrease with increase in the calcination temperature from 300˚C to 600˚Cdue to increasing particle size and degree of agglomeration in the materials. Specific surface area of 2%Fe-HAP calcined at 300˚C increases in comparison to pristine HAP from 66.80 m^2g^{-1} to 122.09m^2g^{-1}. Corresponding total pore volume does not increase significantly, that implies the formation of smaller particle size due to doping of Fe(III) in

HAP. Moreover, decrease in specific surface area and total pore volume of 6%Fe-HAP is significant whilst increase in calcinations temperature of the sample is made from 300˚C to 600˚C.

4.3.6 Particle size and its distribution

Particle size analysis of Fe-HAP powder was performed using dynamic light scattering technique.The particle size distribution is shown in Figure 4.10.The average particle size of Fe-HAP is 0.95μm which is smaller than that of pure HAP (4.15 μm) as expected. Decrease in crystallite sizes of HAP and Fe-HAP calculated from XRD patterns (Table 4.3) also show the influence of strain in lattice parameter due to the incorporation of Fe(III) in HAP.

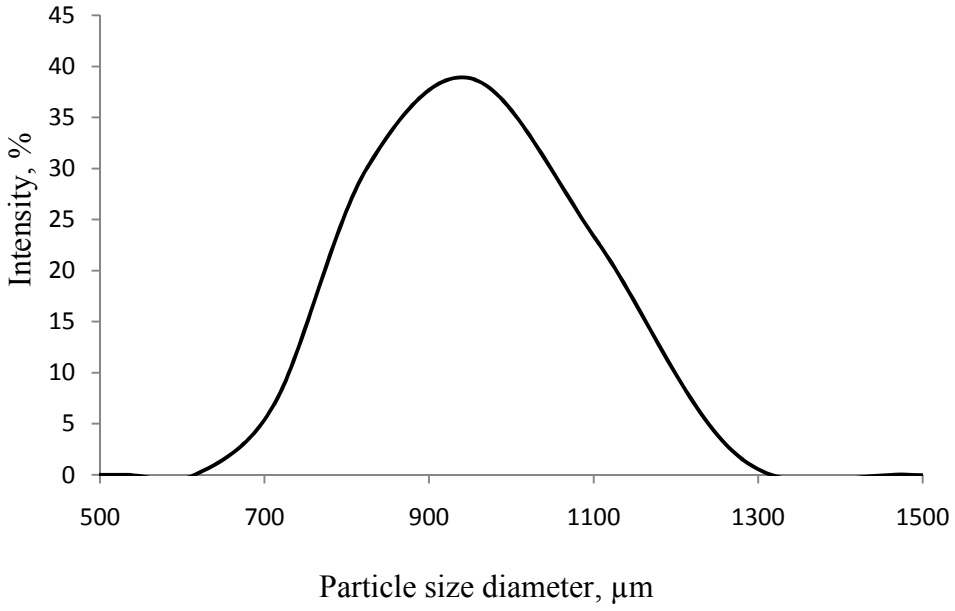

Figure 4.10 Particle size distribution of 2%Fe-HAP6

4.4 Conclusions

Fe-HAPs with different Fe content would be synthesized from waste material following wet chemical method. Characterization of Fe-HAP was carried out using FT-IR, XRD,

SEM, EDS, particle size analysis and BET surface area analysis methods. Presence of both A and B type carbonate substitution along with substitution of Ca^{2+} ion with Fe^{3+} ion was observed.This feature is also supported by values of cell parameter *a* and*c* from XRD pattern for a hexagonal system. Doping of Fe^{3+} into HAP powders greatly influence the crystallinity ina trend that the crystallinity decrease with increase in Fe content in the samples. Formation of smaller particles resulted from doping of HAP with Fe(III) is evident from DLS particle size analysis along with SEM and XRD analysis. BET analysis reveals increase of specific surface area of Fe-HAP in comparison to pure HAP (Table 4.4). Highest specific surface area was measured for 2% and 4% Fe-HAP calcined at 300°C. Effect of calcinations temperature played an important role in controlling specific surface area along with pore size of the materials. As a consequence, pure HAP and Fe-HAP calcined at 300°C can be used as adsorbents in preference to the HAP and Fe-HAP those are oven dried and calcined at 600°C. Samples treated at 300°C also preserve a single phase HAP crystal along with higher specific surface area and total pore volume. So it can be concluded that Fe-HAPs are successfully synthesized from waste material which can be used as adsorbent for the removal of heavy metals from aqueous system.

References

1. Corami A., Mignardi S., Ferrini V., "Cadmium removalfrom single- and multi-metal (Cd^{2+}, Pb^{2+}, Zn^{2+}, Cu^{2+}) solutionsby sorption on hydroxyapatite,"*J. Colloid. Interf.Sci.*, **2008**, 317, 402–408.
2. Barabas R., Pop A.,Bogya E.S.,Dejeu V.,"Synthesisandproperties of intelligent biomaterials. In 4th edition of theNational Symposium of Biomaterials,"*Biomater. Med. Surg. Appl.*, **2007**, 18-20, 1-12.
3. Ramesh S.T., Rameshbabu N., Gandhimathi R., Srikanth Kumar M., NidheeshP.V., "Adsorptiveremoval of Pb(II) from aqueous solution using nano-sized hydroxyapatite," *Appl. Water Sci.*, **2013**, 3, 105–113.
4. Liao D., Zheng W., Yang Q., Yue X., Guo L., Zeng G.,"Removal of lead(II) from aqueoussolutions using carbonate hydroxyapatite extracted from eggshell waste," *J. Hazard.Mater.*,**2010**, 177, 126–130.

5. Oliveira L.K., Melo C.A., Goveia D., Lobo F.A., Hernández M.A.A., Fraceto L.F., Rosa A.H., "Adsorption/desorption of arsenic by tropical peat:influence of organic matter, iron and aluminium", *Environ. Technol.*,**2015**, 36, 149-159.
6. TrommerR.M., Santos L.A., Bergmann C.P.,"Alternative technique forhydroxyapatite coatings", *Surf. Coat. Technol.*, **2007**, 201, 9587–9593.
7. PrakashK. H., OoiC. P., KumarR., KhorK. A., CheangP.,"Effect ofsuper saturation level on the size and morphology of hydroxyapatiteprecipitate,"*2006IEEEConf. Emerg. Technol. Nanoelec.*, Singapore,**2006,** 345-349.
8. SammonsR. L., ThackrayA. C., LedoH. M., MarquisP. M., JonesI. P., YongP., MacaskieL. E., "Characterisation and sintering of nanophase hydroxyapatitesynthesised by a species of Serratia," *J. Phys. Conf. Series*, **2007**, 93, 1-7.
9. FuruzonoT., WalshD., SatoK., SonodaK., TanakaJ., "Effect of reaction temperature on the morphology and size ofhydroxyapatitenanoparticles in an emulsion system," *J. Mater. Sci. Lett.*, **2001**, 20, 111-114.
10. PalardM., ChampionE., FoucaudS., "Synthesis of silicate hydroxyapatite $Ca_{10}(PO_4)_{6-x}(SiO_4)_x(OH)_{2-x}$,"*J. Solid StateChem.*, **2008**, 181, 1950-1960.
11. ´Sl´osarczyk A, Paszkiewicz Z, Paluszkiewicz C, "FTIRand XRDevaluation of carbonated hydroxyapatite powderssynthesized by wetmethods", *J. Mol. Struct.*, **2005**, 744, 657–61.
12. Luna-ZaragozaD., Romero-GuzmanE.T., Reyes-GutierrezL.R., "Surface and physicochemical characterization of phosphates vivianite, $Fe_2(PO_4)_3$ and hydroxyapatite, $Ca_5(PO_4)_3OH$", *J. Miner. Mater.Charac. Eng.*, **2009**, 8, 591-609.
13. FleetM.E., "Infrared spectra of carbonate apatites:ν_2-region bands",*Biomaterials*, **2009**, 30, 1473–1481.
14. Paluszkiewicz C, Ślósarczyk A, Pijocha D., "Synthesis, structural properties and thermal stability of Mn-dopedhydroxyapatite", *J. Mol. Struct.*, **2010**, 976, 301-9.
15. KamalH., HezmaA. M., "Spectroscopic investigation and magnetic study of iron, manganese, copper and cobalt-doped hydroxyapatite nanopowders", *Phys. Sci. Int. J.,* **2015**,7, 137-151.

16. LowH. R., PhonthammachaiN., MaignanA., StewartG. A., BastowT. J.,MaL. L.,WhiteT. J., "The crystal chemistry of ferric oxyhydroxyapatite", *Inorg. Chem.,***2008**, 47, 11774-11782.
17. Ahmed, S., Ahsan, M., "Synthesis of Cahydroxyapatite bioceramic from eggshell anditscharacterization", *Bangladesh J. Sci. Ind. Res.,***2008**, 43, 497-508.
18. Pon-On W., Meejoo S., Tang I-M., "Substitution of manganese and iron into hydroxyapatite core/shell nanoparticles", *Mater. Res. Bull.*, **2008**, 43, 2137-2144.
19. SongN., LiuY., ZhangY., TanY. N., GroverL. M., "Synthesis andcharacterization of ironsubstituted apatite", *Adv. Appl. Ceram.,* **2012**, 111, 466-471.
20. SchroederL. W., MathewM.,"Cation ordering in $Ca_2La_8(SiO_4)_6O_2$,"*J. Solid State Chem.*, **1978**, 26, 383-387.
21. YasukawaA., OuchiS., KandoriK., IshikawaT.,"Preparation andcharacterization of magnesium-calcium hydroxyapatites," *J. Mater. Chem.*, **1996**, 6, 1401-1405.
22. LowH. R.,RitterC., WhiteT. J., "Crystal structure refinements of the 2*H* and 2*M* pseudomorphs of ferriccarbonate-hydroxyapatite", *Dalton Trans.*,**2010**, 39, 6488-6495.
23. Borum-NicholasL., Wilson JrO.C., "Surface modification of hydroxyapatitePart I. dodecyl alcohol", *Biomaterials*,**2003**, 24, 3671-3679.
24. Markovic S., Veselinovic L., Lukic M.J., Karanovic L., Bracko I., Ignjatovic N., Uskokovic D., "Synthetical bone-like and biologicalhydroxyapatites: a comparative studyof crystal structure andmorphology", *Biomed. Mater*.,**2011**, 6, 045005(13pp).
25. Mason G., "The effect of pore space connectivity on the hysteresis of capillary condensation in adsorption-desorption isotherm", *J. Colloid. Interf. Sci.*, **1982**, 88, 36-46.

CHAPTER 5

Synthesis and characterization of Cu(II) doped HAPfrom eggshell

5.1 Introduction

Although hydroxyapatite is the major component of biological hard tissues, it has been accepted as an excellent adsorbent for many divalent metal cations.[1-5] As HAP is inexpensive and efficient for the removal of variety of metals, it has been widely usedtoimmobilize a wide range of heavy metals in water andsoils.[1-5] Though HAP is reported as a good adsorbent for the removal of cationic metal ions, it has less significant adsorptioncapacity towards anions in aqueous system such as arsenate and chromate ions.[6] Improvement of adsorption capacity of HAP for anionic species in aqueous medium is important forexpanding its ability. Presence of heavy metals in anionic form in the aqueous environment has raised serious health concernsand there is always need for cost-effective remediation methods[7-9] and HAP offers the potential in this regard. Doping of Cu(II) may significantly enhances adsorption capacity by specific binding with the heavy metals in its anionic form and thereby has received a surge of interest in recent days for adsorption studies.

5.2 Materials and methods

Cu-HAP was synthesized following the procedure described in Chapter 4, nevertheless the method is explained here in brief. Acidic solution of treated waste material (eggshell) was used as Ca^{2+} ion precursor and aqueous solution of copper nitrate was added to Ca^{2+} ionsolution prior to the addition of PO_4^{3-} ion precursor. Mixture was then stirred for 24 hrs just after making it basic with aqueous ammonia. Development of bluish green precipitate suggested the formation of Cu-HAP which was filtered, dried and collected. Figure 3.1 shows the schematic diagram for synthesis of Cu-HAP. Table 5.1 illustrates the quantity of the doping salt used in the synthetic method. Synthesized and thermally

treated Cu-HAPs are labeled on the basis of Cu content in the samples and temperature selected for calcinations as the affix of the temperatures in hundred as shown in Table 5.1. Synthesized products were oven dried at 100°C and calcined at 300°C and 600°C for 30 minutes soaking time while heating rate was maintained at 3°Cmin^{-1}.

Table 5.1: Quantity of Cu(II)-salt used in synthesis of Cu-HAP and sample identification

Sample	Wt % $Cu(NO_3)_2$	Firing temperature, °C	Identification of samples
Pure HAP	0.0	-	-
2%Cu-HAP	2.0	100	2% Cu-HAP1
		300	2% Cu-HAP3
		600	2% Cu-HAP6
4%Cu-HAP	4.0	100	4% Cu-HAP1
		300	4% Cu-HAP3
		600	4% Cu-HAP6
6%Cu-HAP	6.0	100	6% Cu-HAP1
		300	6% Cu-HAP3
		600	6% Cu-HAP6

5.3 Characterization of Cu-HAP

For the characterization of synthesized Cu-HAP samples (oven dried and thermally treated) EDS, XRD, FT-IR, SEM, DLS particle size analyzer, BET surface area analyzer were used.

5.3.1 Elemental analysis

Chemical compositions of all the synthesized samples were determined through EDS analysis. Figure 5.1 shows the presence of Cu along with Ca, P and O with a small

amount of carbon in the synthesized Cu-HAP. As Cu-salt was used in the synthesis of Cu-HAP, presence of Cu is expected in the samples. The (Ca+Cu)/P ratio of the sample is calculated as 1.40which is less than the ideal value of 1.67 for bones. Synthesis of non-stoichiometric Cu-HAP may be attributed to the presence of small amount of carbon in the products.

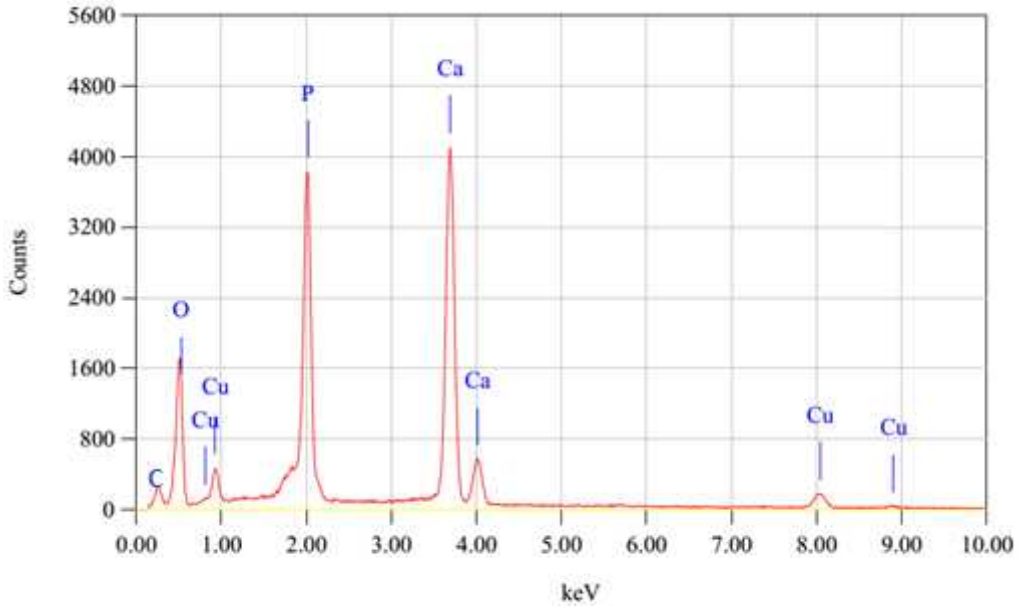

Figure 5.1 EDS spectrum ofCu(II) doped HAP from eggshell

5.3.2 FT-IR analysis

Presence of characteristic phosphate group andhydroxyl group in synthesized Cu-HAP were identified through FT-IRspectrophotometer.FT-IR spectra of Cu-HAP calcined at 600°C with different weight percent of Cu^{2+}ions are depicted in Figure 5.2 while the spectra for oven dried and calcined Cu-HAPs are compared in Figures 5.3. The absorption bands at1090-1030cm^{-1} are due to the ν_3 stretching of PO_4^{3-} group, doublet at approximately 601–606 cm^{-1} and 560–566 $cm^{-1}$are due to the ν_4 bendingmode of PO_4^{3-} group and very weak bands located at 956–962 $cm^{-1}$are attributed to ν_1 stretching mode of PO_4^{3-}present in synthesized Cu-HAP.[10] The peak at 1627 cm^{-1} and broad peak at

approximately 3440 cm^{-1} correspond to the water of adsorbed on the surface of samples. The weak absorption peak at approximately 3537 cm^{-1} can be ascribed to the stretching vibration mode of the structural OH^- group in the lattice. The absorption peaks at 870, 1319, 1419, and 1457 cm^{-1} indicate B-type substitution of carbonate group in HAP.[11,12]Incorporation of CO_3^{2-} ions suggests substitution of phosphate in the apatite lattice. Spectra of the samples indicate the occurrence of B-type substitution.[11,12]Cu-HAP sample does not show typical absorption band at 1540 cm^{-1} that is found in A-type carbonate substitutionin HAP which indicates absence of A-type carbonate.[11,12]

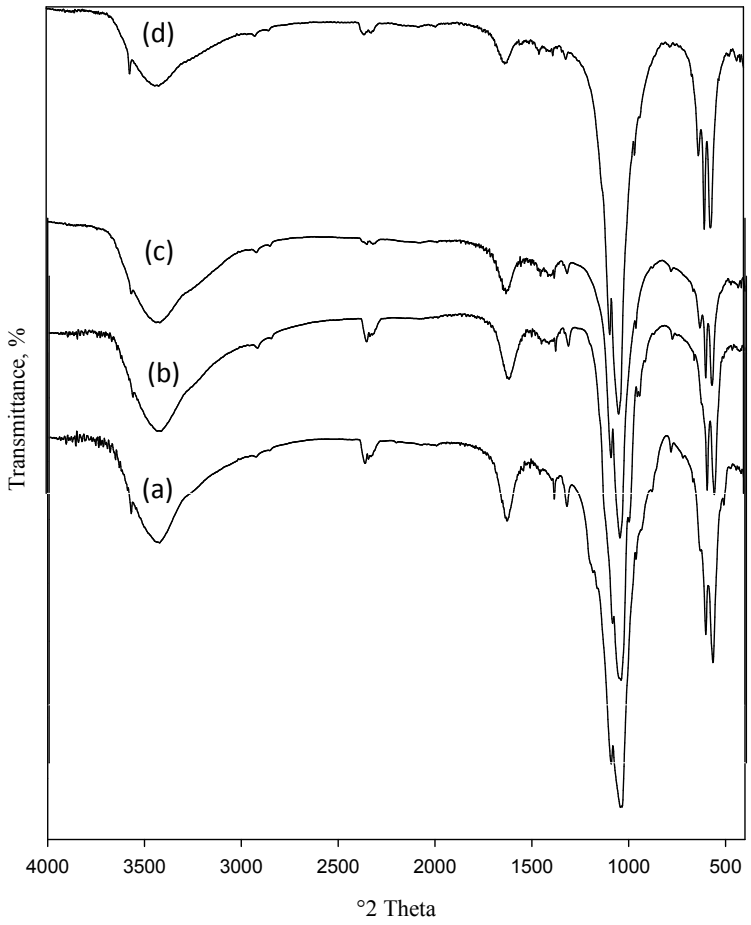

Figure 5.2 FT-IR spectra of Cu-HAPcalcined at 600°C synthesized from eggshell containing (a) 0%, (b) 2%, (c) 4% and (d) 6 wt% Cu

Presence of CO_3^{2-} group in the samples can be explained by the incorporation of CO_2 from environment, as the synthesis was carried out in air at ambient temperature. Increase of calcination temperature decreases the band intensity at ~2364 cm^{-1} assigned for CO_3^{2-} group in the samples. Researchers found that presence of carbonate group in HAP structure facilitates incorporation of cation in HAP.[13] It has already been discussed in Chapter 4 that in the unit cell calcium ions occupied ten sites of HAP crystal. Four of them denoted as Ca-I, form channelsparallel to the c-axis(Site I), and the remaining six, named Ca-II (Site II), arelocated around hydroxyl channels and form calcium triangles. It is reported that cations larger than Ca^{2+} ion can occupy calcium type (II) sites in the apatite lattice, whereas the smaller cations preferred calcium type (I) sites.[14,15] As Cu^{2+} ion has smaller radii (0.77 Å) than Ca^{2+}ion (0.99 Å), preferred site of substitution would be Ca-I. Splitting of ν_3 stretching of PO_4^{3-}group in the range 900-1200 cm^{-1} gradually diminishes as copper content increases in Cu-HAP (Figure 5.3 a, d and g). This implies that substitution takes place at Ca-I site which is responsible for broadening of the vibration band, which is also accountable to the amorphous structure of Cu-HAP. This feature is also supported by the XRD patterns of Cu-HAP samples. Besides, vibration band for structural OH at 3537 cm^{-1}starts to appear as a shoulder after calcinations of Cu-HAP samples at 600°C, whichis mostly merged with the broad band of adsorbed H_2O. In addition, band at ~635 cm^{-1} that is responsible for OH libration mode appears in FT-IR spectra for 4% and 6%Cu-HAP calcined at 600°C. It is known that OH group can undergo libration if it is subject to constraint that restricts its orientation. This may occur due to partial substitution of Cu for Ca-II site in the structure. This OH libration is absent in 2%Cu-HAP calcined at 600°C. Calcination temperature affects presence of structural OH, which is not seen in 2%Cu-HAP6. This indicates absence of OH group in HAP structure, consequently which suggests the presence of a second phase in 2%Cu-HAP6 along with HAP phase. XRD pattern of the sample strongly support this fact. Nevertheless, broad band at 3000-3650 $cm^{-1}$and smaller band at ~1620 cm^{-1}do not show any significant change due to increase in Cu content in Cu-HAP.

Major FT-IR peaks and their corresponding assignments are presented in Table 5.2.

Table 5 .2 Major absorption band positions and their assignments of different wt% of Cu-HAP treated at different temperatures

Observed band position, cm^{-1}									Corresponding assignments
2 wt%Cu-HAP calcined at			4 wt%Cu-HAPcalcined at			6 wt%Cu-HAPcalcined at			
100 °C	300 °C	600 °C	100 °C	300 °C	600 °C	100 °C	300 °C	600 °C	
561	563	565	565	569	565	563	567	569	PO_4^{3-} bending
601	601	601	601	603	603	603	603	603	
_	_	_	_	_	633	_	_	635	Structural OH^-
1035	1037	1051	1037	1041	1053	1035	1039	1040	PO_4^{3-} stretching
1319	1319	1319	1384	1421	_	1417	1419	_	CO_3^{2-} stretching
1635	1627	1627	1635	1641	1614	1635	1631	1635	H_2O adsorbed
2364	2364	2362	_	2312	_	2365	2340	_	CO_3^{2-}stretching
3441	3444	3439	3446	3446	3425	3446	3442	3448	H_2O adsorbed
_	_	_	_	3552	3537	_	_	3577	Structural OH^-

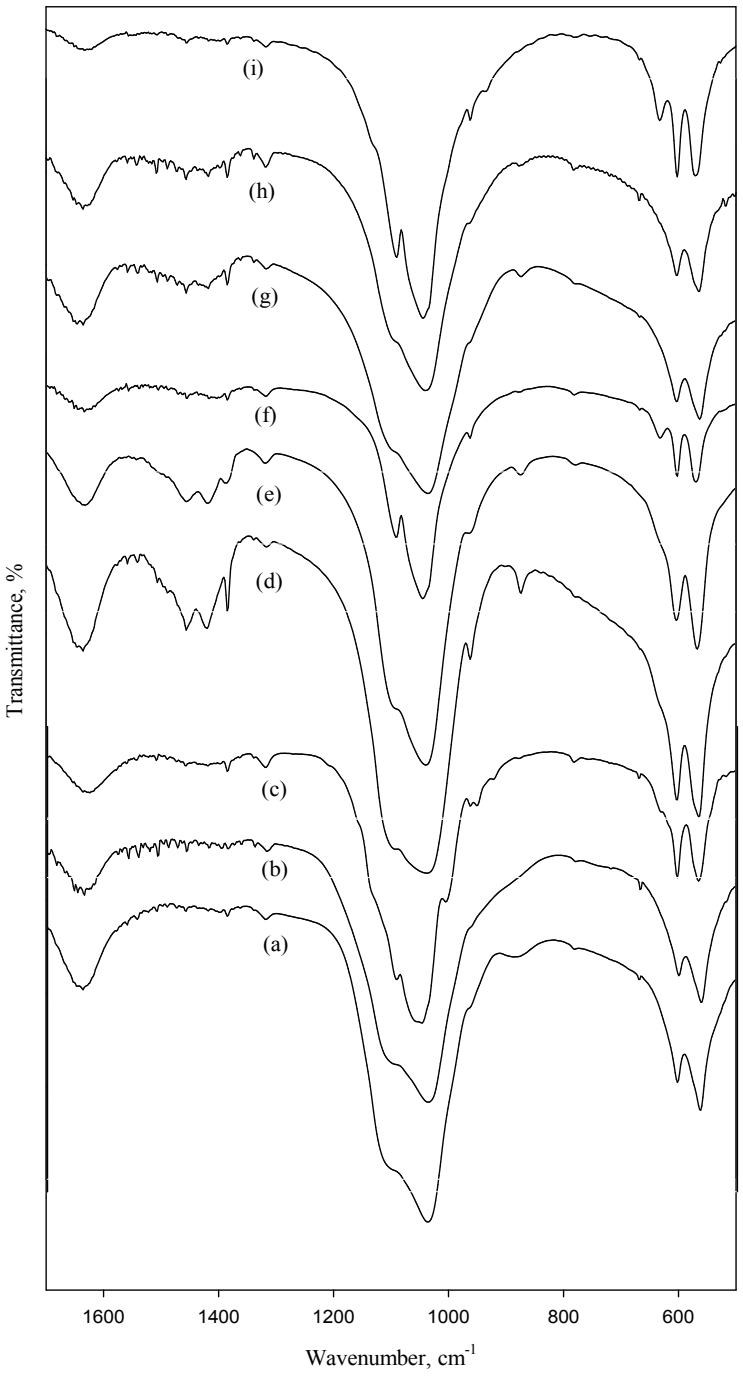

Figure 5.3 FT-IR spectra of thermally treated Cu-HAP from eggshell, 2%Cu-HAP thermally treated at (a) 100°C, (b) 300°C, (c) 600°C; 4%Cu-HAP thermally treated at (d) 100°C, (e) 300°C, (f) 600°C; 6%Cu-HAP thermally treated at (g) 100°C, (h) 300°C, (i) 600°C

5.3.3 XRD analysis

Structure of dried and calcined samples wasassessed using an X-ray powderdiffractometer. Figure 5.4 shows XRD patterns of oven dried synthesized pure and Cu-HAP samples and Figure 5.5 illustrates the patterns of both oven dried and calcined Cu-HAP synthesized with various quantity of Cu(II). Presence of strong diffractionpeaks corresponding to HAP phase at 2θ position ~31.84° for (211) reflection plane togetherwith other two peaks at 32.18 and32.89 °2θconfirmthe formation of HAP phase in the samples.[16]

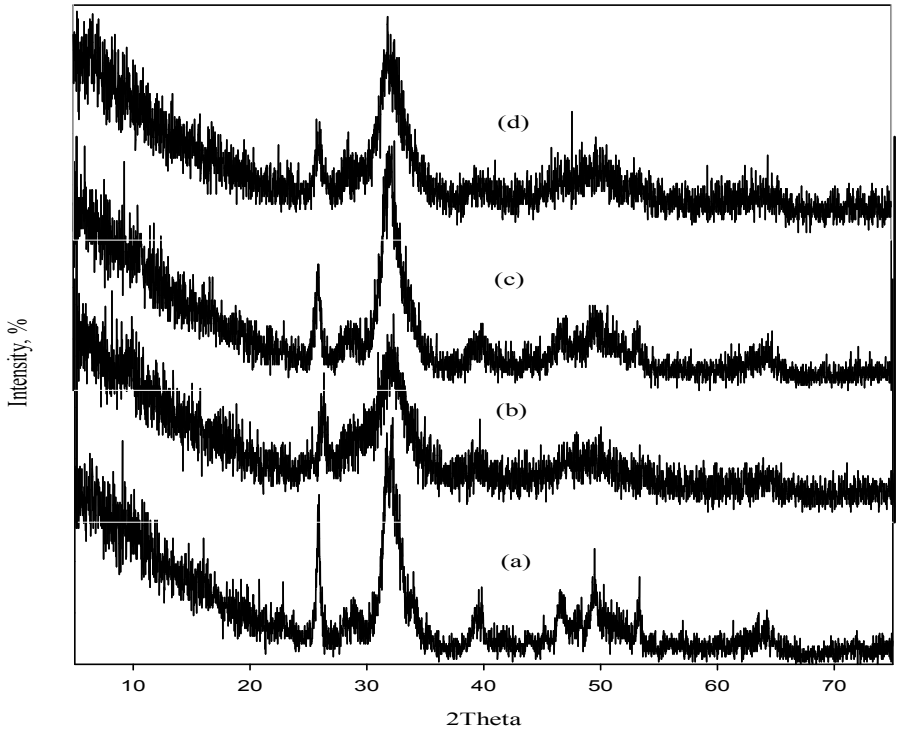

.Figure 5.4 XRD patterns of oven dried synthesized Cu-HAP containing (a) 0, (b) 2, (c) 4 and (d) 6 wt% Cu.

XRD patterns in Figures 5.4 and 5.5 are in good agreement with ICSD File No. 26204 which is hexagonal HAP and shows the presence of single phased HAP (except Figure 5.5c). Major diffraction peak at 31.92 for (211) plane of Cu-HAP become broader as shown in Figure 5.4, due to the substitution of $Cu^{2+}$for Ca^{2+} in the samples. Moreover increase of copper content in the samples decreases the intensity of diffraction peak for (002) reflection plane. This indicates amorphous nature of the synthesized Cu-HAP. Generally, Cu^{2+} ions tend to substitute Ca^{2+} ions as it has smaller radii (0.77 Å) than Ca^{2+} (0.99 Å) which increases surface area and decrease crystallinity of the samples.[17] Amorphous phase of Cu-HAP increases with increase of Cu content in the samples, while crystallinity of the samples increases with increase in calcination temperature.

XRD pattern of 2%Cu-HAP6 in Figure 5.5 (c) indicates presence of a second phase along with HAP phase in the sample. XRD pattern shows major peak at 2θ position 31.27 for (210) reflection plane along with peak at 2θ position 34.68 for (220) plane which is almost in equal intensity of the major peak. This pattern is in agreement with JCPDS-ICDD File 09-0169 *for β-TCP.*[18] *Presence of β-tricalcium phosphate in 2%Cu-HAP6 is also supported by FT-IR spectrum (Figures 5.2b and 5.3c) of sample which indicates the absence of weak vibration band* (3572cm^{-1}) *and libration band* (635 cm^{-1}) *for structural OH group.*

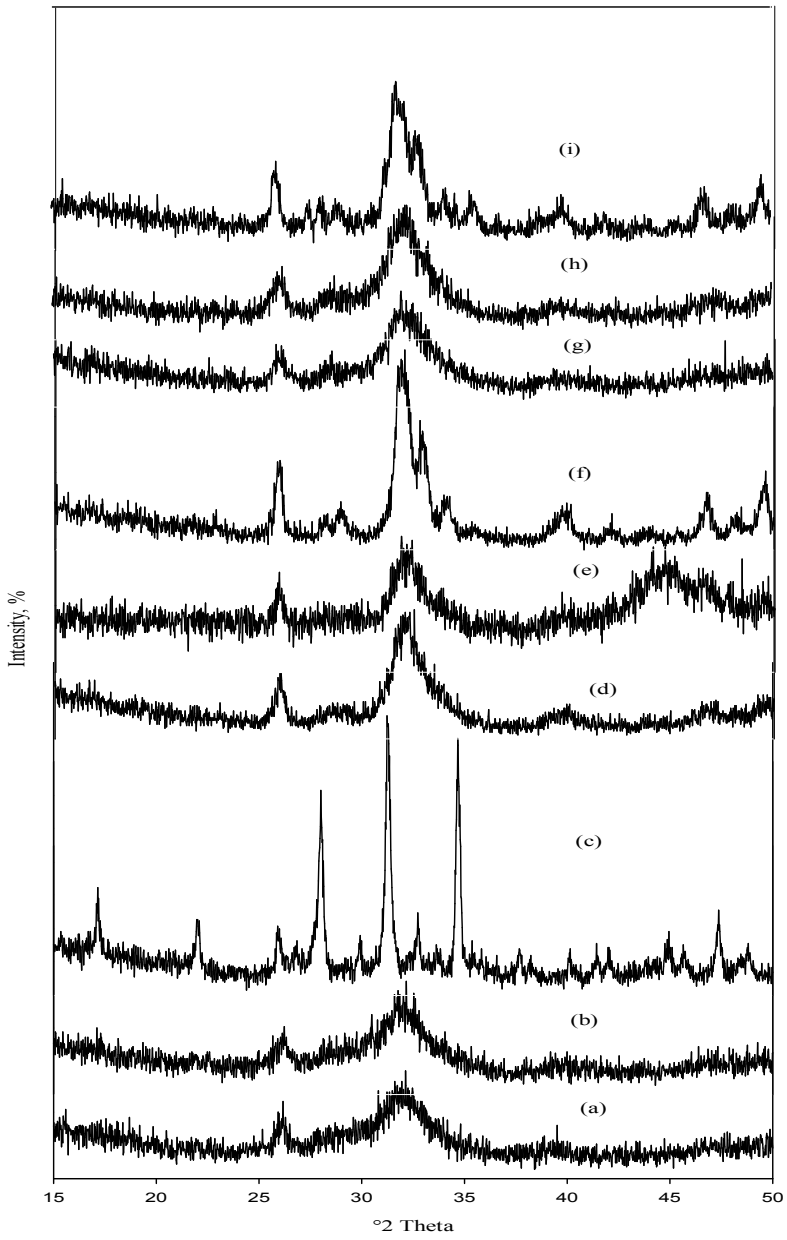

Figure 5.5 XRD patterns of thermally treated synthesized 2 wt% Cu-HAP (a) 100°C, (b) 300°C, (c) 600°C, 4 wt% Cu-HAP (d) 100°C, (e) 300°C, (f) 600°C, 6 wt% Cu-HAP (g) 100°C,(h) 300°C and (i) 600°C

The crystallographic parameters of the synthesized Cu-HAP are calculated using Equations 2.1-2.3 mentioned in Chapter 2. Lattice parameters along with major peak positions of Cu-HAP phase calculated from XRD data are summarized in Table 5.3.

Table 5.3 Comparison of *d*-spacing values and the corresponding plane with crystallite sizes and unit cell volume of the synthesized Cu-HAPs and the JCPDS Standard Data.

Sample		*d*-spacing (Å)	Position (2θ)	(h k l)	Crystallite size, nm	Cell parameter, Å	Unit cell volume, $(Å)^3$
JCPDS		3.4399 2.8131 2.7776 2.7185		0 0 2 2 1 1 1 1 2 3 0 0	-	a= b= 9.42 c = 6.88	528.71
2%Cu-HAP at	100°C	3.4103 2.7802	26.11 32.17	0 0 2 2 1 1	74.34	a=b=9.39 c =6.82	520.77
	300°C	3.4063 2.8038	26.16 31.92	0 0 2 2 1 1	15.21	a = b=9.40 c = 6.81	521.11
	600°C	3.4357 2.8608 2.5866	25.93 31.27 34.68	4 1 0 2 1 0 22 0	78.83	a= 10.35 c = 37.49	638.26
4%Cu-HAP at	100°C	3.4331 3.1035 1.7210	25.95 28.77 53.23	0 0 2 2 1 0 0 0 4	15.24	a= b= 9.48 c = 6.87	534.69
	300°C	3.4421 2.7889	25.89 32.09	0 0 2 211	17.33	a= b= 9.40 c = 6.88	526.47
	600°C	3.4402 2.8105 2.7818 2.7234	25.90 31.84 32.18 32.89	0 0 2 2 1 1 0 1 2 3 0 0	20.35	a= b= 9.43 c = 6.88	529.84
6%Cu-HAP at	100°C	3.4211 2.8062	26.05 31.89	0 0 2 2 1 1	12.15	a= b= 9.14 c = 6.84	494.86
	300°C	3.4243 2.7831	26.02 32.16	0 0 2 2 1 1	15.12	a= b= 9.34 c = 6.85	517.51
	600°C	3.4412 2.8178 2.7312	25.89 31.76 32.79	0 0 2 2 1 1 3 0 0	23.07	a=b= 9.44 c = 6.88	530.96

Table 5.3 shows that the crystallite size of oven dried Cu-HAP decreases with increase in Cu content in the samples. Substitution of larger Ca^{2+} ion with relatively smaller Cu^{2+} ionforms strains in the HAP lattice, which affects the crystallite size at higher Cu content in Cu-HAP. It is reported that larger ions prefer to substitute Ca in the Ca-II site for HAP and provokes an increment in lattice parameter *a*but reduces latticeparameter*c* and reverse statement is true for substitution at Ca-I site.[14-15] Cu-HAP (oven dried and treated at 300°C) show slight decrease in both cell parameters *a* and *c*. This implies that substitution of Cu^{2+} ion takes place in both Ca-I and Ca-II sites. This is also supported by FT-IR spectra of the related samples. However, increase in cell parameter *a* with no change in cell parameter *c* of 4% and 6%Cu-HAP6 indicates substitution at Ca-II site of the samples. This fact is also evident in FT-IR spectra of corresponding samples. An increase in unit cell volume with increasing Cu content confirmed the substitution of Cu onto the OH sites in the hexagonal channels of the apatite structure.[19]

5.3.4 SEM analysis

The particles of the 2 wt% Cu-HAP calcined at 600°C are homogenously distributed on the surface and consists of slightly elongated spherical structure as shown in the Figure 5.6.The size of the agglomerates tends to increase as the amount of dopant increased and also calcination temperature increases the agglomeration of the particles of Cu-HAP.

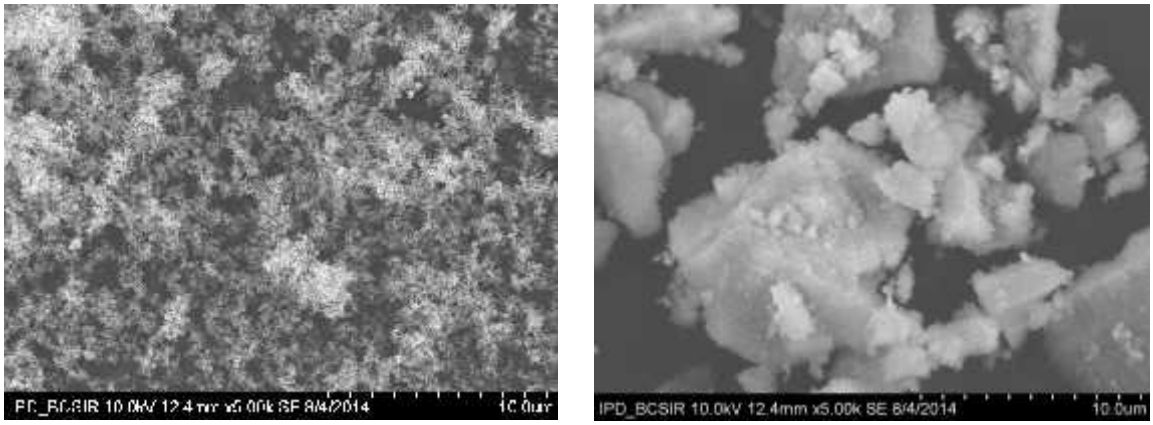

(a) (b)

Figure 5.6 SEM micrographs of thermally treated at 600°C Cu-HAP with (a) 2 wt% and (b) 4 wt% Cu.

5.3.5 Analysis of surface area

High surface area of a material is one of the most important criterion to be a good adsorbent. Therefore it is necessary to measure surface area of Cu-HAP to evaluate the adsorption efficiency of that material. Synthesized Cu-HAPs were analyzed by gas adsorption technique and pore distribution and specific surface areas of the samples were measured using the data obtained from the analysis.

Analysis of nitrogen adsorption behavior of Cu-HAP

Synthesized Cu-HAPs were analyzed to determine surface area and total pore volume using N_2 gas (at 77K) adsorption/desorption isotherm. Figure 5.7 presents the isotherms for Cu-HAP both oven dried and calcined at 300°C. Adsorption–desorption isotherm for 2%Cu-HAP1 shows in Figure 5.7(a) illustrates type III isotherm with no hysteresis loop. This indicates adsorption on a non-porous surface and surface area of the sample is very low. Type III isotherm with narrowH1 hysteresis loop for 2%Cu-HAP3 in Figure 5.7 (b) indicates the presence of a narrow distribution of relatively uniform cylindrical or tubular pores.[20]BJH plot of 2%Cu-HAP3 in Figure 5.8 (b) supports the fact.

Type IV isotherm is observed in Figure 5.7 (c) with hysteresis loop for 6% Cu-HAP3 which indicates the association of capillary condensation and evaporation taking place in mesopores during adsorption and desorption.At lower relative pressure ($P/P_0 < 0.4$) formation of a plateau in the isotherm profile indicatesformation of an adsorbate monolayer on pore surface and then followed by multilayer formation. Type H2 hysteresis loop suggests the presence of highly interconnected pores in the material.

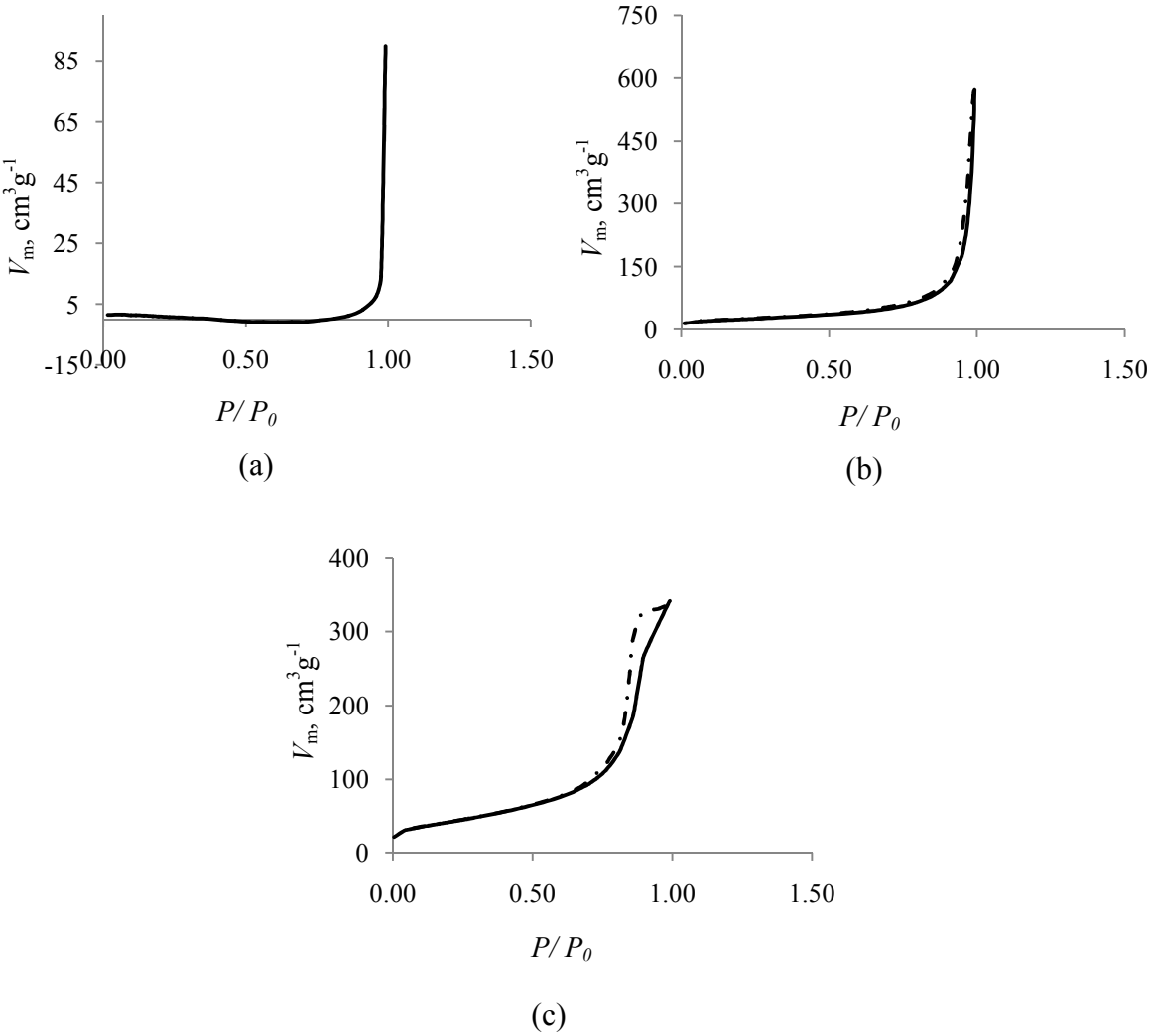

Figure 5.7 Adsorption/ desorption isotherm of Cu-HAP (a) 2 wt% dried at 100°C, (b) 2 wt% and (c) 6 wt% calcined at 300°C

Analysis of adsorption data for Cu-HAP by BET isotherm

Parameters obtained by the analysis of BET plot and BJH plot for Cu-HAP samples are given in Table 5.4. Lower BET surface area and the pore volumes of oven dried 2 wt% Cu-HAP can be explained by the blockage of internal porosity by incorporated Cu^{2+} ions. Since mean pore diameter of the oven dried sample is larger than calcined Cu-HAP sample, blocked pores would be micropores, resulting in a decrease of specific surface area and total pore volume.BJH plot in Figure 5.8 (a) shows the pore sizedistribution

which indicates the presence of macropores along with mesopores in the sample. Surface area of calcined Cu-HAP increases with increasing doping content, however total pore volume decreases with decrease of BET crystallite size of the samples. Increase in amount of copper in Cu-HAP increase specific surface area which indicates incorporation of Cu^{2+} ions in Ca sites on HAP.

Effect of doping of Cu^{2+}ion is also observed in BET particle size of the samples (Table 5.4).

Table 5.4 Data obtained from analysis of BET isotherms and BJH plot for Cu-HAP

Cu-HAP	BET surface area m^2g^{-1}	BJH total pore volume cm^3g^{-1}	BET mean pore diameter nm	BJH pore radius, nm	BET mean particle size nm
2 wt% dried at 100°C	6.50	0.1311	83.15	46.13	292.11
2 wt% calcined at 300°C	86.44	0.8803	38.04	14.13	21.97
6 wt% dried at 300°C	153.39	0.5383	13.73	6.95	12.38

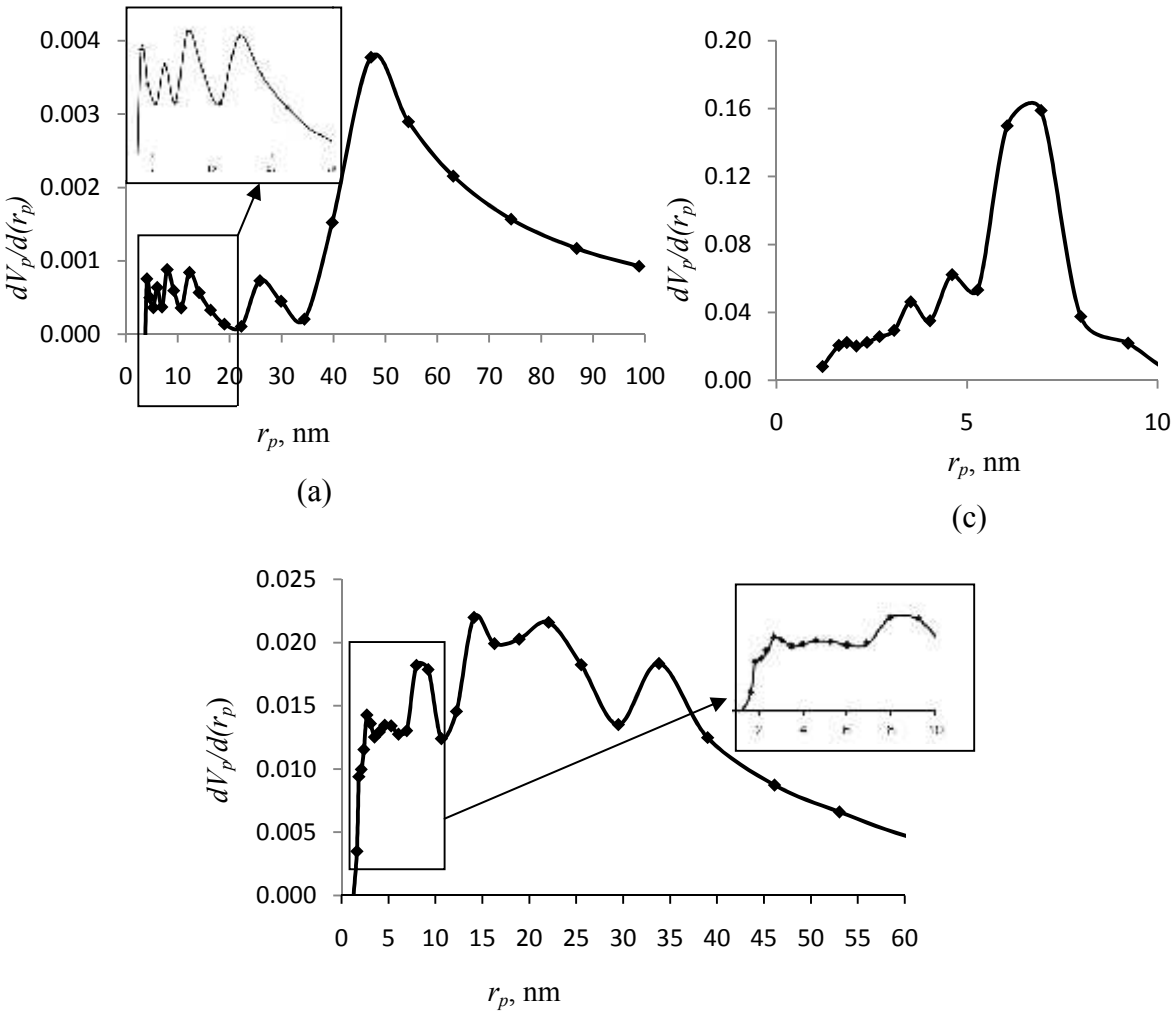

Figure 5.8 Differential curves of BJH plot of a N_2 adsorption isotherm of Cu-HAP samples (a) 2%Cu dried at 100°C, (b) 2% and (c) 6%Cu-HAP calcined at 300°C

5.3.6 Particle size and its distribution

Dynamic light scattering technique was used to determine the particle size of Cu-HAP powder and particle size distribution curve is shown in Figure 5.9.It shows the average particle size of Cu-HAP is2.67 μm which is larger than that of Fe-HAP. Crystallite sizes measured from XRD data of Fe-HAP and Cu-HAP show similar behaviour which can be explained by the smaller cation size of Fe^{3+} ion (0.64 Å) in compared to Cu^{2+} ion (0.77 Å).

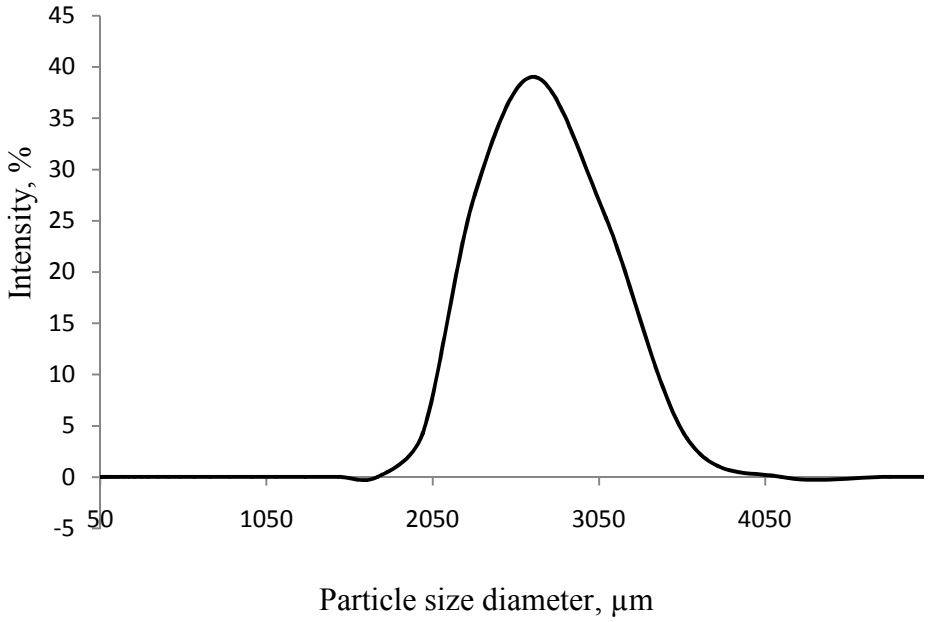

Figure 5.9 Particle size distributions of 2%Cu-HAP6

5.4 Conclusions

Copper substituted hydroxyapatite would be synthesized by wet chemical precipitation methodand calcined at 300°C and 600°C for30 min. Formation of single HAP phase is affirmed using powder XRD andFT-IR techniques. Presence of secondary phase (β-TCP) is noticed with increase of calcination temperature from 300°C to 600°C in case of 2%Cu-HAP.

Partial substitution of calcium by Cu in synthesized Cu-HAP leads to decrease in HAP cell unit parameters and reduction of crystallite size with increase in copper content in Cu-HAP and it is also affected by calcination temperature. Effect of calcination temperature also played an important role in controlling specific surface area along with pore size of the materials. BET analysis reveals an increase of specific surface area of Cu-HAP in comparison to pure HAP. Surface area of Cu-HAP calcined at 300°C is higher than oven dried samples. Highest specific surface area is measured for 2% and 6% Cu-HAP calcined at 300°C. As a consequence, Cu-HAP calcined at 300°C can be used as a competent adsorbent in preference to HAP and oven dried Cu-HAP. Samples treated

at 300°C also preserved a single phase HAP crystal along with higher specific surface area and total pore volume. So it can be concluded that Cu-HAPs are successfully synthesized from waste material which can be used as an improved adsorbent for the removal of heavy metals from aqueous system.

References

1. Suzuki T., HatsushikaT., Hayakawa Y., "Synthetic hydroxyapatitesemployed as inorganic cation-exchangers", *J. Chem. Soc.FaradayTras.,* **1981**, 77, 1059-1062.
2. Suzuki T.,Hatsushika T., Hayakawa Y., "Synthetic hydroxyapatitesemployed as inorganic cation-exchangers, Part 2",*J.Chem.Soc. Faraday Tras.,* **1982**, 78, 3605-3611.
3. Ma Q., Logan T. Traina S., "Lead immobilization from aqueoussolutions and contaminated soils using phosphate rocks", *Environ. Sci. Technol.,* **1995**, 29, 1118-1126.
4. Chen X., Wright J., Conca J., Feurrung L., "Evaluation of heavymetal remediation using mineral apatite", *Water Air Soil Pollut.,* **1997**, 98, 57-78.
5. Seaman J. C., Arey J. S., Bertsch P. M., "Immobilization of nickeland other metals in contaminated sediments by hydroxyapatiteaddition", *J. Environ. Qual.,* **2001**, 30, 460- 469.
6. Mopuri N., SumathiS., "Removal of cadmium (ii) and nickel (ii) ions bycopper substituted hydroxyapatite", *Int. J. Appl. Eng. Res.*,2013,8, 2179-2181.
7. Kinniburgh D. G., Smedley P. L. Eds., "Arsenic Contamination of Groundwater in Bangladesh Vol-2", *Final Report; BGSTechnical Report WC/00/19*; British Geological Survey:Keyworth,UK, **2001**.
8. Mandal B., Suzuki K., "Arsenic round the world: a review", *Talanta,* **2002**, 58, 201–235.
9. Mohan D., Pittman C., "Arsenic removal from water/wastewaterusing adsorbents-a critical review", *J. Hazard.Mater.,* **2007**,142,1-53.
10. RauJ.V., NunzianteCesaroS., FerroD., BarinovS.M., FadeevaI.V., "FTIR study of carbonate loss from carbonated apatites in the wide temperature range", *J.Biomed.Mater.Res. Part B: Appl. Biomater*., **2004**, 2, 441-447.

11. Chen C.W., Oakes C.S., Byrappa K., Riman R.E., Brown K., TenHuisen K.S., JanasV.F., "Synthesis, characterization, and dispersion properties ofhydroxyapatite prepared by mechanochemical-hydrothermal methods", *J. Mater.Chem.,* **2004**, 14,2425-2432.
12. Regnier P., Lasaga A.C., Berner R.A., Han O.H., Zilm K.W., "Mechanism ofCO_3^{2-} substitution in carbonate-fluorapatite: Evidence from FTIR spectroscopy,13C NMR, and quantum mechanical calculations", *Am. Miner.,* **1994**, 79,809–818.
13. Paluszkiewicz C., Ślósarczyk A, Pijocha D., "Synthesis, structural properties and thermal stability of Mn-dopedhydroxyapatite", *J. Mol. Struct.*, **2010**, 976, 301-309.
14. SchroederL. W., MathewM.,"Cation ordering in $Ca_2La_8(SiO_4)_6O_2$,"*J. Solid State Chem.*, **1978**, 26, 383-387.
15. YasukawaA., OuchiS., KandoriK., IshikawaT., "Preparation andcharacterizationof magnesium-calcium hydroxyapatites," *J.Mater. Chem.*, **1996**, 6, 1401-1405.
16. AhmedS., AhsanM., "Synthesis of ca-hydroxyapatite bioceramic from eggshell and itscharacterization", *Bangladesh J. Sci. Ind. Res.*, **2008**, 43, 501-512.
17. Liu G., Talley J.W., Na C., Larson S., Wolfe L.G., "Copper doping improves hydroxyapatite sorption for arsenatein simulatedgroundwaters",*Environ. Sci. Technol.,* **2010**, 44, 1366-1372.
18. Pillai R.S., Sglavo V.M., "Effect of MgO addition onsolid state synthesis and thermal behaviorof beta-tricalcium phosphate", *Ceram. Int.*, **2015**, 41, 2512–2518.
19. Imrie F.E., Skakle J.M.S., Gibson I.R., "Preparation of copper-dopedhydroxyapatite with varying x in thecomposition$Ca_{10}(PO_4)_6Cu_xO_yH_z$ ", *Bioceram. Dev. Appl.,***2013**, S1:005.
20. Matthias T., "Physical adsorptioncharacterization of nanoporousmaterials" *Chem. Ing. Tech.*, **2010**, 82, 1059-1073.

CHAPTER 6

Synthesis and characterization of nano HAPfrom eggshell and its application in removal of heavy metals from aqueous medium

6.1 Introduction

Nano HAP with appropriate stoichiometry, morphology and purity, have received considerable attention due to its wide application in high technology biomedical fields and environmental remediation. NanoHAPwhich has a grain size less than 100 nm in at least one directionhas high surface area.[1] Biological apatites available from fish scales and animal bones also have high surface area[2] which contribute to their high reactivity. As a consequence biological apatites display a variety of chemical substitutions in the HAP structure.[2] As eggshell is one of the richest source of calcium, it has been used to synthesize HAP using various methods in the recent years. For sustainable development and environmental remediation wastes should be recycled, reused and channeled towards the production of valueaddedproducts. Utilization of eggshell in the synthesis of nano HAP can be one of the significant steps towards the waste recycling technology. The mostfrequently used methods for the preparation of HAP nano particles are ultrasonic, co- precipitation, sol-gel, hydrothermal, microwave assisted irradiation etc.[3] A few works have been reported on nano HAP synthesis by microemulsion method using ionic and mixed surfactants.[4] The water-in-oil microemulsion system contains reverse micelles dispersed in acontinuous oil phase. Each reverse micelle consists of aqueous droplets (one reagent) surrounded by certainsurfactant species suspended inthe oil phase. Following the addition of the second microemulsioncontaining another reagent, fusion–fission between the reverse micelles causes the reaction between calcium and phosphateions andfinally formation of HAP nanocrystals takes place. Microwave-assisted synthesis of nano HAP from precursors prepared from eggshell has been reported by Parsons and Mallick.[5] The aim of this work is to synthesis nano HAP using eggshells as a

source of calcium ions by microemulsion method. The nano HAP has the potential as an efficient adsorbent for the removal of toxic metals from aqueous system.

6.2 Materials and Methods

6.2.1 Synthesis of nano-HAP using microemulsion

In order to synthesize nano HAP using microemulsion method, calcium acetate was first prepared from eggshell and used as Ca^{2+} ion source.

(i) Synthesis of calcium acetate/precursor from eggshell

A desired quantity of eggshell was dissolved in 4% acetic acid solution for 24 h at room temperature (30°C). The insoluble organic part and the inner membrane of eggshell were removed from the solution. After removal of the inner membrane this was filtered to obtain a clear solution. Evaporation of this clear solution resulted in white solid powder of calcium acetate. This was then calcined at 300°C for 3 h and preserved for characterization. Figure 6.1 shows the schematic diagram of the synthesis of calcium acetate from eggshell.

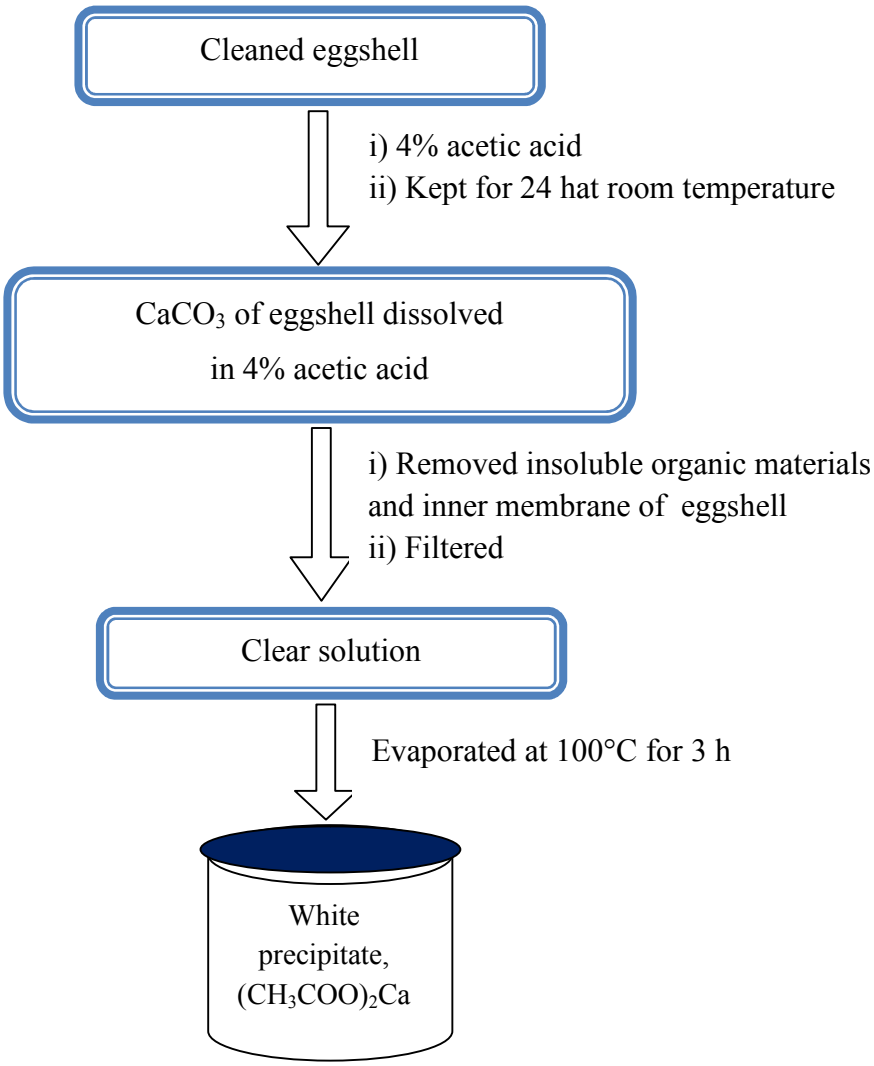

Figure 6.1 Schematic diagram for synthesis of calcium acetate from eggshell

(ii) Synthesis of nano-HAP using microemulsion method

A quaternary reverse micelle system, tritonX-100 (TX-100)/cyclohexane/*n*-pentanol/water, was used for the synthesis of nano HAP. Two reverse micelle compositions of same volume were prepared by adding an aqueous solution of synthesized calcium acetate in composition-1 and $(NH_4)_2HPO_4$ in composition-2 containing TX-100 in cycloheaxane and *n*-pentanol with $[H_2O]/[surfactant]$ ratio W_0=7.8. The two compositions were mixed and stirred for 4 h and then centrifuged at 3000 rpm for 20 mins just after addition of ethanol to precipitate out nano HAP.

Schematic diagram of synthesis of nano HAP is shown in Figure 6.2. Concentrations of calcium ion and phosphate ion precursors were maintained in such a manner that the Ca/P ratio remains approximately 1.66 as in HAP found in bones and teeth. Compositions of the two reverse micelle solutions are showed in Table 6.1.

Table 6.1: Compositions of microemulsion for nano-HAP synthesis

Microemulsion	Wt% of				Water to surfactant ratio, W_0
	TX-100	Ca^{2+}or PO_4^{3-} aqueous solution	Cyclohexane	1-pentanol	
Composition-1	10	2.2850	83	4.7540	7.8
Composition-2	10	2.2850	83	4.7540	

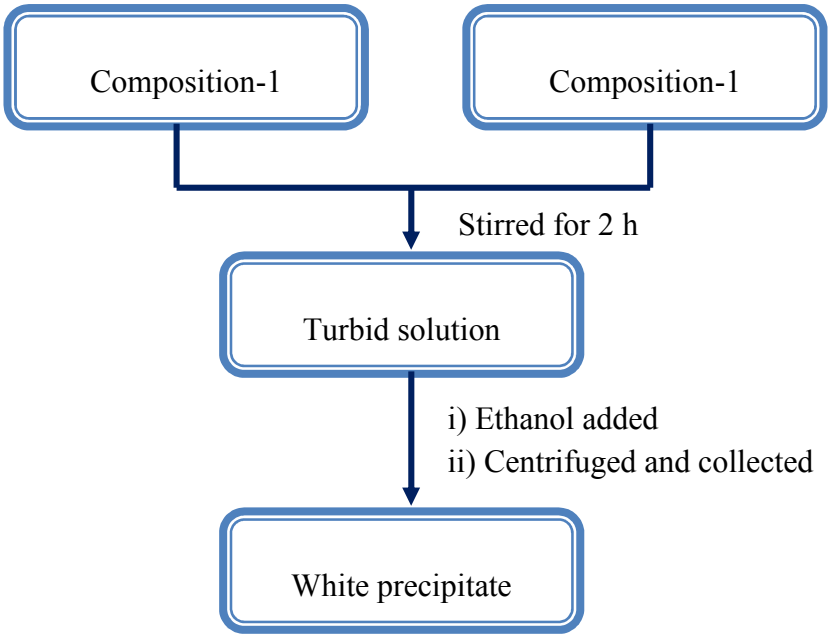

Figure 6.2 Schematic diagram for synthesis of nano HAP from eggshell

A white precipitate was the final product which was collected after thorough washing and drying at 100°C for 3 h.

6.2.2 Removal of arsenic from aqueous system using nano HAP

As(V) solution of a specific initial concentration was prepared by proper dilution of stock solution (1000 mgL^{-1}). 10 mL of the stock solution was added to a reagent bottle containing optimum adsorbent dosage for equilibrium time 60 min. Adsorbents used in this study were oven dried and calcined at 300°C and 600°C. All the studies were performed at an optimum pH 9.0 for As(V) solution. Adsorption of As(V) on HAP and nano HAP was also carried out at pH 7 which shows the minimum adsorption efficiency for HAP1 and HAP3 . All the adsorption experiments were performed at ambient temperature (30º ± 1º C). The contents were shaken at 150 rpm and then centrifuged at 2000 rpm for 15 mins. and the supernatant liquid was analyzed for As(V) ion concentration using hydride generated system HG-AAS (NOVAA 350, Analytik Jena, Germany).

6.3 Characterization of calcium acetate

6.3.1 FT-IR analysis

Figure 6.3 shows the FT-IR spectrum of synthesized calcium acetate in the region from 400-4000 cm^{-1}. Two weak bands at 3032 and 2920 cm^{-1} are due the anti-symmetric $\nu_{as.}(CH_3)$ and symmetric $\nu_s(CH_3)$ methyl stretching vibrations, respectively.[6] Broad band at 3436 cm^{-1} for $Ca(CH_3COO)_2$ is due to H-bonded ν(O-H) stretching vibration. Figure 6.2 shows the region of the spectrum from 1200-1600 cm^{-1} which is dominated by CH_3 bending and C-O stretching vibrations.The small broad peak present at 1320 cm^{-1} is due to the symmetric methyl bending vibrations of the acetate anion. The antisymmetric methyl bending vibration is observed at 1420 cm^{-1} for calcium acetate species.[6] Two bands observed at around 1450$cm^{-1}$are attributed to the symmetric stretching vibration of the C-O bond.[6]The calcium acetate displays an intense series of bands at 1540, 1562 and 1607 cm^{-1} which is the result of antisymmetric C-O stretching vibrations.This assignment

of the C-O antisymmetric stretching vibration over such a wide range of wave numbers is in agreement with literature.[6] The compound exhibits a stretching vibration at 662cm^{-1} which is due to out of plane stretching vibrations of the O-C-O fragment.The in-plane bending vibration of the methyl group appears as a single broad peak at 1022cm^{-1}.

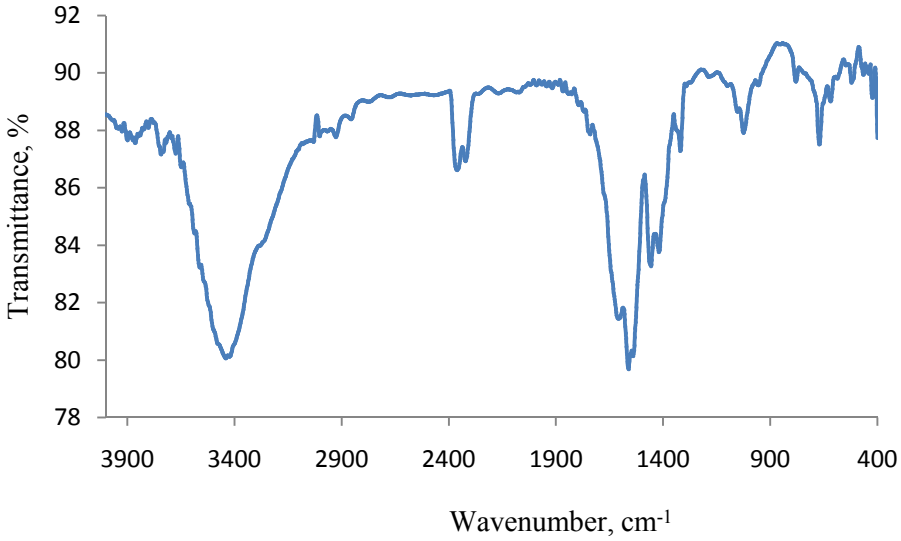

Figure 6.3 FT-IR spectrum of calcium acetate prepared from eggshell

6.3.2 XRD analysis

X-ray diffraction pattern of the synthesized calcium acetate compound was recorded (Figure 6.4) to confirm its crystallographic structure. XRD patternconfirms the formation of calcium acetate as it is in good agreement with reference pattern of calcium acetate hydrate 00-019-0199.[6]Diffraction pattern in the region from 5-10 degree 2θ are significant for the calcium acetate crystal.

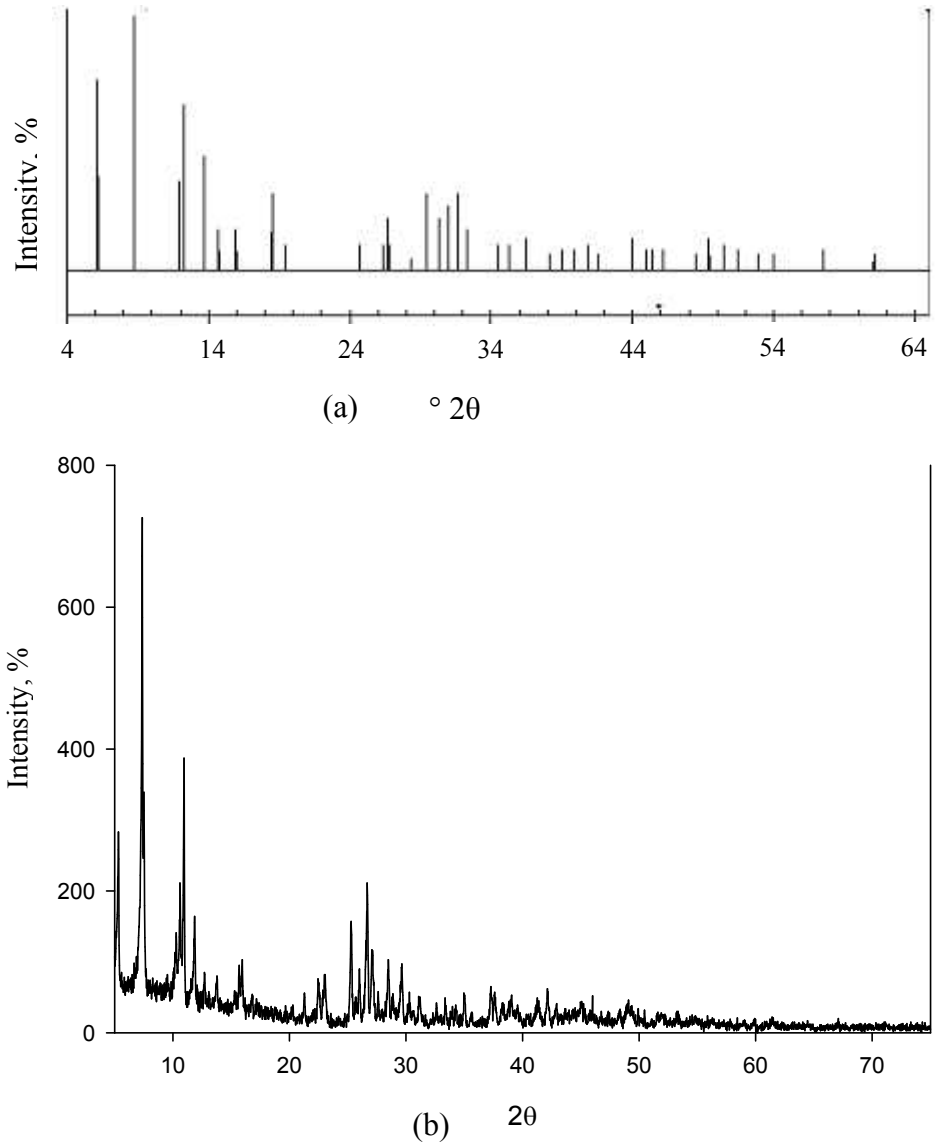

Figure 6.4 XRD pattern of calcium acetate (a) reference pattern of calcium acetate hydrate 00-019-0199 (b) synthesized from eggshell

6.4 Characterization of nano HAP

6.4.1 FT-IR analysis

Figure 6.4 shows the FT-IR spectra (both oven dried and calcined) of synthesized nano HAP. FT- IR spectra of nano HAP exhibits well defined absorption bands characteristic of HAP phase.[7] Presence of phosphate group in nano HAP from eggshell (Figure 6.5)

can be attributed by double bands at 563 and 601cm^{-1} which refer to asymmetric and symmetric deformation modes ν_4 of phosphate group. Intensive absorption band in the range of 1030-1095 cm^{-1} corresponds to a band characteristic of asymmetric stretching mode ν_3 of PO_4^{3-} group. The broad band in the range 3430–3444 cm^{-1} can be attributed to traces of water incorporated in HAP structure, together with the weak band around 1627cm^{-1} of H–O–H bending mode.[8] A shoulder is observed at 3649 cm^{-1} after calciningsynthesized nano HAP at 600°C. This implies the presence of structural OH group in the product which was masked by the broad H_2O absorption band in the spectra for oven dried nano HAP from eggshell (Figure 6.5a and b).The absorption bands at 862, 1319, and1382 cm^{-1} indicate the presence of CO_3^{2-} group, which suggests that carbonate ions are substituted for certain phosphate positions in the apatite lattice and B-type substitution takes place.[9,10] The band position and their corresponding assignments are given in Table 6.2.

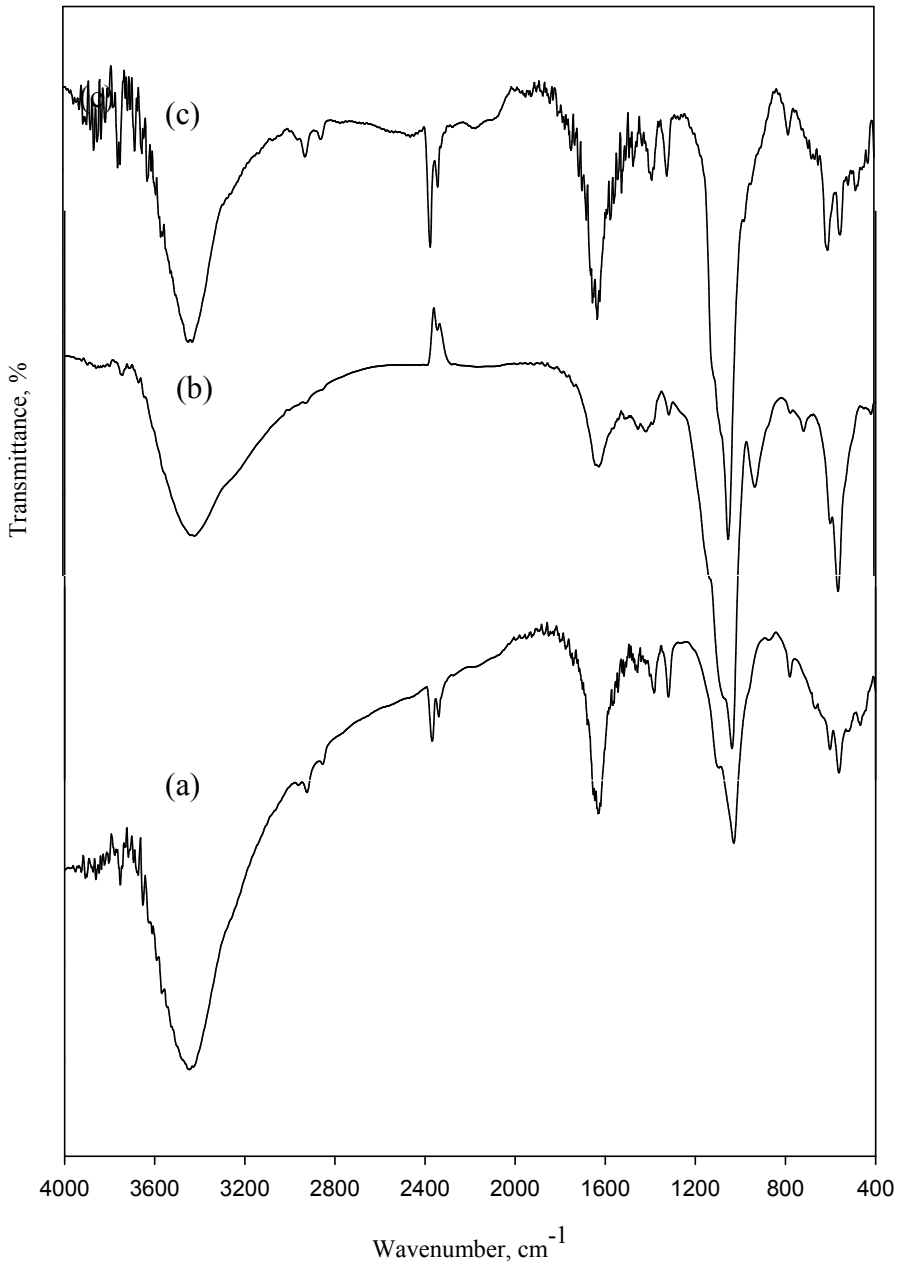

Figure 6.5 FT-IR spectra of nano HAP synthesized from calcium acetate (a) oven dried at 100°C, calcined at (b) 300°C and (c) 600°C

Table 6.2 FT-IR band positions and their corresponding assignments of synthesized pure and thermally treated nano HAP

Observed band position, cm^{-1}			Corresponding assignments
Nano HAP(calcium acetate) treated at			
100°C	**300°C**	**600°C**	
563	567	551	PO_4^{3-} bending
601	602	609	
1029	1037	1047	PO_4^{3-} stretching
1319 1382	1317 1390	1319 1382	CO_3^{2-} stretching
1627	1628	1627	Adsorbed H_2O
2368	_	2368	CO_3^{2-} stretching
3444	3423	3444	Structural OH^- and adsorbed H_2O
_	_	3649	Structural OH^-

6.4.2 XRD analysis

The structure of dried and calcined nano HAP wasassessed using an X-ray powder diffractometer. Figures 6.6(a) and (b) show XRD patterns of both oven dried (100°C) and calcined (600°C) nano HAPs respectively. Presence of strong diffractionpeak at 2θ position ~31.98° (Figure 6.6a) for (211) reflection plane confirmthe formation of HAP phase in the oven dried nano HAP.[11] On theother side, both β-tricalcium phosphate and hydroxyapatite phases exist in the nano HAP sample calcined at 600°C (Figure 6.6b). XRD pattern shows major peak at 2θ position 30.64 for (210) reflection plane along with

peak at 2θ position 33.95 for (220) plane which is almost in equal intensity of the major peak. This pattern is in agreement with JCPDS-ICDD File 09-0169 *for β-TCP.*[12] *The* presence of poorly crystalline HAP phase *at* 2θ position 32.02 for (211) plane in Figure 6.5 (b) indicates the existence of *HAP phase in nano HAP6 along with β-TCP*.

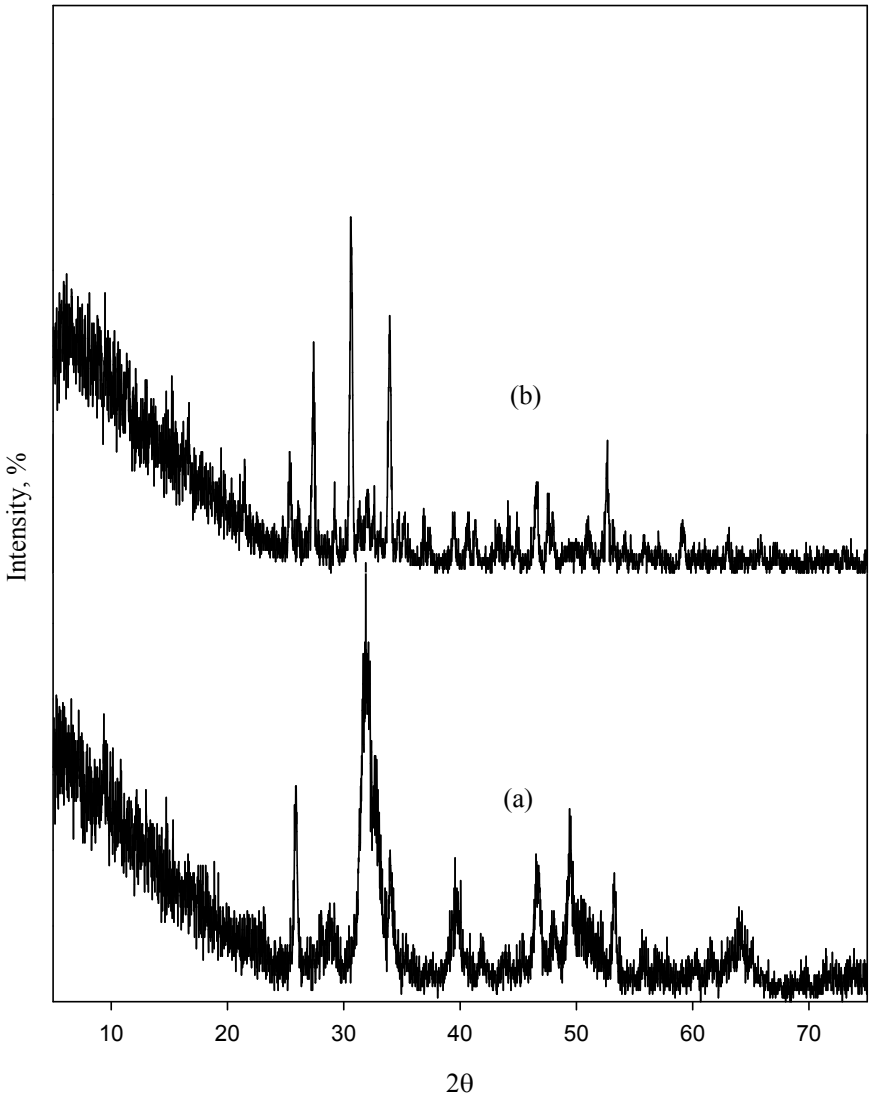

Figure 6.6 XRD patterns of nano HAP from eggshell derived calcium acetate thermally treated at (a) 100°C and (b) 600°C

The crystallographic parameters of the synthesized nano HAP are calculated using equations 2.1-2.3 mentioned in Chapter 2. Lattice parameters along with major peak positions of nano HAP phase calculated from XRD data are summarized in Table 6.3.

Table 6.3 Comparison of *d*-spacing values and the corresponding plane with crystallite sizes and unit cell volume of the synthesized nano HAP and the JCPDS Standard Data.

Sample			*d*-spacing (Å)	Position (2θ)	(h k l)	Crystallite size, nm	Cell parameter, Å	Unit cell volume, $(Å)^3$
JCPDS			3.4399 2.8131 2.7776 2.7185	25.87 31.77 32.19 32.90	0 0 2 2 1 1 1 1 2 3 0 0	-	a= b= 9.42 c = 6.88	528.71
Nano HAP treated at	100°C		3.4414 2.7986	25.89 31.98	0 0 2 2 1 1	13.58	a=b=9.36 c =6.88	522.00
	600°C	HAP phase	3.4177 2.7951 1.7390	26.07 32.02 52.63	0 0 2 2 1 1 0 0 4	40.79	a=b=9.58 c = 6.84	543.65
		β-TCP phase	2.9179 2.5861	30.64 34.69	2 1 0 22 0	69.89	a=b=10.34 c =23.81	2204.61

Table 6.3 shows that the crystallite size of nano HAP increases with increase in calcination temperature. Substitution in the Ca-II site of HAP provokes an increment in lattice parameter *a*but reduces latticeparameter*c* and reverse statement is true for substitution at Ca-I site.[13,14] Figure 6.5 (a) shows a decrease in cell parameter *a* and no significant change in cell parameter *c*. It indicates the carbonate substitution at Ca-I site which is also known as B-type substitution. FT-IR spectra also support this B-type substitution in HAP structure. Presence of both phases (HAP and β-TCP) in Figure 6.5 (b) shows an increase in cell parameter *a* and decrease in cell parameter *c.* Crystallite size of the samples increase with increase in calcination temperatures.

6.4.3 SEM analysis

SEM micrographs in Figure 6.7 (a) and (b) show the morphology of synthesized nano HAP thermally treated at 600°C. Image of nano HAP shows elongated spheroid shape with particle size of approximately 100 nm. The crystallite size of nano HAP increased from 13.58 nm to 40.79 nm with increase in calcination temperature from 100°C to 600°C. Hence agglomeration of nano HAP particles is observed at higher calcinations temperature.

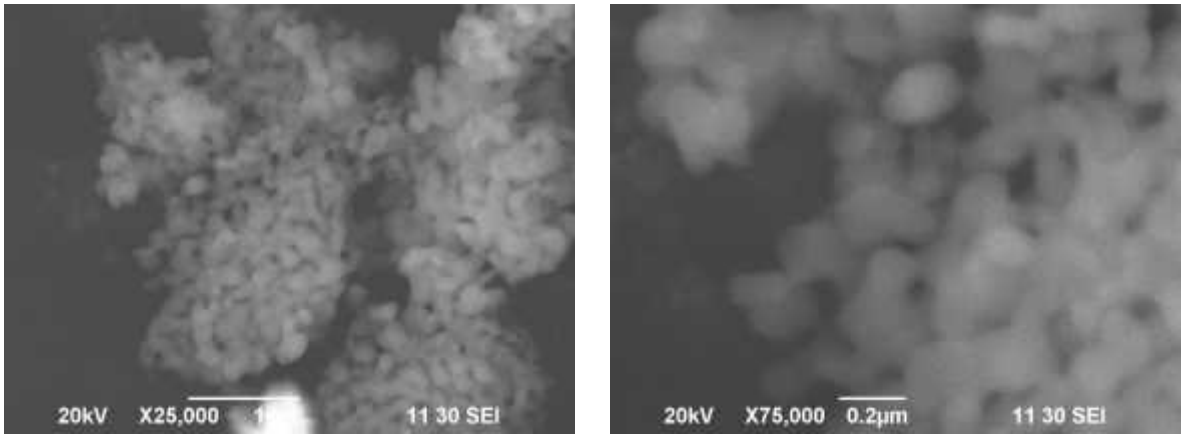

(a) (b)

Figure 6.7 SEM micrographs of synthesized nano HAP treated at 600°C magnification (a) 25,000 times and (b) 75,ooo times

6.4.4 Analysis of surface area

Specific surface area of a material is an important property for the study of adsorption capacity and for describing pore type of the porous media. Gas adsorption techniques are widely used to characterize the pore structures and surface areas of various materials.

Analysis of nitrogen adsorption behavior of nano HAP

N_2gas (at 77K) is mostcommonly used for surface area and mesopore characterization. The shape of the isotherm and its hysteresis pattern provide useful information about

theadsorption mechanism, the solid and gas interactions, and can be used to qualitativelypredict the types of pores present in the adsorbent. IUPAC classification of the adsorption isotherms into six types (Type I to VI), along with four hysteresis patterntypes (H1 to H4) are mentioned in Chapter 1.[15] Figure 6.8 (a) shows N_2 gas adsorption/desorption isotherm for thermally treated nano HAP. Theisothermof nano HAPcalcined at 600°C resembles type III with a small hysteresis loop,suggesting the existence of mesopores in the sample.[16]A vertical H1 type hysteresis loop in the isotherm in the narrow range of P/P_0(0.90 to 0.99)indicatesthe presence of uniform cylindricaltype pores.[16]

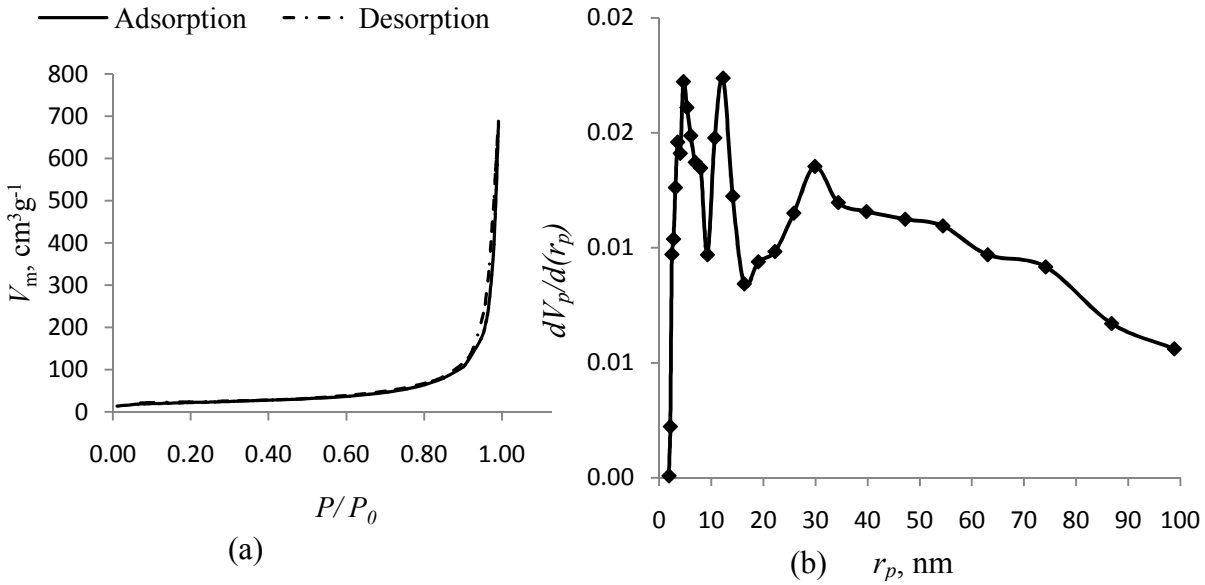

Figure 6.8 Nano HAP calcined at 600°C (a) adsorption/ desorption isotherm, (b) differential curve of BJH plot

Analysis of adsorption data for nano HAP by BET isotherm

Parameters measured by BET analysis of calcined nano HAP are presented in Table 6.4, parameters of calcined pure HAP are also mentioned for the comparison. Surface area of

calcined nano HAP is measured as 79.23 m^2g^{-1} which is approximately 3.5 times higher than the pure HAP.

Table 6.4 Data obtained from analysis of BET isotherms and BJH plot for nano HAP

Synthesized HAP calcined at 600°C	BET surface area m^2g^{-1}	BJH total pore volume cm^3g^{-1}	BET mean pore diameter nm	BJH pore radius, nm	BET mean particle size nm
Pure HAP	22.40	0.3436	59.21	29.5	83.97
Nano HAP	79.23	1.00	51.21	12.24	23.96

Pore size distribution (Figure 6.8b) obtained from BJH plot indicates that most of the pores are in the mesopore region along with macropores in the sample. Decrease in BET particle size for nano HAP6 increase the total pore volume of the sample, which indicates an increase in interparticle and intraparticle pores in nano HAP6.

6.4.5 Particle size and its distribution

Particle size distribution of nano HAP was analyzed by DLS technique. Figure 6.9 (a), (b) and (c) show the particle size distributions of nano HAP in microemulsion, oven dried at 100°C and calcined at 600°C respectively. Immediate after preparation of nano HAP in microemulsions the diameter was measured 12 nm. Presence of particles with average diameter size of 16 and 295 nm (Fig. 6.9b) indicate the agglomeration of the nano particle while it is oven dried at 100°C. Nano HAP calcined at 600°C has average particle size of 600 nm, which indicates increase in agglomeration with increase in calcination temperature. At low temperature particle growth is faster than crystalline growth, and the process of crystalline growth is favored by increase in calcination

temperature. However, DLS measures the hydrodynamic size of the particle, so particle size of HAP may be smaller than that measured by DLS technique.

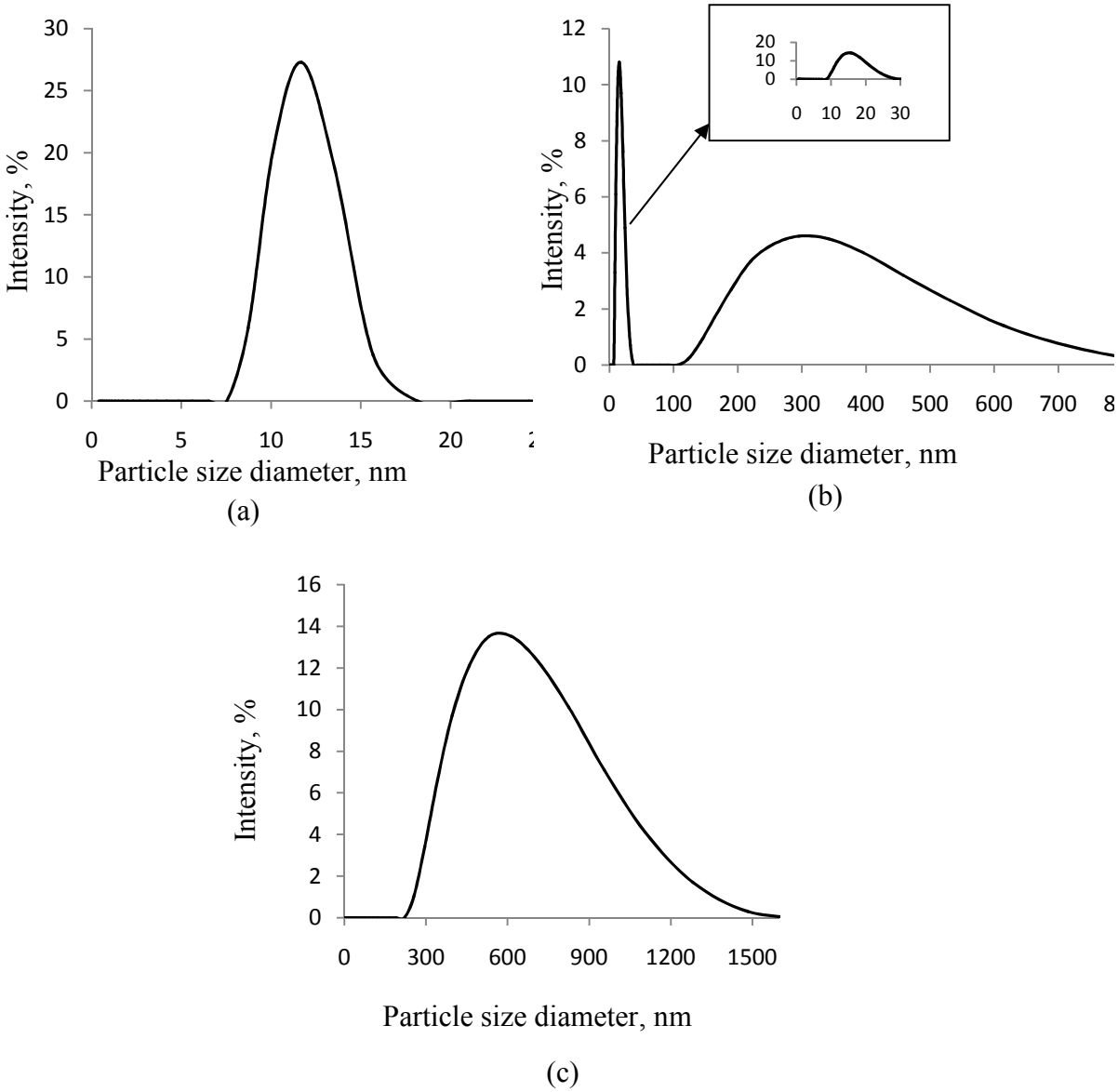

Figure 6.9 Particle size distribution of nano HAP (a) in microemulsion (b) oven dried at 100°C and (c) calcined at 600°C

6.5 Application of nano HAP in removal of heavy metals from aqueous system

HAP stabilizes a wide range of metals suchas chromium, cobalt, cadmium, zinc, nickel,plutonium, lead, arsenic etc.[17-18] Adsorbent property of synthesized pure HAP will be discussed in Chapter 7. The ability to remove heavy metals of pure HAP is not significant particularly for removal of arsenate and chromate from aqueous system. While Nano HAP particle is a promising adsorbent in the removal of heavy metals due to its properties and low cost synthesis. Recent advancements in nano technology gave rise to many nanoparticle adsorbents. The smaller the size of these nanoparticles, the larger the surface area provided for the contaminants to get adsorbed.

6.5.1 Arsenic removal efficiency of nano HAP

Figure 6.9 (a) and (b) show As(V) removal efficiency of nano HAP at pH 9.0 and pH 7.0 respectively. Figure 6.10(a) shows that at equilibrium condition arsenic removal efficiency of HAP6 is calculated 20.13%, 22.48% for HAP3 and 32.08% for nano HAP6. Higher As(V) removal efficiency of nano HAP6 could be explained by higher surface area of the sample as compared to HAP6. Arsenic removal efficiency of pure HAP was lowest at pH 7.0, so efficiency of nano HAP was checked at pH 7.0. A significant increase in arsenic removal efficiency is observed for nano HAP1, which is 38.27% and on the contrary this efficiency is 0.97% for pure HAP1.

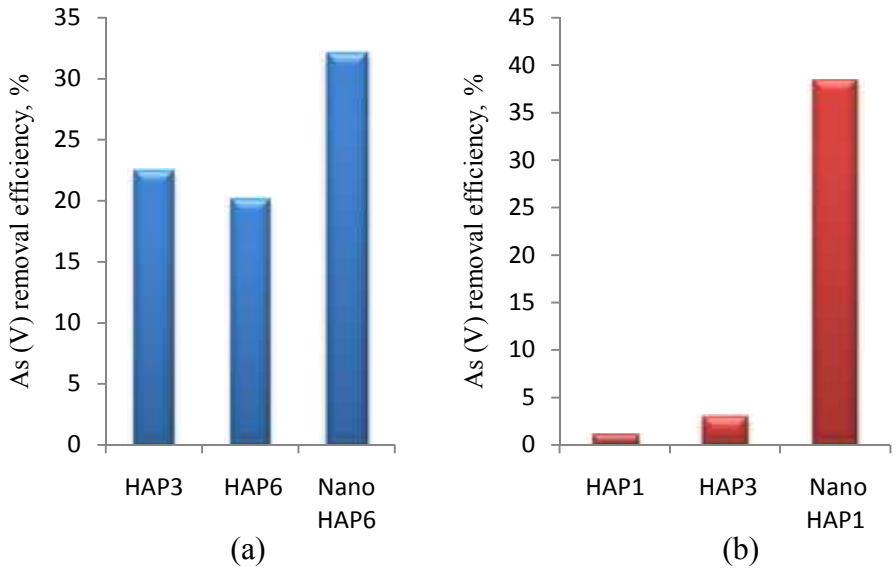

Figure 6.10 As(V) removal efficiency of pure and nano HAP at pH (a) 9.0 and (b) 7.0

6.6 Conclusions

Nano HAP could be synthesized by microemulsion method using non-ionic surfactant Triton X-100 and *n*-pentanol as oil phase, while calcium and phosphate precursors were used as water phase. Surfactant could be completely removed by thermally treating the nano HAP at 100°C and 600°C. A second phase can be identified in the product calcined at 600°C. Crystallinity of the products increases with increase in calcined temperatures and synthesized nano HAP shows higher surface area than that of pure HAP.

Arsenic removal efficiency of nano HAP was tested at pH 7.0 and 9.0, which shows a significant increase in arsenic removal efficiency in comparison to synthesized HAP micro particles. Nano HAP shows a promising development in removal of arsenic from aqueous system at pH 7.0, which would be helpful for the removal of arsenic from ground water as well.

For the first time, calcium precursor synthesized from eggshells was used to synthesis nano HAP by microemulsion method. Synthesized nano HAP is a useful product with great potential for the removal of arsenic from aqueous media. Additionally, synthesis of

nano HAP from eggshells will create a new dimension in waste management system by both using and reducing the environmental pollution.

References

1. Vallet-Regí M, González-Calbet J M, "Calcium phosphates as substitution ofbone Tissues", *Prog. Solid State Chem.*, **2004**, 32, 1-31.
2. Bajić Z.J., Djokić V.R., Veličković Z.S., Vuruna M.M., Ristić M.D., Issa N.B., Marinković A.D., "Equilibrium, kineticandthermodynamic studies on removal of Cd(II), Pb(II) and As(V) fromwastewater usingcarp (cyprinuscarpio) scales", *Dig. J. Nanomat. Biostruc.*,**2013**, 8, 1581–1590.
3. Anitha P., PandyaHaresh M., "Comprehensive review of preparationmethodologies of nano hydroxyapatite", *J. Environ. Nanotechnol*., **2014**, 3,
   101-121.
4. Singh S., Bhardwaj P., Singh V., Aggarwal S., Mandal U.K., "Synthesis of nano crystalline calcium phosphate in microemulsion-effect of nature of surfactants", *J. Colloid. Interf. Sci.*, **2008**, 319, 322-329.
5. ParsonsN.R., Mallick K.K.,"Rapid synthesis of nanocrystalline hydroxyapatite Frombiowaste eggshell viamicrowave irradiation for tissue engineeringapplications",*International Conference of Undergraduate Research (ICUR)*, **2013**, Univ. of Warwick, UK.
6. Frost Ray L., Musumeci Anthony W., Waclawik Eric R., "A spectroscopic study of the mineral paceite (calcium acetate)", *Spectrochim. Acta A,* **2007**, 67, 649-661.
7. XuG., AksayI. A., GrovesJ. T., "Continuous crystalline carbonate apatite thin films- abiomimetic approach," *J. Am. Chem. Soc.,* **2001**, 123, 2196-2203.
8. PrabakaranK., Rajeswari S., "Development of hydroxyapatite from natural fish bone through heat treatment", *Trends Biomater.Artif. Organ.*, **2006**, 20, 20-23.
9. Chen C.W., Oakes C.S., Byrappa K., Riman R.E., Brown K., TenHuisen K.S., JanasV.F., "Synthesis, characterization, and dispersion properties ofhydroxyapatite

prepared by mechanochemical-hydrothermal methods", *J. Mater.Chem.,* **2004**,14,2425-2432.

10. Regnier P., Lasaga A.C., Berner R.A., Han O.H., ZilmK.W., "Mechanism of CO_3^{2-} substitution in carbonate-fluorapatite: evidence from FT-IR spectroscopy,13C NMR, and quantum mechanical calculations", *Am. Miner.,* **1994**, 79,809–818.
11. AhmedS., AhsanM., "Synthesis of ca-hydroxyapatite bioceramic from eggshell and itscharacterization", *Bang. J. Sci. Ind. Res.*, **2008**, 43, 501-512.
12. Pillai R.S., Sglavo V.M., "Effect of MgO addition onsolidstate synthesis and thermal behaviorof beta-tricalcium phosphate", *Ceram. Int.*, **2015**, 41, 2512–2518.
13. SchroederL.W., MathewM.,"Cation ordering in $Ca_2La_8(SiO_4)_6O_2$,", *J. Solid State Chem.*, **1978**, 26, 383-387.
14. YasukawaA.,OuchiS., KandoriK., IshikawaT., "Preparation andcharacterization of magnesium-calcium hydroxyapatites," , *J. Mater. Chem.*, **1996**, 6, 1401-1405.
15. SingK., Everett D., Haul R., Moscou L., Peirotti R., Rouquerol J., "IUPAC commission on colloid and surface chemistry including catalysis", *Pure Appl. Chem*.,**1985**, 57,603–619.
16. Ki-Joong Kim, Ho-GeunAhn, "The effect of pore structure of zeolite on the adsorption of VOCs and their desorption properties by microwave heating", *Microporous Mesoporous Mater.,* **2012**,152, 78-83.
17. Omar W., Al-Itawi H., "Removal of Pb^{2+}ions from aqueous solutions by adsorption on kaolinite clay", *A. J. Appl.Sci*.,**2007**, 4, 502-507.
18. Czerniczyniec M., Farias S., MagallanesJ., Cicerone D., "Arsenic (V) adsorptiononto biogenic hydroxyapatite: solutioncompositioneffects", *Water, Air, Soil Pollut*., **2003**, 180,75-82.

CHAPTER 7

Treatment of waste water containing heavy metals using synthesized pure and doped HAP

7.1 Introduction

Hydroxyapatite is an important biomaterial and has been extensively used in biomedical field.[1] Due to its structural similarity with the mineral component of bones and teeth, HAP is often used for hard tissue repair. Besides biomedical applications, HAP has the high ability of ion exchange against cations and also a good adsorbent for inorganic materials.[2-6] Due to the large specific area, high thermal and chemical stability and high ionic exchange capacity HAP is selected as an adsorbent.[7] The prime focus of this chapter is to investigate the efficiency of synthesized pure and doped HAPs in treating heavy metals, in particular As(V), Pb(II) and Cr(VI) which often contaminate water resources in our country. Arsenic contamination has emerged as an alarming problem in this region over the decades. Arsenic has been reported in significant concentration in various countries such as Bangladesh, Chile, China and India.[8] Additionally Chromium(VI) from tannery industries and Pb(II) from other industries have increased the contamination level in many folds and this is now a big threat for us. In fact, environmental pollution caused by heavy metals is of great concern of the researchers due to negative impact of heavy metals on living organisms. In recent years, considerable effort has been made for the decontamination of the aqueous system. Adsorption process has been superior to other traditional methods used for the removal of heavy metals due to its low cost and is considered one of the most important processes of removing heavy metals from various wastewater sources.[9] In this study, we aimed at removing selected heavy metals from aqueous media by adsorption technique using synthesized and thermally treated pure and doped HAPs.

7.1.1 Heavy metals contamination problem in Bangladesh: Present scenario

There are many industries in Bangladesh, namely tannery, paper and pulps, textiles, carbides, pharmaceuticals, pesticides etc. which discharge heavy metals like cadmium, lead, chromium, mercury, zinc, arsenic with their effluents and wastes.[10] Even trace amounts of these metals, inhibit the activity of enzymes in living cells.[11] Therefore their discharge into the environment must be minimized and carefully controlled. In the following discussion arsenic contamination in Bangladesh is highlighted, as removal of arsenic from aqueous system has so far been thoroughly studied here.

Arsenic contaminated tube well water was first detected in Bangladesh in early 1990s.[12] Natural sources including some minerals are the major reasons for high level of arsenic contamination in natural water, together with some anthropogenic activities such as, extensive use of arsenic in pigments, wood preservatives, paints, dyes, pharmaceuticals, semiconductors, insecticides and herbicides.[13] About 70% of arsenic is used in pesticides.[14] The United States Environmental Protection Agency (EPA) set the maximum contaminant level (MCL) for arsenic at 10 μgL^{-1} in January 2001.[15] Before 2001, the MCL was 50 μgL^{-1}, still the arsenic limit in Bangladesh is set to 50 μgL^{-1}.[16]

The visible symptoms caused by long term arsenic exposures include lesions, hardening of the skin, dark spots on hands and feet along with skin cancer and internal cancers of other organs, which can be fatal.[17] Currently Bangladesh is facing the world's most serious arsenic crisis and it is estimated that 40-60 million people of the country's total population are at risk of exposure to arsenic in their drinking water over the Bangladesh standard of 50 μgL^{-1}.[18,19] The high exposure of arsenic has led to arsenicosis in millions of people in Bangladesh and the issue has yet to be resolved.

As mentioned in Chapter1, arsenic exists in nature in the oxidation states +V (arsenate), +III (arsenite), 0 (arsenic) and -III (arsine). In aqueous systems, arsenic exhibits anionic behavior. Moreover, change in pH of the system is always associated with protonation/deprotonation of the arsenic species in both arsenate and arsenite which is depicted in Figure 7.1.[20]

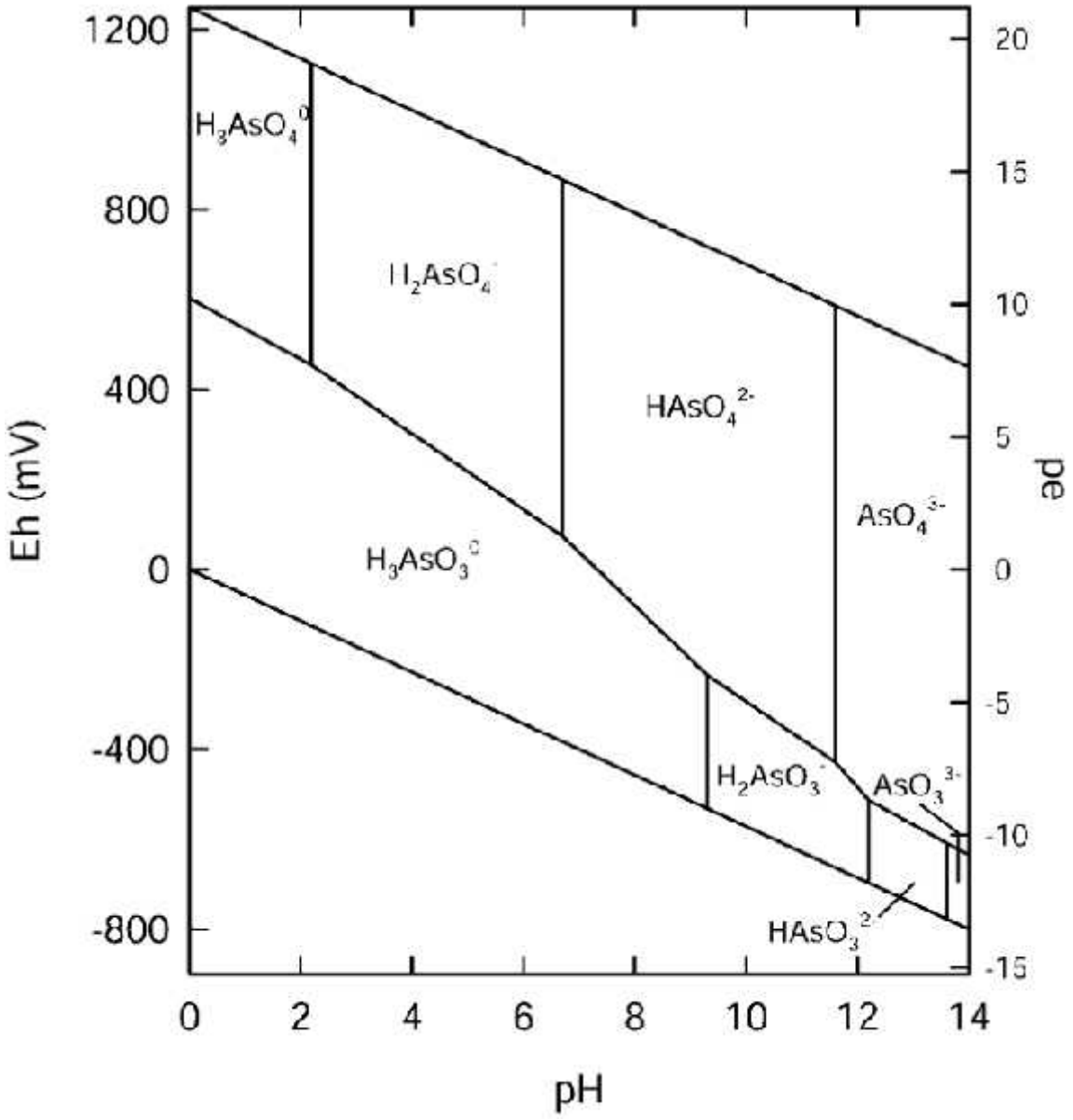

Figure 7.1 Pe-pH diagram for arsenic species

One of the conditions that may affect arsenic valence and speciation is pH that is described in the Figure 7.1 and it can be stated that in the pH range of 4.0 to 10.0, As(V) species are negatively charged in water, and As(III) species are neutral in charge.[19] In Bangladesh, standard pH value for waste from industrial units is determined to be in the range 6.0-9.0, however researchers found the pH values in the range 3.0-9.0 in waste

water samples in Bangladesh.[21] Consequently As(V) species has been selected for this study which exists in anionic species in aqueous media.

Chromium is often released into the environment from tanneries, laboratory analysis, electroplating, paint and dyestuff, rubber and plastics, textile industries, oxidants and cleaning agents.[22] Several studies showed the serious contamination of soil and water of Hazaribagh tannery area with Cr, Zn, and Pb in addition to some organic pollutants.[23] The Department of Environment (DoE) of Bangladesh has categorized this area as a red zone. Moreover, increased use of fertilizer, paints and anti-rust agents increase Pb(II) contamination in water. Chromium is a highly toxic heavy metal for microorganisms, humans, animals and plants. Lead has harmful effect on human nervous system and children are more susceptible to lead poisoning.

According to the EPA the maximum permissible limit for Cr(VI) for discharge into inland surface water is 0.1 mg L^{-1} and in potable water is 0.05 mg L^{-1} and for Pb(II) it is 0.015 mgL^{-1}.[24]

Chromium in environment occurs in both +VI and +III oxidation states. In contrast to the low mobility of Cr(III), Cr(VI) is more soluble, mobile and toxic. It is noteworthy that chromium is thermodynamically stable in both Cr(VI) and Cr(III) state in the presence of atmospheric oxygen depending on pH. Under oxidizing conditions, Cr(III) is stable as Cr^{3+} at pH < 2.0 and Cr(VI) is stable at higher pH. Pe-pH diagram of chromium species is presented in Figure 7.2.

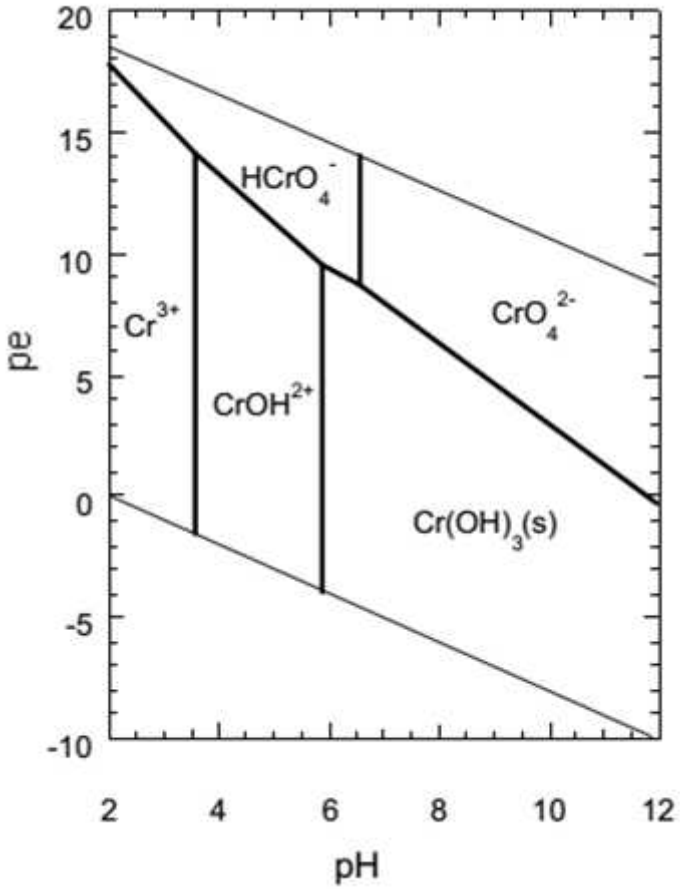

Figure 7.2 Pe-pH diagram for chromium species

Cr(VI) is predominantly present in the form of hydrogenchromate ($HCrO^{-4}$) between pH 1.0 and 6.5 and chromate (CrO_2^{-4}) at higher pH values. In concentrated, acidic solutions, dichromate ($Cr_2O_2^{-7}$) may exist, but it reverts rapidly to hydrogenchromate or chromate upon dilution or neutralization. Chromium(VI) compounds are found to be more toxic than Cr(III) compounds because of the high solubility and mobility of Cr(VI) in water.

7.2 Materials and methods

7.2.1 Preparation of standards and reagent

Stock solution of As(V) (1000 mg L^{-1}) was prepared by dissolving specific quantity of sodium arsenate ($NaH_2AsO_4.7H_2O$) in de-ionized water. Subsequently working solutions

of required concentrations for the adsorption experiments were prepared from the stock solution by proper dilution. For the analysis of As(V), 500 mL reducing solution was prepared by dissolving 0.5 g NaOH and 1.5 g $NaBH_4$, in de-ionized water and adding water up to the mark in a volumetric flask. $NaBH_4$ was always prepared immediately before use. Hydrochloric acid and potassium iodide (KI) solution were prepared according to the standard operating procedure (SOP) used to determine As(V) by HG-AAS.

Standard solutions for chromium and lead were prepared following the similar procedure used in the case of arsenic. The concentration of the Cr(VI) was measured by UV spectrophotometer (Hitachi, UV 2910, Japan) and concentration of Pb(II) was determined by flame-AAS (NOVAA 350, Analytik Jena, Germany).

7.2.2 Determination of Zero Point Charge (ZPC)

It is well established that pH of the zero point charge (pH_{ZPC}) plays an important role in the adsorption process, hence prior to the adsorption study pH_{ZPC} was determined according to the procedure reported by Rivera-Utrilla *et. al.*[25] For this work, 50 mL of 0.01 M of sodium chloride (NaCl) solution was placed in a 100 mL Erlenmeyer flask with stopper. The pH of the solution was adjusted to 2.0–9.0 by adding 0.1 M HCl or 0.1 M sodium hydroxide solutions and 0.15 g of adsorbents (pure HAP, Fe-HAP and Cu-HAP each separately) were added to the solution. The mixtures were then kept for 24 hrs. at 30°C. The final pH value of each suspension was recorded after 24 hrs. using a pH meter (H1 2211pH Meter, HANNA instruments). The ZPC of the sample was calculated by plotting ΔpH (initial pH – final pH) versus pHi (initial pH) and shown in Figure 7.3.

7.2.3 Adsorption of heavy metals on pure and doped HAP

Adsorption experiments were carried out in series of 100 mL reagent bottle with stopper by adding specific amount (1-10 gL^{-1}) of the synthesized pure HAP, Fe-HAP and Cu-HAP in 50 mL of synthetic metal ion solution. Stoppers were provided to avoid change in concentration due to evaporation. The pH of the test solutions was adjusted using

required amount of 0.1M HCl or 0.1M NaOH solution. All the adsorption experiments were performed in ambient temperature (30º ± 1º C). The reagent bottle containing the substrate solution and the adsorbent were shaken at 150 rpm for the desired period of contact time in an electrically thermostatic shaking water bath (SBS40, Stuart, Bibby Scientific, UK). The time required to reach the equilibrium condition was estimated at regular interval of time till equilibrium was reached. The contents were then centrifuged at 2000 rpm for 15 mins and the supernatant liquid was analyzed for heavy metal ions concentration using appropriate instrument. As(V) concentration was measured by hydride generated system HG-AAS (NOVAA 350, Analytik Jena, Germany). Standards for calibration were prepared from the As(V) stock solution supplied by Sigma-Aldrich, Switzerland, concentrations of the standard solutions were 2, 5, 10 and 20 μgL^{-1}. The samples and standards for arsenic analysis were reduced from As^{5+} to As^{3+} prior to analysis and this was achieved by adding a reducing solution of 50% (w/v) KI. 10 mL volume of standard or sample was placed in a 100 mL volumetric flask and 1/2 mL of 50% KI solution and 5 mL of concentrated HCl was added. The volumetric flask was filled up to the mark with de-ionized water and after 30-60 min the samples were ready for necessary measurements. All glass containers were cleaned properly followed by washing with de-ionized water before use to avoid any contamination. The produced hydrides are volatile and transported to a quartz cell which is heated to 950°C by means of an argon carrier gas.

The adsorption capacity of the metal ion adsorbed per gram of adsorbent was calculated according to the following equation.

$$q_e = (C_i - C_f)\, V/M \qquad (7.1)$$

Percent of adsorption efficiency was calculated following the equation,

$$\text{Adsorption efficiency, \%} = (C_i - C_f) \times 100 / C_i \qquad (7.2)$$

Where C_i and C_f are the initial and final concentrations of the As(V) in the aqueous solution in μgL^{-1}, V is the volume of the adsorbate solution in L and M is the mass of the adsorbents in g used, so adsorption capacity will be μgg^{-1}.

Various parameters were considered while carrying out the adsorption study:

i. Effect of contact time
ii. Effect of pH
iii. Effect of adsorbent dosage
iv. Effect of initial metal ion concentration

7.3 Results and discussion

7.3.1 Zero Point Charge (ZPC) of pure and doped HAP

The pH $_{ZPC}$ can be defined as the pH at which charges on the surface of the adsorbents become zero. A plot of ΔpH (initial pH – final pH) versus pHi (initial pH) is shown in Figure 7.3. This plot was used to calculate the ZPC value for each adsorbent. The ZPC values were calculated from the intercept of the curve.

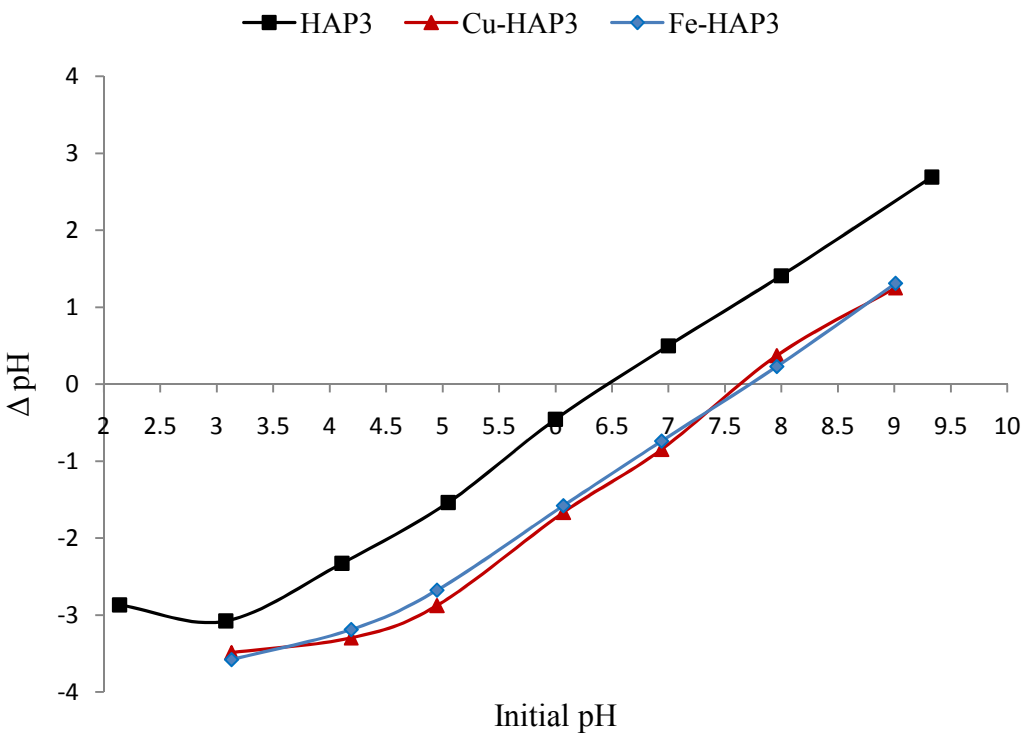

Figure 7.3 Determination of zero point charge (ZPC) of thermally treated pure and doped HAP

Results of pH_{ZPC} of thermally treated pure and doped HAP are illustrated in Table 7.1.

Table 7.1 Results of ZPC for pure and doped HAP

Sample calcined at 300°C	pH at ZPC
HAP	6.5
Cu-HAP	7.6
Fe-HAP	7.8

Results indicate that at $pH < pH_{ZPC}$, adsorbents possess positive charge on their surface, at $pH > pH_{ZPC}$ the surface contain negative charge.

7.3.2 Selection of pure and doped HAP as adsorbents

As discussed in the preceding chapters, it is obvious that BET specific surface area, pore volume, and mean pore diameter of the pure and doped HAP increase when the materials are thermally treated at 300°C in all cases. XRD patterns are almost similar for all samples which indicate that apatite phases remain unchanged in the synthesized doped HAP. BET specific surface area increases with increase in copper content in the doped samples from 2 wt% to 6 wt%. In case of Fe-HAP samples BET surface area shows higher value for 2 wt% and 4 wt%Fe-HAP3, and then decreases with increase in iron content from 4 wt% to 6 wt%. Therefore, pure and doped HAP calcined at 300°C are expected to be good adsorbents and have been selected for the study of the removal of heavy metal ions from waste water.

7.3.3 Adsorption of As(V) on synthesized pure and doped HAP

7.3.3.1 Effect of pH

pH is one of the most important factors which influences the adsorption process and strongly controls the speciation of the arsenic in aqueous system (Figure 7.1). pH of the

solution determines the availability of the specific arsenic species for adsorption in a particular environment. The effect of pH on adsorption of arsenate ion on thermally treated synthesized pure and doped HAP was investigated by varying the solution pH from 2.0 to 9.0. Other conditions for adsorption of arsenate ion on HAP and doped HAP were established by the experiments, while temperature was maintained at 30°C with contact time 60 min and As(V) concentration was 100 µg L^{-1}, adsorbent dose was maintained 1 gL^{-1}. Figures 7.4 and 7.5 show the effects of pH on adsorption of As(V) on pure HAP, Cu-HAP and Fe-HAP.

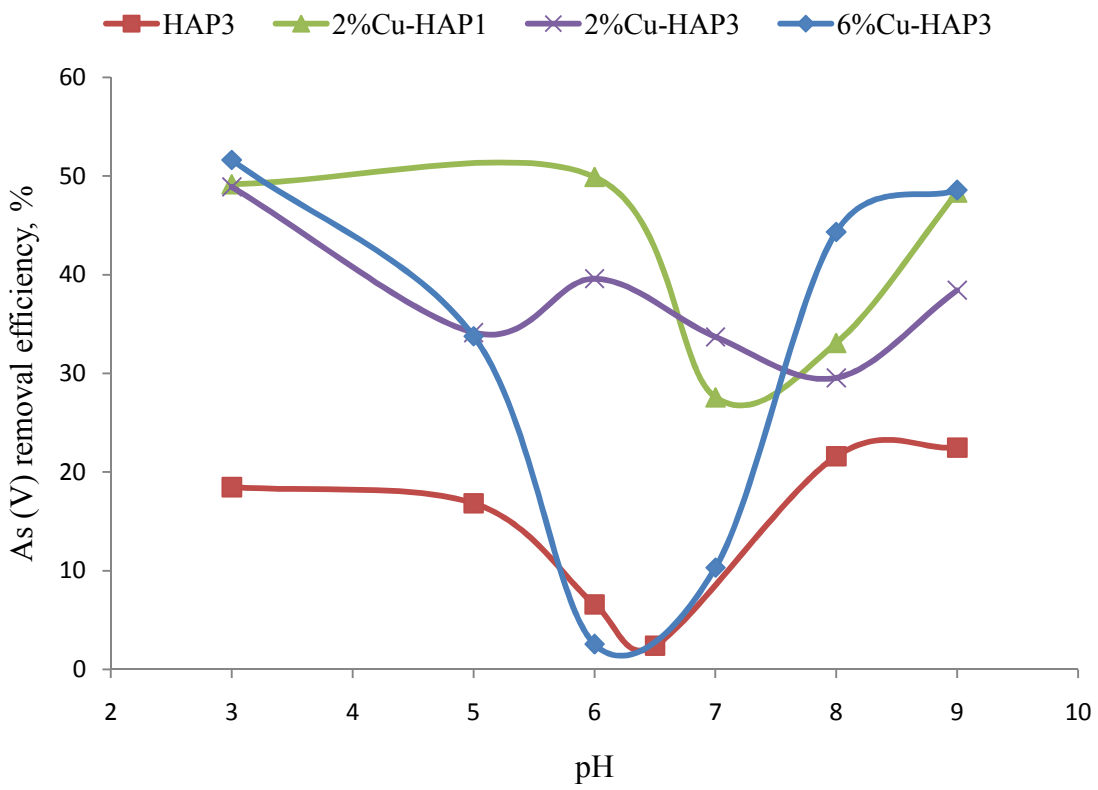

Figure 7.4 Effect of pH on removal of As(V) using thermal treated pure and Cu-HAP

It is worth mentioning that the influence of pH at values lower than 3.0 could not be studied due to the fact that the adsorbents was not stable at pH lower than 3.0. Figure 7.1 shows that in aqueous system As(V) (arsenate) is stable in oxidative condition and exists as a monovalent ($H_2AsO_4^-$) anion at pH range of 3.0-6.8 or as divalent ($HAsO_4^{2-}$) anion

at pH range of 7.0-11.0. At lower pH, surface of HAP and Cu-HAP become highly protonated (< pH_{PZC}) which is favorable for removal of As(V) as the species exists as monovalent anion. For this reason, relatively higher removal efficiency for As(V) is observed at low pH. Moreover, lowest removal efficiency is observed at pH 6.0-7.0, which may be attributed to the pH_{ZPC} values for HAP and Cu-HAP (pH_{ZPC} 6.5 and 7.6). A neutral charge condition is developed on surface of the selected adsorbents at pH 6.0-7.0. With further increase in pH, As(V) removal efficiency of the adsorbents and efficiency increases to reach a maximum at pH 9.0. Adsorption of As(V) anionic species on negatively charged surface (> pH_{PZC}) of the adsorbents can be easily visualized. This indicates the exchange of arsenate for phosphate in the HAP structure.[26]

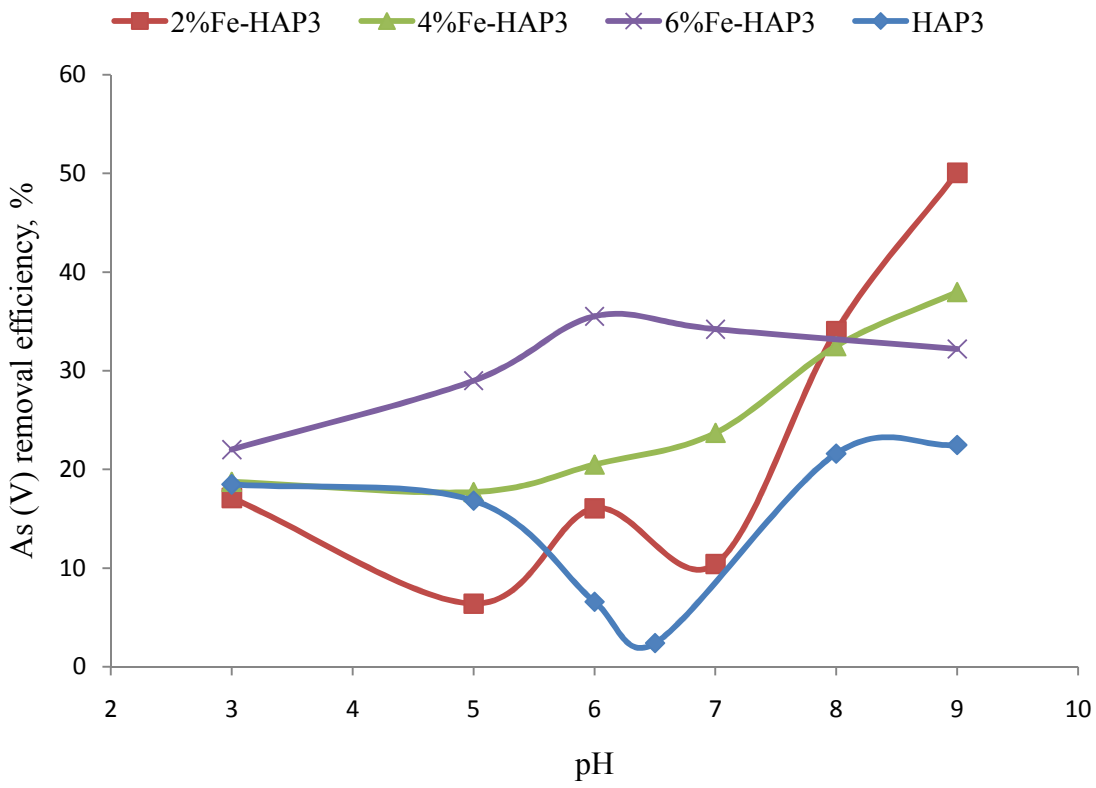

Figure 7.5 Effect of pH on removal of As(V) using thermal treated pure and Fe-HAP

Several Fe(III) oxides, poorly crystalline hydrous ferric oxides (ferrihydrite), zero valent iron (ZVI) and other iron coated materials are well-known for their ability to remove arsenic from aqueous solutions.[27-31] ZVI and other iron compounds have high efficiencies for arsenate removal only at low pH values.[32] In this study, synthesized Fe-HAP show higher efficiency for removal of As(V) from aqueous system at pH 9.0 (Figure 7.5). A gradual increase in arsenic removal efficiency is observed with increase in pH from 3.0 to pH 9.0 for calcined 2% and 4%Fe-HAP. This result indicates the probability of anion exchange between arsenate and phosphate due to their similar ionic radii (AsO_4^{3-}: 248 nm and PO_4^{3-}: 238 nm). However 6%Fe-HAP3 shows higher As(V) removal efficiency at pH 6.0 which is below pH_{PZC} of the sample. This implies the adsorption of anionic arsenate species is also favorable on cationic surface of 6%Fe-HAP3. It is also remarkable that arsenic adsorption decreases with increase of iron content in Fe-HAP. This may be due to the decrease in total surface area of the Fe-HAP samples and also blocking of pores by Fe^{3+} ion, as indicated by the specific surface area analysis as discussed in Chapter 4.

7.3.3.2 Effect of contact time

Contact time is also an important factor that affects the removal efficiency of the adsorbent. Figure 7.6 shows the effect of contact time on the percentage removal of As(V) using pure and doped HAP at optimum pH and at 30°C temperature, initial As(V) concentration was 100 μgL^{-1}.

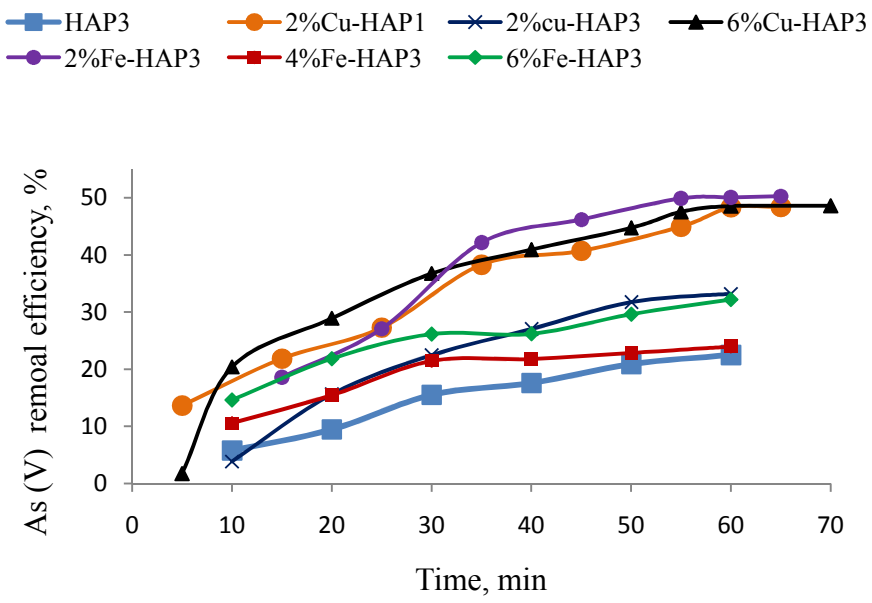

Figure 7.6 Effect of contact time on adsorption of As(V) on pure and doped HAP

The percentage of As(V) removal efficiency increase with increasing the contact time. Most of adsorption takes place in the initial 20-30 min and then increases slowly and reaches the maximum adsorption in about 50 to 60 min for all adsorbents. For thermally treated pure HAP 15.5% adsorption occurs in the first 30 min and thereafter the rate of adsorption is found to be slow (22.48%) and reaches equilibrium at 60 min. Nevertheless initial adsorption efficiency of Cu-HAP and Fe-HAP are in the range of 23-38% and 23-42% respectively which finally reached at equilibrium with 33-49% and 24-50% adsorption efficiency. It is obvious from Figure 7.6 that doping of pure HAP increases the adsorption capacity by approximately two fold for both Fe(III) and Cu(II) doped products. Rate of removal of As(V) is higher at the initial stage, due to the availability of more active sites on the surface of pure as well as doped HAP. The rate is slower at the later stages of contact time probably due to the electrostatic hindrances between negatively charged arsenate species adsorbed on the surface of adsorbents and also due to the reduction of active sites on adsorbents.[33] Another reason of slower adsorption rate of later part of curve in Figure 7.7, may be due to the slower rate of diffusion of arsenate ions on metal ion doped HAP.[34]

7.3.3.3 Effect of adsorbent dosage

Figure 7.7 shows the effect of dosage variation of pure and doped HAP on As(V) removal keeping the equilibrium conditions constant. Mass of adsorbent used is an important parameter for the adsorption process because this factor determines the efficiency of an adsorbent for a given initial concentration of the adsorbate. The equilibrium conditions for studying the adsorption of arsenate are as follows: temperature- 30°C, contact time- 60 min, pH- 9.0 and initial concentration of arsenate ion- 100 μgL^{-1}.

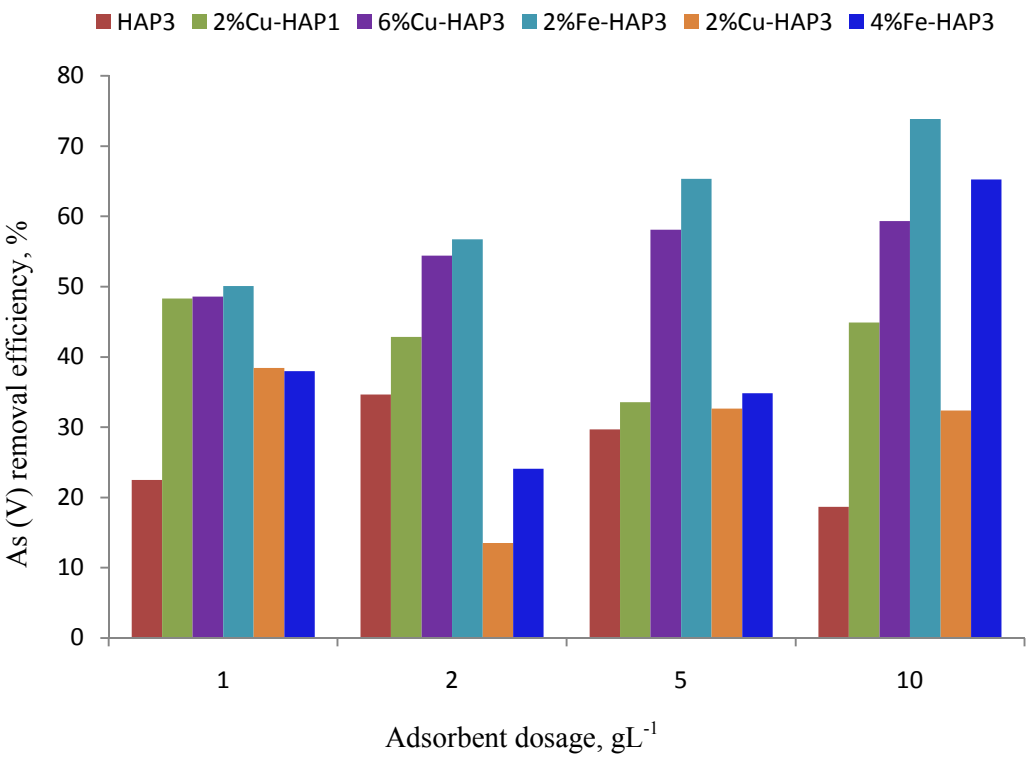

Figure 7.7 Effect of adsorbent dosage on adsorption of As(V) on pure and doped HAP

Figure 7.7 shows adsorption of arsenate on pure HAP3 decreases from 22.48% to 18.69% as adsorbent dosage increases from 1 gL^{-1} to 10 gL^{-1} with a slight increase in the adsorption capacity at HAP3 dosages of 2 and 5 gL^{-1}. Adsorption of As(V) from aqueous media involves exchange of phosphate ion with arsenate ion and concentration of

phosphate ion in the solution enhances with increase of exchange of arsenate and phosphate ions. As a consequence, adsorption of arsenate ion on HAP is reduced due to presence of higher phosphate content in solution while quantity of HAP increases in the adsorption system.[35] Another reason for reduced adsorption capacity of pure HAP3 is due to the lower surface area of the sample which contains less active sites for adsorption. It is also evident from Figure 7.7 that adsorption capacity of 2%Fe-HAP3 enhances from 50% to 74% with the increase of adsorbent dosage from 1 gL^{-1} to 10 gL^{-1}. Adsorption capacity of 4%Fe-HAP3 increases from 38% to 65% for similar increment of adsorbent dosage. For 6%Cu-HAP3 this capacity enhances from 49% to 60% while this increment is not significant in case of oven dried and thermally treated 2%Cu-HAP. In cases of doped HAP, specific surface area of the calcined products are higher in comparison to the pure HAP, so higher adsorption efficiency is observed due to the availability of active sites on the materials. Moreover, incorporation of ferric ion in HAP structure enhances As (V) adsorption capacity of Fe-HAP in comparison to pure HAP.[36]

7.3.3.4 Effect of initial As(V) concentration

Initial concentrations of arsenate ion were varied in the range of 65-170 μgL^{-1} and adsorption on pure and doped HAP samples were investigated maintaining adsorbent dosage 2 gL^{-1} at pH 9.0 for 60 min at 30°C temperature. Figure 7.8 reveals that adsorption efficiency is higher at lower initial arsenic concentration (50 and 90 μgL^{-1}) and gradually decreases with increase in initial arsenic concentration. The reason for the decrease in As(V) removal efficiency at higher initial concentration may be due to saturation of the active sites of the adsorbent by the As(V) and hence, further increase in As(V) concentration does not bring about an increase in adsorption significantly.

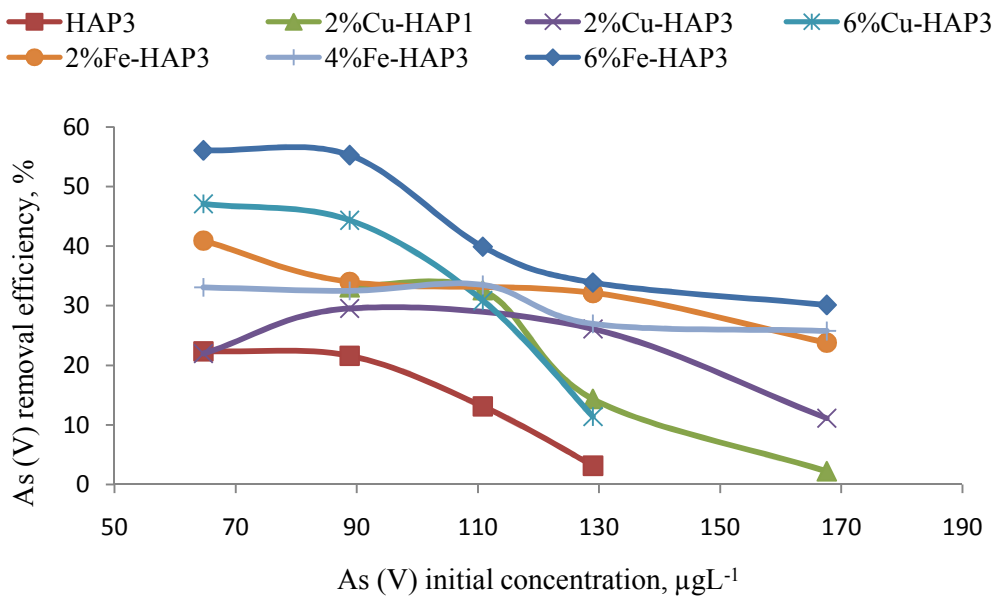

Figure 7.8 Effect of initial As(V) concentration on adsorption on pure and doped HAP

From Figure 7.8 it is observed that Fe-HAP shows a gradual decrease in adsorption efficiency with increase in initial As(V) concentration, from 56% to 30% for 6%Fe-HAP3, from 33% to 26% for 4%Fe-HAP3 and from 41% to 24% for 2%Fe-HAP3. On the other hand, arsenate removal efficiency rapidly decreased from 22% to 3% for pure HAP on variation of initial As(V) ion concentration. Nevertheless, Cu-HAP shows (Figure 7.8) a sharp decrease in As(V) removal efficiency with increase in initial As(V) concentrations and these are: from 47% to 11% for 6%Cu-HAP3, from 22% to 11% for 2%Cu-HAP3 with an initial slight increase to 29.56% and from 33% to 2.21% for 2%Cu-HAP1. Presence of Fe^{3+} ions in the adsorbents enhances the adsorption efficiency in comparison to pure and Cu-HAP.[36]

7.3.4 Adsorption of Cr(VI) and Pb(II) using synthesized pure and doped HAP

After revealing the arsenic removal efficiency of synthesized pure and doped HAPs, investigation was continued for the study of removal of Cr(VI) and Pb(II) from aqueous system with the same adsorbents.

7.3.4.1 Effect of pH

Chromium removal

Figure 7.9 shows the effect of pH on Cr(VI) and Pb(II) removal using selected synthesized HAPs. Adsorbents were selected by considering the efficiency of HAPs in removing arsenic from aqueous system. Hence HAP3, 6%Cu-HAP3 and 6%Fe-HAP3 were selected for this adsorption study. Here pH was varied from 3.0 to 9.0 and other conditions for adsorption of chromate ion on HAP and doped HAP were kept constant as temperature was maintained at 30°C with contact time 20 min and Cr(VI) initial concentration was 100 μgL^{-1}, adsorbent dose was maintained 1 gL^{-1}.

Cr(VI) adsorption efficiency for HAP3 shows its maximum value 35% at pH 9.0, while this value is 90% for 6%Cu-HAP3 at pH 6.0. This indicates the anionic exchange of chromate and phosphate ion in pure HAP3 structure at a pH higher than pH_{ZPC} of the sample. Furthermore, in case of 6%Cu-HAP3 removal of chromate ion takes place at pH less than pH_{ZPC} which implies that adsorption efficiency takes place largely due to the electrostatic attraction between positively charged surface of the sample and $HCrO^{4-}$ ion in the solution. Figure 7.2 shows the presence of $HCrO^{4-}$ ion in aqueous solution at pH range 0.0 to 6.5. On the contrary, chromium removal efficiency of 6%Fe-HAP3 shows (Figure 7.9) a maximum value 27% at pH 3.0. This result also explains the electrostatic attraction between surface cation of the sample and chromate ion in solution. Nevertheless 6%Cu-HAP3 shows high potential in removing chromate ion due to its higher surface area in comparison to other two adsorbents.

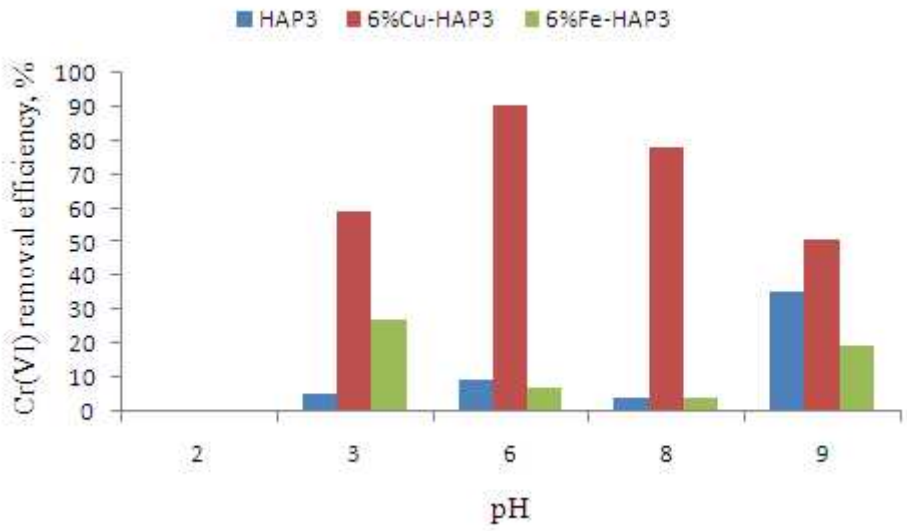

Figure 7.9 Effect of pH on thermal treated pure and doped HAP in removal of Cr(VI) from aqueous system

Lead removal

Selection of the adsorption was done by the assessment of the adsorbents used in removal of arsenate and chromate ions from aqueous system. Higher surface area of 6%Cu-HAP3 and 2%Fe-HAP3 is considered as an important property of a potential adsorbent and Figure 7.9 shows higher Cr(VI) removal efficiency using 6%Cu-HAP3. 2%Cu-HAP1 was selected for its high efficacy in removing arsenate ion and HAP3 was selected for making a comparison with other adsorbents under study. In this part of experiment pH was varied from 3.0 to 8.0 and other conditions for adsorption of lead ion on HAP and doped HAP were kept constant as temperature was maintained at 30°C with contact time 30 min and Pb(II) initial concentration was 5 mg L^{-1}, adsorbent dose was maintained 1 gL^{-1}. Figure 7.10 shows the lead removal efficiency of the selected adsorbents at different pH. Pb(II) removal efficiency of HAP3 and 2%Cu-HAP1 at pH 3.0 are 84.13% and 86.80% respectively. This implies that exchange of Ca^{2+} ion with Pb^{2+} ion takes place at pH 3.0 which is less than pH_{ZPC} of the samples.

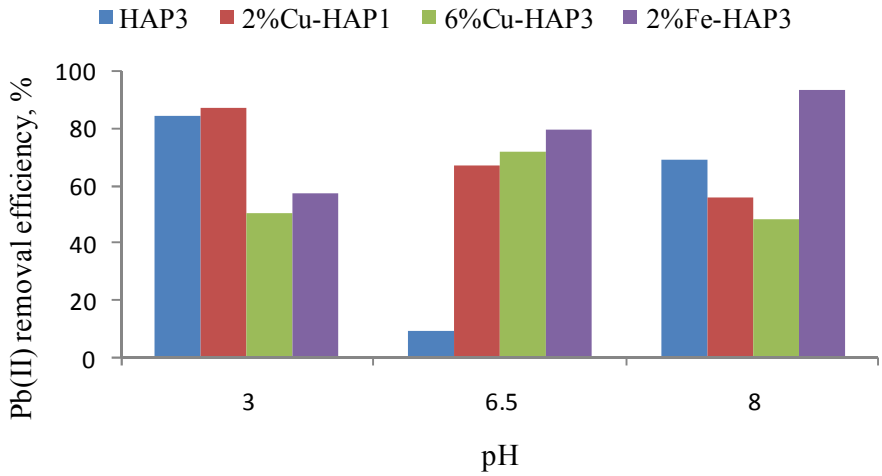

Figure 7.10 Effect of pH on thermal treated pure and doped HAP in removal of Pb(II) from aqueous system

6%Cu-HAP3 shows its maximum lead removal efficiency 71.70% at pH 6.5 which is also less than pH_{ZPC} of the sample. Furthermore 2%Fe-HAP3 shows an increased efficacy with 93.14% in removal of lead ion at pH 8.0. This indicates both ion exchange of Ca^{2+} ion by Pb^{2+} ion and electrostatic attraction between Pb^{2+} ion and PO_4^{3-} ion on HAP surface occurs in removing lead from aqueous medium.

7.3.4.2 Effect of contact time

Chromium removal

Removal of chromate ion from aqueous solution depends on the contact time of the adsorbent and adsorbate solution keeping other adsorption parameters constant. Experiment was conducted by varying the contact time from 5 to 25 min. Adsorption of chromate ion from aqueous system was studied while other conditions were kept constant. The percent of removal of chromate ion increases with increase in contact time from 5 min to 25 min and reaches at equilibrium at 20 min (Figure 7.11) for all selected adsorbents at the same adsorption condition.

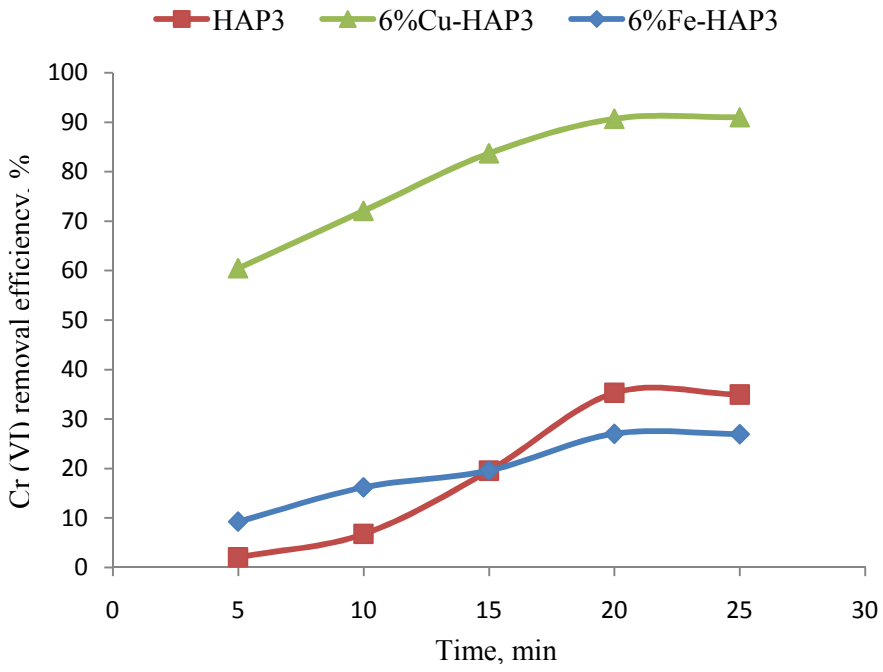

Figure 7.11 Effect of contact time on thermal treated pure and doped HAP for removal of Cr(VI) from aqueous system

The chromate ion removal efficiency increases initially due to the availability of more active sites on the surface of pure and doped HAP. 6%Cu-HAP3 shows the maximum Cr(VI) removal efficiency 90.70% at pH 6.0 and temperature 30°C. Pure HAP3 shows higher efficiency (35.29%) for the removal of chromate ion than that of 6%Fe-HAP3 which is 27.03%. High efficiency of 6%Cu-HAP3 can be explained by higher surface area of the sample compare to HAP3 and 6%Fe-HAP3 samples. It is known that at pH > 6.5, Cr(VI) anions are present in solution as CrO_4^{2-}, but the principal species are $HCrO_4^-$ at pH 6.5 which is used in this adsorption process. The adsorption of CrO_4^{2-} requires two adsorption sites, whereas in the case of $HCrO_4^-$ one active adsorption site is needed. As a result higher Cr(VI) adsorption capacity is obtained at pH 6.0.

Lead removal

Lead adsorption study was carried out as a function of contact time. The adsorption capability of thermally pure HAP was compared with that of thermally doped HAP in

Figure 7.12. It can be seen that the removal efficiency increases with the increasing of the contact time for all adsorbents used in this study. The maximum value of removal efficiency of HAP3 is 84.13% reached at equilibrium at 40 min, while in case of 2%Fe-HAP3 is 93.14% reached at equilibrium at 30 min. Pb(II) removal efficiency of 2%Cu-HAP1 and 6%Cu-HAP3 are 86.80% and 71.70% respectively which reached at equilibrium at 30 min. The shorter period necessary to reach the equilibrium indicates strong interactions between Pb(II) and doped HAP. Pb(II) removal efficiencies of pure and doped HAP were measured at the pH at which the corresponding adsorbent shows a maximum efficiency. The faster rate for Pb(II) removal process and the high value of the removal efficiency direct to the conclusion that the synthesized Fe doped HAP can be successfully used in the retention of lead ions from aqueous system.

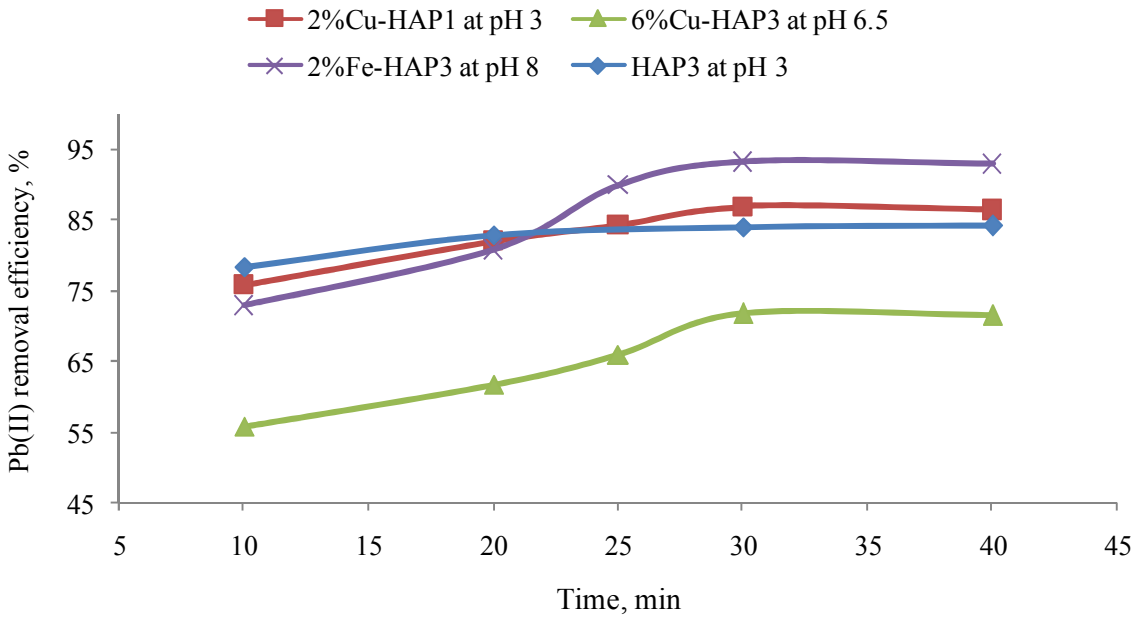

Figure 7.12 Effect of contact time on thermally treated pure and doped HAP for removal of Pb(II) from aqueous system

7.3.5 Adsorption isotherm for As(V)

Adsorption is generally described through isotherms, the amount of adsorbate on the adsorbent as a function of its pressure or concentration at constant temperature.[37]

Adsorption of As(V) on pure and doped HAP were carried out at 30°C temperature at pH 9.0 and by varying the initial concentration of As(V). The adsorption isotherm shows the relationship between adsorbate concentration and degree of accumulation on adsorbent surface. In other words, isotherm also can provide information on the capacity of the adsorbent or the amount required for removing a unit mass of pollutant under the operating conditions. In this study, adsorption isotherms are developed by exposing different initial concentration of As(V) in 10 mL of liquid for 60 min at optimum pH 9.0 and at 30°C temperature for synthesized pure and doped HAP. Adsorption behaviors of thermally treated pure and doped HAP are studied using isotherms, namely, Langmuir, Freundlich and Temkin adsorption isotherms.

7.3.5.1 Langmuir isotherm

The Langmuir adsorption isotherm describes quantitatively the build up of a layer of molecules on an adsorbent surface as a function of the concentration of the adsorbed material in the liquid phase in which it is in contact. The Langmuir isotherm is the simplest of all mechanistic models and it is based on the assumptions that adsorption cannot proceed beyond monolayer coverage on a surface containing finite number of adsorption sites. It also assumes that adsorbent surface have adsorbent sites of same adsorption energy and there is no lateral interaction between adsorbed molecules. When the whole surface of the adsorbent is completely covered by a unimolecular layer of the adsorbate further adsorption is not possible and it indicates a saturation of adsorption.

The Langmuir isotherm model can be represented as follows

$$q_e = q_{max} \frac{K_L C_e}{1 + K_L C_e} \tag{7.3}$$

Linear form of Langmuir isotherm model can be shown as follows

$$\frac{C_e}{q_e} = \frac{1}{k_L q_m} + \frac{C_e}{q_m} \tag{7.4}$$

Where q_e is the adsorption capacity at equilibrium ($\mu g g^{-1}$), q_{max} is the theoretical maximum adsorption capacity of the adsorbent ($\mu g g^{-1}$), K_L is the Langmuir constant ($L\mu g^{-1}$) and C_e is the equilibrium As(V) concentration in the solution ($\mu g L^{-1}$). The Langmuir adsorption isotherm data for As(V) adsorption on pure and doped HAP are graphically presented as a function of C_e vs C_e/q_e in Figure 7.13. The values of q_m and K_L are calculated from slope and intercept of the graphs respectively which is presented in Table 7.2.

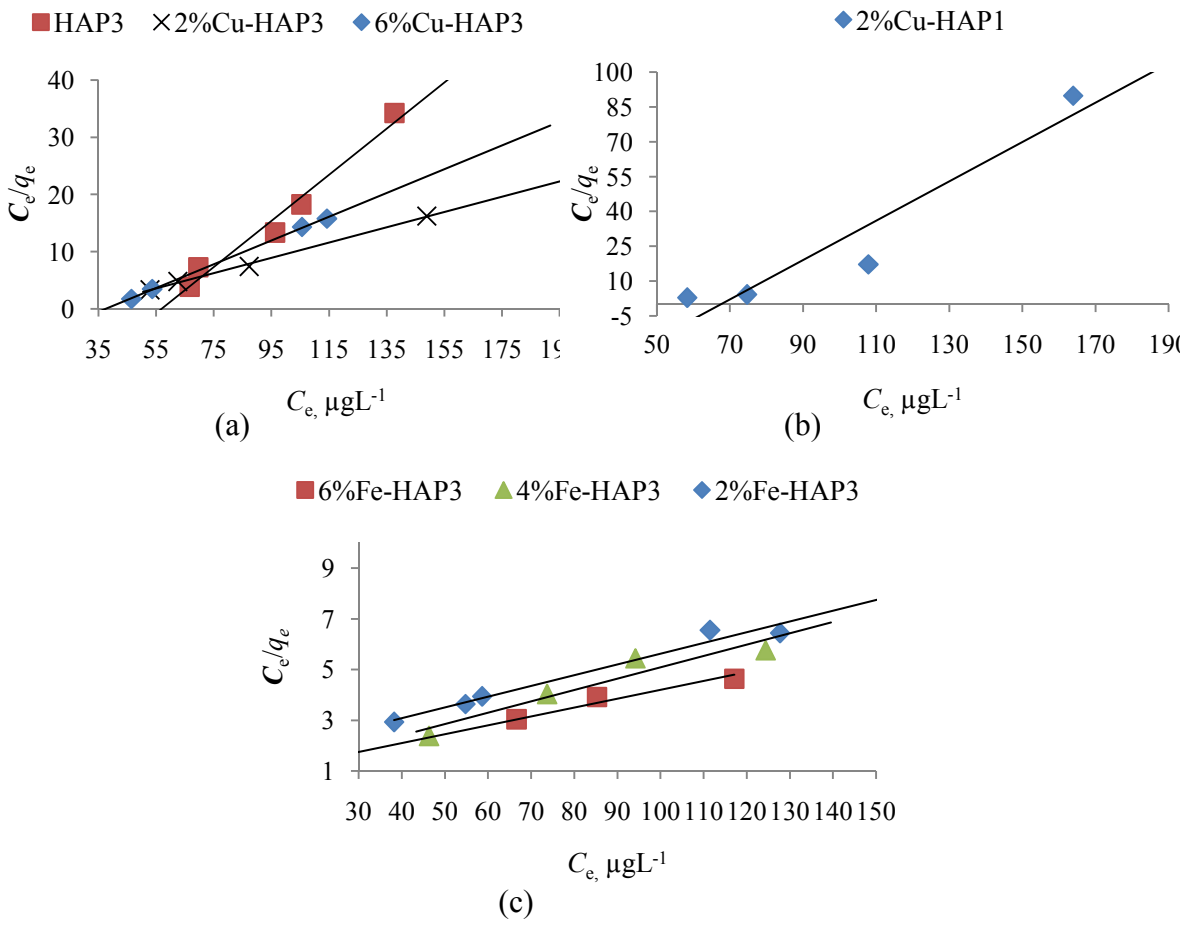

Fig. 7.13 Langmuir isotherm plot for As(V) adsorption on (a) thermally treated pure and Cu-HAP, (b) oven dried 2%Cu-HAP and (c) thermally treated Fe-HAP

A dimensionless equilibrium parameter, R_L which is the essential characteristics of Langmuir isotherm describes the type of isotherm. R_L can be calculated from Langmuir

constant k_L and the initial concentration of the adsorbate solution, C_0 by following equation and results are given in Table 7.2.

$$R_L = \frac{1}{1 + k_L C_o} \quad (7.5)$$

Where C_0 (μgL^{-1}) is the initial As(V) ion concentration and k_L ($L\mu g^{-1}$) is Langmuir constant. The value of R_L indicates the shape of the isotherm to be either linear (R_L=1), unfavourable (R_L> 1), favourable (0 <R_L< 1), or irreversible (R_L= 0).

Though the values of correlation coefficients (R^2) (Table 7.2) for all the adsorbents are higher than 0.9, negative values of Langmuir constant for pure HAP and Cu-HAP indicate that the adsorption behavior for As(V) removal system do not follow the assumption on which the Langmuir model is based on. Nevertheless R^2 values as well as Langmuir constant for Fe-HAP show that the data are fitted well to Langmuir isotherm model. Moreover in this study, R_L values for As(V) ion adsorption ranged from 0.20-0.37 for 2%Fe-HAP3, 0.08-0.14 for 4%Fe-HAP3 and 0.11-0.24 for 6%Fe-HAP3 which implies that adsorption is favorable for these adsorbents.

7.3.5.2 Freundlich Isotherm

The Freundlich isotherm is chosen to estimate the adsorption intensity of the adsorbent towards the adsorbate. Freundlich derived an empirical adsorption isotherm for heterogeneous system and non-linear equation which is expressed as

$$q_e = K_F C_e^{1/n} \quad (7.6)$$

Linear form of Freundlich equation is

$$\log q_e = \log K_F + (1/n) \log C_e \quad (7.7)$$

Where q_e is the amount adsorbed per unit mass of adsorbent (μgg^{-1}), C_e is the equilibrium adsorbate concentration in solution (μgL^{-1}), K_F and 'n' are Freundlich constants related to

the adsorption capacity and adsorption intensity respectively. Freundlich adsorption data for As(V) on pure and doped HAP are graphically shown as a function of logC_e vs logq_e in Figure 7.14. Parameters calculated from Freundlich equation are shown in Table 7.2. The magnitude of K_F and n shows easy separation of heavy metal ion from wastewater and high adsorption capacity. Whereas, a value of $1/n$ below unity implies chemisorptions process where $1/n$ above one is an indicative of cooperative adsorption.[38] If n lies between 1 and 10, this indicates a favorable adsorption process.

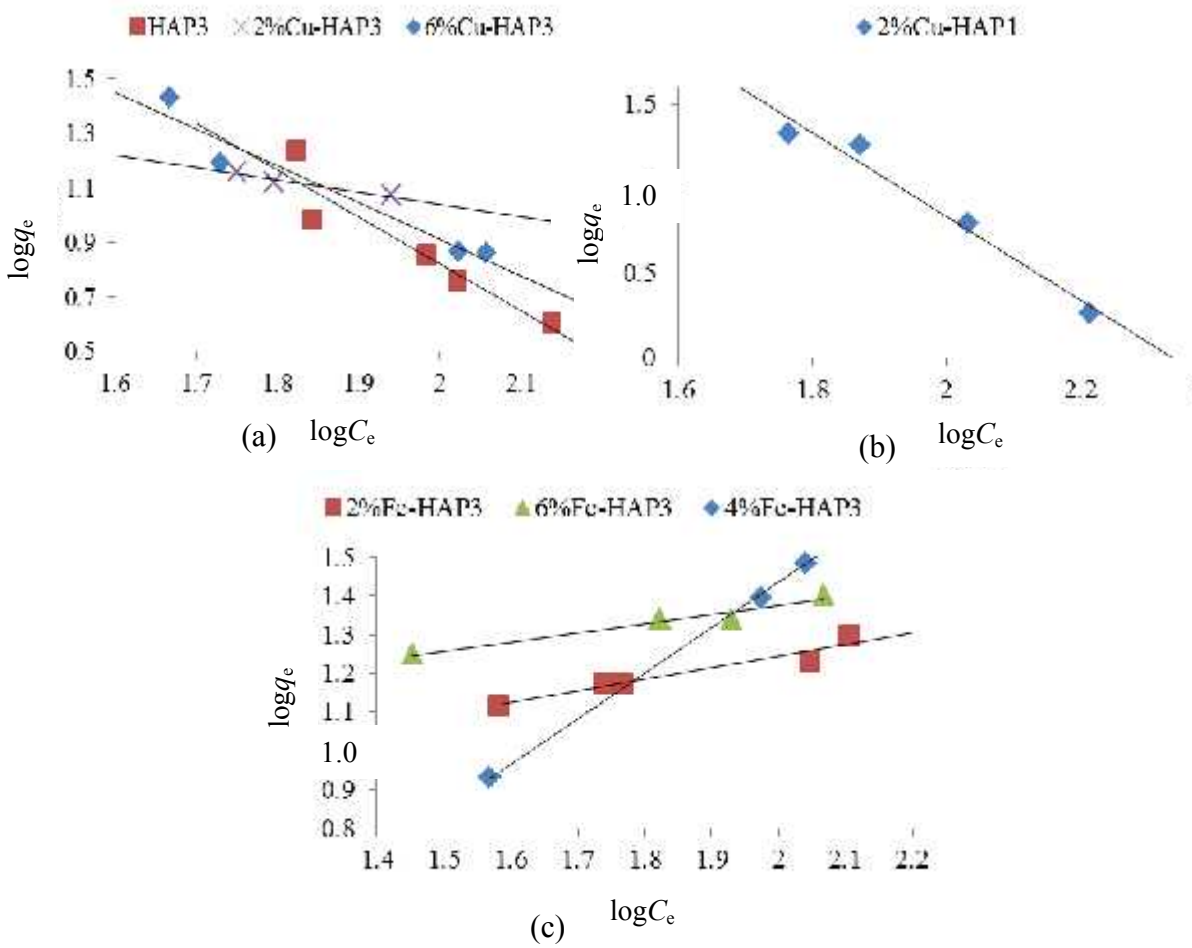

Figure 7.14 Freundlich isotherm plot for As(V) adsorption on (a) thermally treated pure and Cu-HAP, (b) oven dried 2%Cu-HAP and (c) thermally treated Fe-HAP

The value of n, which is related to the distribution of adsorbed ions on the adsorbent surface is found to be negative (Table 7.2) for As(V) ion adsorption on pure and Cu-HAP which indicates unfavourable adsorption. R^2 values of the adsorbents are above 0.9 in all

cases. Values of n for Fe-HAP indicate a favorable condition for adsorption of As(V). The fit of data to Freundlich isotherm model may indicate the heterogeneity of the adsorbed surface.

7.3.5.3 Temkin Isotherm

Temkin isotherm model is used to investigate the adsorption potential of pure and doped HAP to As(V) ion. This model is assuming that the heat of adsorption (ΔH_{ads}) of all molecules in the layer decreased linearly by increase the coverage.[39] The Temkin model considers change of heat of adsorption during adsorption on the surface of the adsorbent. The model is given by

$$q_e = B_1 \ln K_T C_e \qquad (7.8)$$

Linear form of the Temkin model is

$$q_e = B_1 \ln K_T + B_1 \ln C_e \qquad (7.9)$$

Where $B_1 = RT/b$, T is temperature in K, R is universal gas constant (8.314 $Jmol^{-1}k^{-1}$), K_T is the equilibrium binding constant (Lmg^{-1}) and B_1 is related to the heat of adsorption. Figure 7.15 represents plot of q_e versus $\ln C_e$ and calculated parameters are given in Table 7.2.

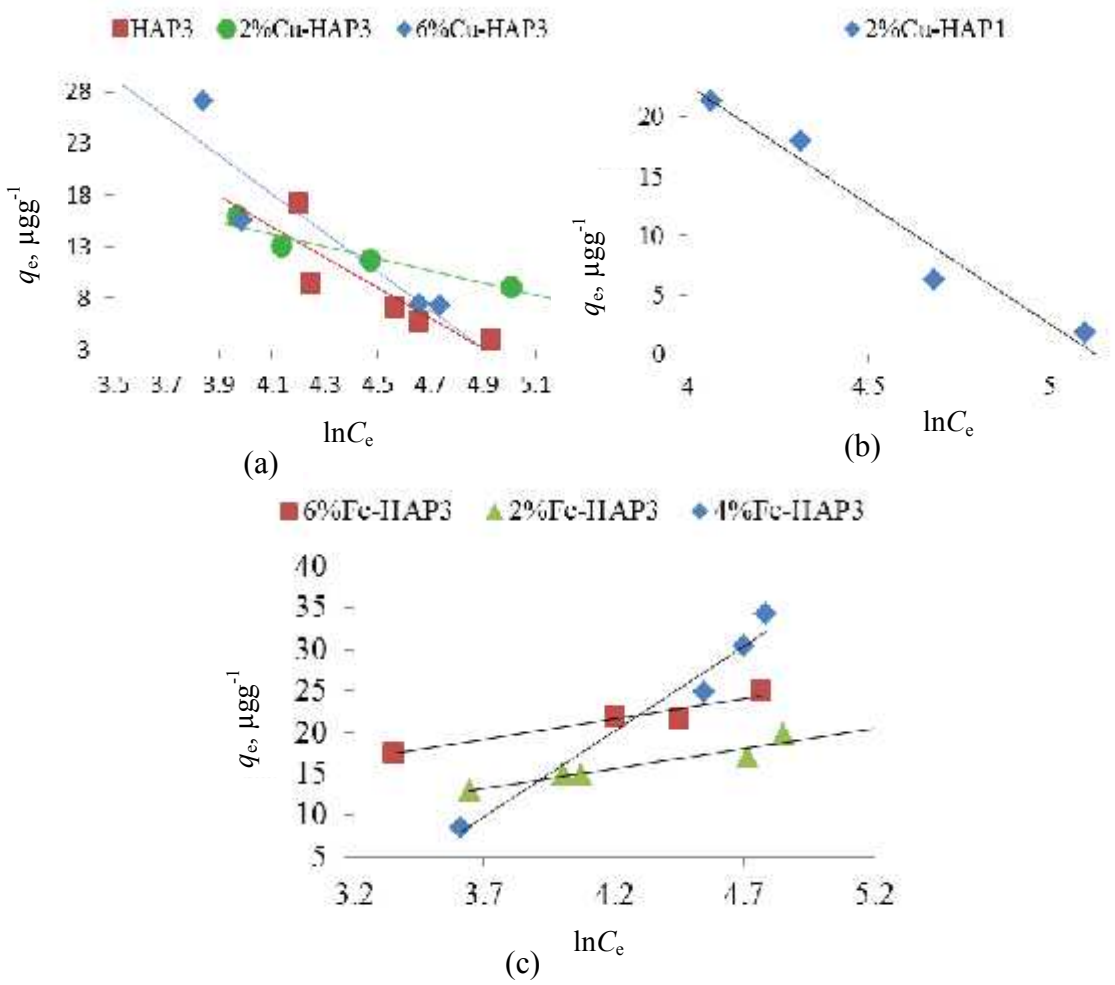

Figure 7.15 Temkin isotherm plot for As(V) adsorption on (a) thermally treated pure and Cu-HAP, (b) oven dried 2%Cu-HAP and (c) thermally treated Fe-HAP

The correlation coefficient (R^2) values for the selected adsorbents are lower for Temkin isotherm model considering the R^2 values of Langmuir and Freundlich models. Moreover, values of B_1 (heat of adsorption) are negative for pure and Cu-HAP samples which indicates this model also does not describe the adsorption process well.

Table 7.2

Adsorption isotherm parameters for As(V) adsorption on thermally treated pure and doped HAP

Sample	Langmuir adsorption isotherm			Freundlich adsorption isotherm			Temkin isotherm		
	q_m $\mu g\ g^{-1}$	Langmuir constant, K_L, $L\ \mu g^{-1}$ $(\times 10^{-2})$	R^2	Freundlich constant, K_F, $(\mu g/g)(L/\mu g)^{1/n}$	Freundlich constant, n	R^2	$B_1 = RT/b$	K_T $(L\mu g^{-1})$ $(\times 10^{-3})$	R^2
HAP3	2.475	-1.75	0.9730	18.03	-0.5827	0.8871	-14.69	6.00	0.7385
2%Cu-HAP1	1.180	-1.48	0.9084	591.43	-0.4054	0.9674	-20.14	5.93	0.9557
2%Cu-HAP3	7.463	-3.48	0.9974	85.55	-2.2416	0.9879	- 5.95	1.51	0.9234
6%Cu-HAP3	4.810	-2.66	0.9994	3932.78	-0.7457	0.9414	-18.68	6.28	0.8432
2%Fe-HAP3	23.64	3.04	0.9700	4.41	3.3367	0.9280	4.84	0.38	0.9075
4%Fe-HAP3	22.37	7.22	0.9074	0.21	0.8530	0.9992	20.60	0.03	0.9727
6%Fe-HAP3	28.65	4.95	0.9826	8.03	4.2550	0.9489	4.91	1.24	0.9297

7.4 Conclusions

Arsenic contamination of water in Bangladesh is a serious issue and it is yet to be resolved. Development of efficient low-cost adsorbent with high ability to remove arsenic from aquatic environment has therefore been a challenging task. Adsorption equilibrium conditions were established by studying the effects of various parameters of As(V) adsorption on pure and doped HAP. Equilibrium was established at pH 9.0, contact time 60 min, As(V) concentration 100 μgL^{-1} and experiment was done at room temperature (30°C). As(V) removal efficiency was investigated in detail and it was observed that the efficiency of HAP increased from 22% to 48% and 50% upon doping with Cu(II) and Fe(III) respectively keeping the equilibrium conditions for adsorption constant. The capacity enhanced to 59% and 74% while adsorbent dosage of copper and iron increased from 1 gL^{-1} to 10 gL^{-1}. Moreover the results show that the arsenate removal efficiency for Fe-HAP and Cu-HAP is two-fold higher than that for pure HAP.

Higher Cr(VI) removal efficiency of 6%Cu-HAP3 indicates the superiority of Copper doped HAP over pure HAP sample as a promising adsorbent. Study of adsorption of Pb(II) shows that pure and doped HAP are powerful adsorbents for removing Pb(II) from aqueous solution. The optimum dose of the selected adsorbents for Pb(II) removal is found to be 0.1 gL^{-1} with the highest removal efficiency of 93.14% for 2%Fe-HAP3. In both cases, adsorption equilibrium was attained quickly. Synthesized pure and doped HAP could represent an economical source for adsorption of Cr(VI) and Pb(II) from aqueous system.

Adsorption behavior was analyzed for adsorption of As(V) adsorption on thermally treated pure HAP, Cu-HAP and Fe-HAP using namely, Langmuir, Freundlich and Temkin adsorption isotherms. The equilibrium data fitted well with Langmuir model for low and high Fe(III) doping (2 and 6 wt%), while for an intermediate doping (4 wt%) Freundlich isotherm was followed. However, negative values for Langmuir isotherm constants, Freundlich constant and B_1, heat of adsorption for Temkin isotherm for As(V) adsorption are obtained for pure and copper doped HAP. This indicates the inadequacy of the isotherm model to explain the adsorption process.

The potential of the pure and copper and iron doped HAP synthesized from eggshell was explored to create a new dimension in waste management system by both efficient uses of such waste materials to reduce environmental pollution.

References

1. Grecu, M., Novac, G., Ionita, D., Ungureanu, C., "Incorporation of tobramycin biomimetic in hydroxyapatite coating on Co-Cr-Mo alloy and its antimicrobial acitivity", Rev. Chim., (Bucharest), **2011**, 62, 352-356.
2. Tamai M., Isshiki T., Nishio K., Nakamura M., Nakahira A., Endoh H., "A metastable phase in thermal decomposition of Ca-deficient hydroxyapatite," *J. Mater. Sci. Mater. Med.*, **2003**, 14, 617-622.
3. Ahn E. S., Gleason N. J., Nakahira A., Ying J. Y.,"Nanostructure processing of hydroxyapatite-based bio-ceramics," *Nano Lett.*, **2001**, 3, 149-153.
4. Nakahira A., Aoki S., Sakamoto K., Yamaguchi S.,"Synthesis and evaluation of various layered octacalcium phosphate by wet-chemical processing," *J. Mater. Sci. Mater. Med.*, **2001**, 12, 793-800.
5. Aoki S., Yamaguchi S., Nakahira A., Suganuma K. "A new approach to an artificial joint based on bio-cartilage/porous α-tricalcium phosphate system," *J. Eur. Ceram. Soc.*, **2003**, 23, 2939-2946.
6. Kleebe H. J., Nakahira A., Pezzotti G., "Microstructure and micro crack formation at grain boundaries in Na_3PO_4-doped hydroxyapatite," *J. Ceram. Soc. Japan*, **2001**, 109, 181-185.
7. Nakahira A., Karatani C., Nishida S., "Evaluation of cadmium removal in solution using various hydroxyapatite and cattle bone," *Phosphorus Res. Bull.*, **2004**, 17, 148-152.
8. Budinova T., Savova D., Tsyntsarski B., Ania C.O.,Cabal B., Parra J.B., Petrov N., "Biomass waste-derived activated carbon for the removal of arsenic and manganese ions from aqueous solutions", *Appl. Surf. Sci*., **2009**, 255, 4650-4657.
9. Simonescu C.M., Dima R., Ferdes M., Meghea A., "Equilibrium and kinetic

studies on the biosorption of Cu (II) onto Aspergillus niger biomass", *Rev. Chim.* (Bucharest), **2012**, 63, 224-228.

10. Mokaddes M.A.A., Nahar B.S., Baten M.A.,"Status of heavy metal contaminations of river water of Dhaka metropolitan city", *J. Environ. Sci. Nat. Resour.,* **2013**, 5, 349–353.
11. Rahman K., "Industrial pollution and control for sustainable development: Training manual on environmental management in Bangladesh", Department of Environment, Dhaka, Bangladesh, **1992**, 184-206.
12. Allan H., Smith,Elena O. Lingas, Rahman Mahfuzar "Contamination of drinking-water by arsenic in Bangladesh: a public health emergency", *Bull. WHO*, **2000**, 78, 1093-1103.
13. U.S. EPA. national primary drinking water regulations; arsenic and clarifications to compliance and new source contaminants monitoring; proposed rule. Federal Register, **2000**, 65, 38888.
14. Kumaresan M., Riyazuddin P., "Overview of speciation chemistry of Arsenic", *Curr. Sci.*, **2001**, 80, 837-846.
15. WHO Arsenic Compounds, Environmental Health Criteria 224, 2nd ed., World Health Organisation, Geneva, **2001**.
16. Arsenic primer: guidance for UNICEF country offices on the investigation and mitigation of arsenic contamination. New York: UNICEF, **2008**.
17. Arsenicosis in Bangladesh, Dhaka, Dhaka Community Hospital (DCH), **1998**, Bangladesh: 1–46.
18. McArthur, J.M. "Arsenic in groundwater: testing pollution mechanisms for sedimentary aquifers in Bangladesh.", *Water Resour. Res.*, **2001**, 37, 109-117.
19. "Harvard Arsenic Project." Harvard University, April 28, **2002**.
20. Smedley P.L., Kinniburgh D.G.,"A review of the source, behavior and distribution of arsenic in natural waters", *Appl. Geochem.*, **2002**, 17, 517-568.
21. Rouf M.A., Islam M.S., Haq M.Z., Ahmed N., Rabeya T., "Characterization of effluents of leather industries in Hazaribagh area of Dhaka city", *Bangladesh J. Sci. Ind. Res.,* **2013**, 48, 155-166.

22. Mondol M.N., Chamon A.S., Faiz B., Elahi S. F., "Chromium in urban soil-plant-water ecosystems", *J. Bangladesh Acad. Sci.,* **2013**, 37, 173-187.

23. Saha G. C., Ali, M. A., "Groundwater contamination in Dhaka City from tannery waste.", *J. Civ. Eng.,* **2001**, 29, 151–165.

24. EPA, Environmental Protection Agency, Environmental Pollution Control Alternatives. EPA/625/5-90/025, EPA/625/4-89/023. *Cincinnati,* US, **1990**.

25. Rivera-Utrilla J., Bautista-Toledo I., ferro-Garca M. A., Morino-Castilla C., "Activated carbon surface modifications by adsorption of bacteria and their effect on aqueous lead adsorption", *J. Chem. Technol. Biotechnol.*, **2001,** 76, 1209-1215.

26. Mitchell P**.**, "Transport of phosphate across the osmotic barrier of *Micrococcus pyogenes:* specificity and kinetics", *J. gen. Microbiol.,* **1954**, 11, 73-82.

27. Pierce M.L., Moore C.B., "Adsorption of arsenite and arsenate on amorphous iron hydroxide", *Water Res.*, **1982**, 16, 1247-1253.

28. Raven K.P., Jain A., Loeppert R.H., "Arsenite and arsenate adsorption on ferrihydrite: kinetics, equilibrium, and adsorption envelopes", *Environ. Sci. Technol*., **1998**, 32, 344-349.

29. Hsia T. H., Lo S. L., Lin C. F., "Characterization of arsenate adsorption on hydrous iron oxide using chemical and physical methods", *Colloid. Surf. A*, **1994**, 105, 1-7.

30. Matis K.A., Zouboulis A.I., Malamas F.B., Afonso M.D.R., Hudson M.J., "Flotation removal of As(V) onto goethite", *Environ. Pollut*., **1997**, 97, 239-245.

31. Sun X.,Doner H. E., "Adsorption and oxidation of arsenite on goethite", *Soil Sci*., **1998**, 163, 278-287.

32. Mohan D., Pittman C., "Arsenic removal from water/waste water using adsorbents-a critical review", *J. Hazard. Mater*., **2007**,142, 1–53.

33. Kannan N, Karrupasamy K., "Low cost adsorbents for the removal of phenyl acetic acid from aqueous solution", *Indian J. Environ. Protect*, **1998**, 18, 683-690.

34. Ghosh U.C., Goswami S., "Studies on adsorption behaviour of Cr(VI) onto synthetic hydrous stannic oxide", *Water SA*, **2005**, 31 , 597-602.

35. Violante A., Pigna M., Ragusa R., "Factors affecting arsenic adsorption/desorption

on/from variable charge minerals and soils", *17th WCSS*, 14-21 August **2002**, Thailand.

36. Lenoble V., Laclautre C., Deluchat V., Bollinger B., "Arsenic removal by adsorption on iron(III) phosphate", *J. Hazard. Mater. B*, **2005**, 123, 262–268.
37. Metcalf Eddy, "Wastewater engineering, treatment and Re-use", **2003**, John Wiley, 1138– 1151.
38. Haghseresht F**.**, Lu G., "Adsorption characteristics of phenolic compounds onto coal-reject-derived adsorbents", *Energy Fuels*, **1998**, 12, 1100–1107.
39. Taha M. Elmorsi, "Equilibrium isotherms and kinetic studies of removal of methylene blue dye by adsorption onto miswak leaves as a natural adsorbent", *J. Environ. Prot.*, **2011**, 2, 817-827.

CHAPTER 8

Kinetic study of As(V) adsorption on pure and doped HAP

8.1 Introduction

Adsorption is one of the most widely applied method for removal of pollutant from contaminated aqueous system.As adsorption is concerned, kinetic aspects is important to know more details about the performance of an adsorbent and mechanism of adsorption.Besides adsorption capacity, kinetic performance of a given adsorbent is also of great significance for the large scale application.The study of adsorption kinetics in wastewater treatment is significant as it describes the solute uptake rate which in turn controls time required forthe removal for completion of adsorption process.Therefore, in order to design an appropriate adsorption treatment plant, it is important to predict the rate at which pollutant is removed from aqueous solution.

Equilibrium conditions for adsorption of As(V) on pure and doped HAP were established from adsorption studies by various different adsorption parameters. Details of the investigation of adsorption capacity of pure and doped HAP samples as well as study of adsorption isotherms are discussed in Chapter 7.

The kinetic studies of adsorption process are crucialbecause the data obtained from such studies are necessaryto understand the variables that influence the adsorption of solutes. The results can also be used to determine theequilibrium time and the rate of adsorption can be usedto develop predictive models for large scale experiments.Adsorption kinetics data were processed according to several kinetic models: first order, pseudofirst order, pseudosecond order, Elovich and intraparticle diffusion model.

8.2 Materials and methods

In this study, As(V) solution of a specific initial concentration was prepared by proper dilution of stock solution (1000 mgL^{-1}). 10 mL of stock solution was transferred to a

reagent bottle containing optimum adsorbent dose for different contact time up to 70 min. All the studies were performed at an optimum pH 9.0 for As(V) solution (Chapter 7). The contents were centrifuged after a definite time interval and the centrifugates were analyzed for residual concentration of As(V) by standard method using HG-AAS.

8.3 Adsorption kinetics

8.3.1 First-order kinetic

The first-order rate equation is generally expressed as[1]:

$$\ln C_t = \ln C_0 - kt \qquad (8.1)$$

Where, k is the rate constant for adsorption. Therefore Plot of $\ln C_t$ Vs t would be a straight line and Figure 8.1 shows the plotsfrom which rate constants $k$were derived from the respective slopes and the initial concentration C_0 of the metal ion can be calculated from the intercept. Regression coefficients (R^2)are summarized in Table 8.1 with the rate constants and initial concentration of the metal ion.

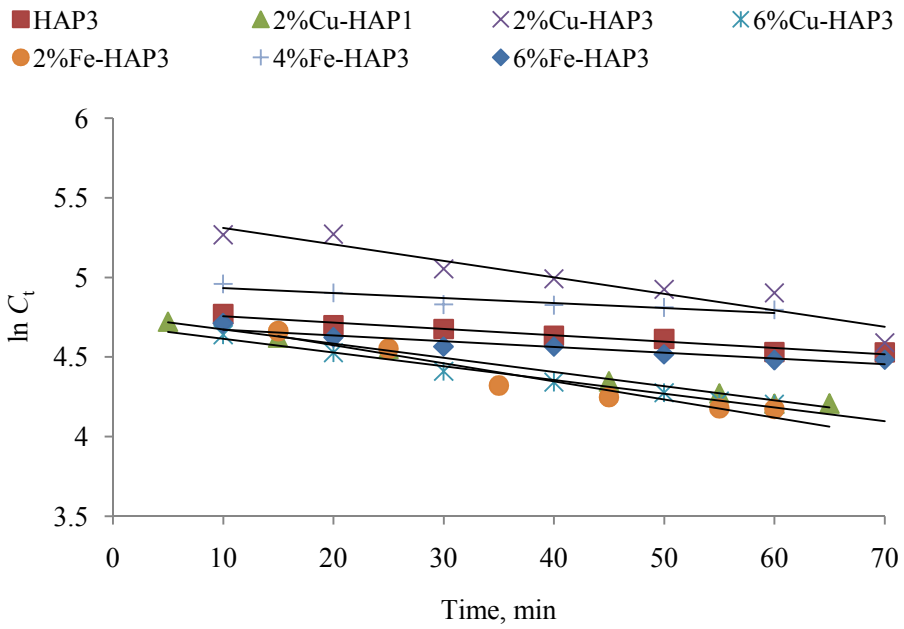

Figure8.1: First-order adsorption kinetics of As(V) on pure and doped HAP Conditions: As(V) concentration 100 µgL^{-1}; contact time: 60 min; 1 gL^{-1} adsorbent mass and pH 9.0 (± 0.1).

The plots in Figure 8.1 are linear for all the adsorbents used in the experiments and the rate constant is lower for thermally treated pure HAP (Table 8.1). Moreover, calculated initial concentrations of arsenic metal ionare not in good agreement with the experimental values and also the correlation coefficient values are not significant whichas shown in Table 8.1. But correlation coefficient values for HAP3 and 2% Cu-HAP1 are closer to unity (0.966 and 0.994, respectively).This indicates the partial fitting of this kinetic model to explain the adsorption process for HAP3 and 2% Cu-HAP1. However, the experimental data do not give a good correlation for other adsorbents.

8.3.2 Pseudo first-order kinetic

The Pseudo first-order kinetic model was proposed by Lagergren[2]and the linear form is generallyexpressed as:

$$\log (q_e - q_t) = \log q_e - k_1 t \quad (8.2)$$

Where, $q_e$and $q_t$are the amounts of As(V) in $\mu g g^{-1}$adsorbed at equilibrium and at time (t) respectively.Plot of $\log(q_e - q_t)$versus t gives a straight line for first-order adsorption kinetics which allows computation ofthe rate constant k_1. Figure 8.2 shows the graph plotted for pseudo first-order kinetic model. Table 8.1 presents values of the parameters measured from this kinetic model.

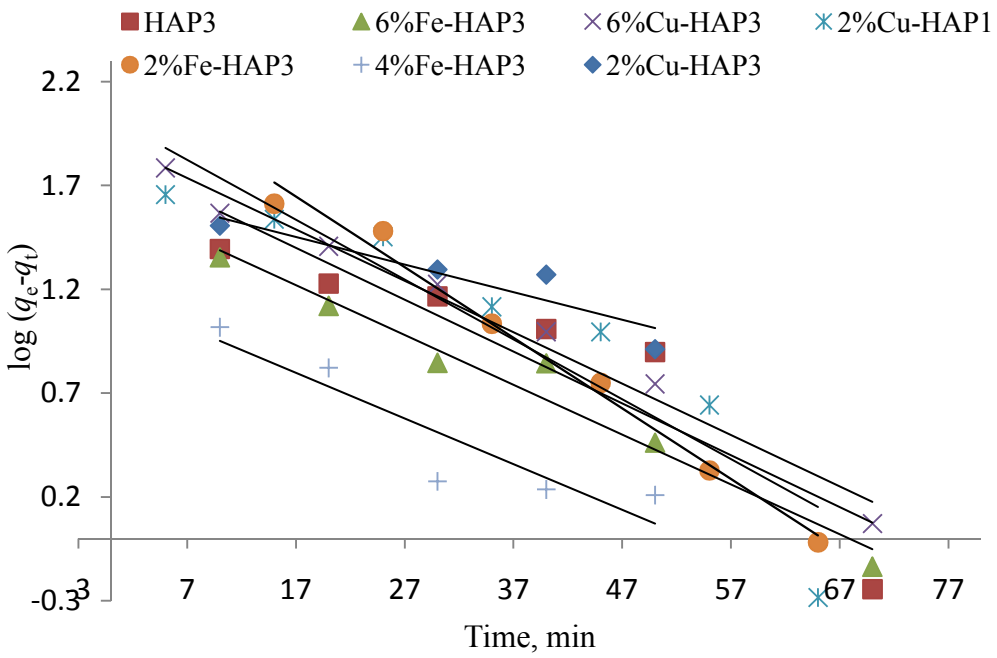

Figure 8.2 Pseudo first-order adsorption kinetics of As(V) on pure and doped HAP, Conditions: As(V) concentration 100 µgL^{-1}; contact time: 60 min; 1 gL^{-1}adsorbent mass and pH 9.0 (± 0.1).

This model is based on the assumption that the rate of adsorption is proportional to the number of free sites available on the adsorbent. From Table 8.1 it can be stated that pseudo first-order fitting gives poorvalue for R^2 for pure HAP, 2%Cu-HAP and 4%Fe-HAP (< 0.9), but it shows slightly higher values for calcined 6%Cu-HAP, 2% and 6%Fe-HAP (>0.9). Nevertheless, certain disagreement betweenthe experimental and calculated $q_e$values implies that the pseudo first order equation does not fit well for all adsorbents in the whole range of contact time. Only 6%Fe-HAP3 partially follows pseudo first-order kinetic model.

8.3.3 Pseudo second-order kinetic

The adsorption kinetic may also be described by the pseudo second-order model using the Ho equation[3]represented as:

$$t/q_t = t/q_e + 1/k_2q_e^2 \qquad (8.3)$$

where k_2 ($g\mu g^{-1}min^{-1}$) is the rate constant of the second-order equation for adsorption of arsenate, q_t (μgg^{-1}) is the amount of arsenate per unit gram of adsorbent at time '*t*' and q_e is the maximum adsorption capacity (μgg^{-1}) for the second-order adsorption.The kinetic plots of t/q_t versus t for As(V) adsorption at ambient temperature (30 ± 1°C) are presented in Figure 8.3.Values ofk_2, q_e and $R^2$are calculated from the plot of t/q_t versus t and the results are presented in Table 8.1.

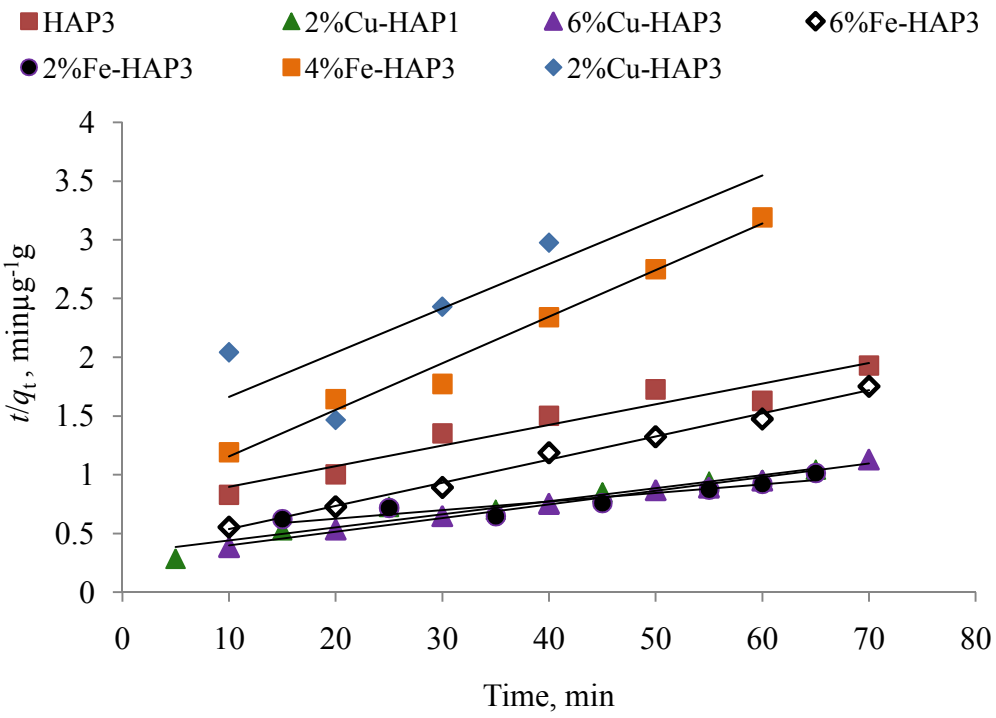

Figure 8.3 Pseudo second-order adsorption kinetics of As(V) on pure and doped HAP, Conditions: As(V) concentration 100 μgL^{-1}; contact time: 60 min; 1 gL^{-1} adsorbent mass and pH 9.0 (± 0.1).

The pseudo second-order kinetic model has often been used to fit the experimental kinetic adsorption data to determine whether or not an adsorption process is dominated by the chemical adsorption phenomenon.R^2 for pseudo second order equation are in the range of 0.93 -0.99 for the adsorption of the As(V) for all adsorbentswith the exception noted for R^2 values of 2%Cu-HAP3 and 2%Fe-HAP3 (≤ 0.8). Although the calculated

$q_e$values are slightly overestimated compared to their experimental counterparts, this model fits well for thermally treated 6%Cu-HAP, 4% and 6%Fe-HAP.

8.3.4 Elovich kinetic

Adsorption data can also be analyzed using theElovich equation[4]andlinear form of this model is expressed as:

$$q_t = 1/\beta \ln(\alpha\beta) + 1/\beta \ln(t) \qquad (8.4)$$

Where q_t is the amount of metal ions adsorbed on adsorbents ($\mu g g^{-1}$) at time t (min), $\alpha$is the initial adsorption rate constant($\mu g g^{-1}$.min) andthe parameter βisthe constant ($g\mu g^{-1}$)related to the extent of surfacecoverage and activation energy for chemisorptions, both are the Elovich constants. Values of α and $\beta$are calculated from slope and intercept of the plot q_t versus ln(t).Figure 8.4 shows the kinetic plots of q_t versus ln(t) and $v$alues are given in Table 8.1.

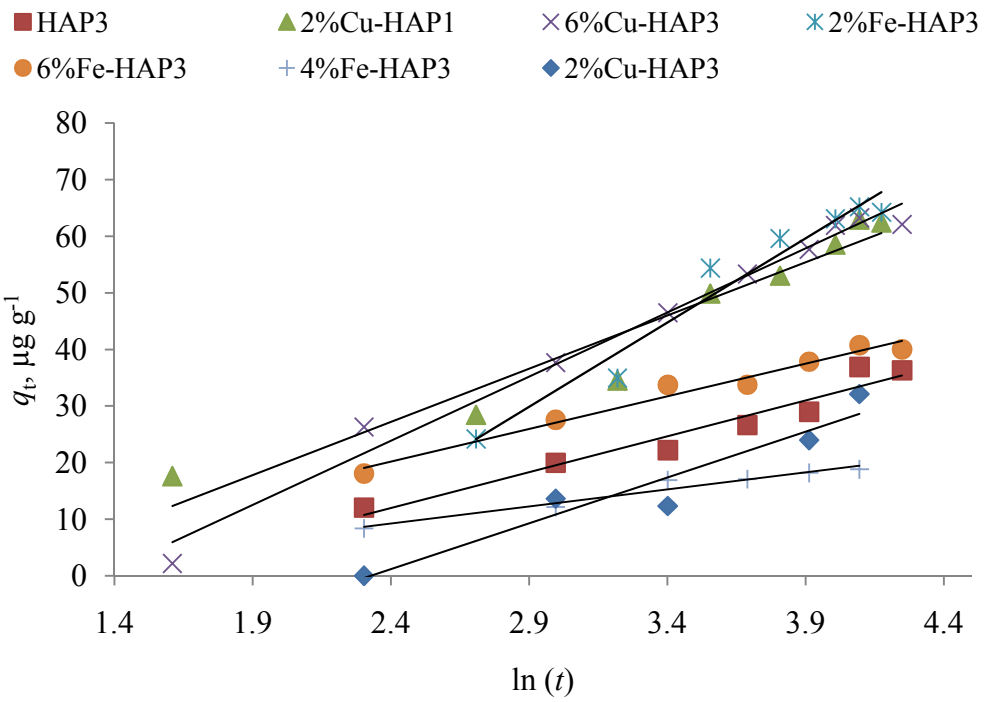

Figure 8.4Elovich adsorption kinetics of As(V) on pure and doped HAP, Conditions: As(V) concentration 100 µgL^{-1}; contact time: 60 min; 1 gL^{-1}adsorbent mass and pH 9.0 (± 0.1).

Elovich's equation is often applied to describe the adsorption ofgas onto solid systems[5], but recently this has also been used to describethe adsorption process of pollutants from aqueoussolutions.[6,7] Table 8.1 shows that the calculated values of αare higher than that of ß for all adsorbents.These values show that initial adsorption rate is very high and much of the arsenate is adsorbed rapidly on pure HAP and doped HAP. Although adsorption of arsenate on pure HAP is much slower than doped HAP, values of R^2 for this model are higher(>0.9) for all adsorbents.

8.3.5 Intraparticle diffusion model

During adsorption, there is a possibility of the adsorbate to diffuse into the interiorpores of the adsorbent. This can be examined by the relationship between amount of adsorbed adsorbate and square root of contact timegiven by the following equation[8]:

$$q_t = K_{id}\, t_{1/2} + C \qquad (8.5)$$

Where q_t is the adsorption capacity ($\mu g g^{-1}$) at t time (min), K_{id} is the intraparticle diffusion rate constant and C($\mu g\ g^{-1}$) is constant gives an indication of thickness of the boundary layer.This is known as intraparticle diffusion kinetic model and the linear plots of $q_t$versus $t^{1/2}$ are shown in Figure 8.5.

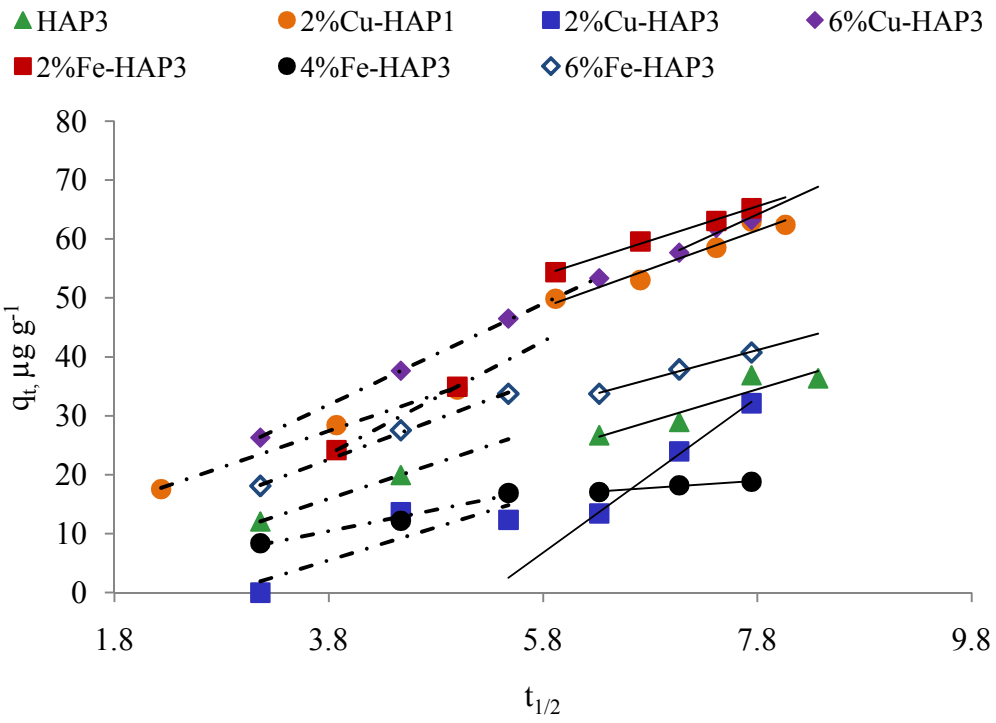

Figure 8.5Intraparticle diffusionadsorption kinetics of As(V) on pure and doped HAP, Conditions: As(V) concentration 100 µgL^{-1}; contact time: 60 min; 1 gL^{-1} adsorbent mass and pH 9.0 (± 0.1)

The intraparticle diffusion plot (Figure 8.5) shows that the lines do not pass through the origin and this indicates that the intra-particle diffusion is not the only rate-controlling step.[9]It is observed that the intra-particle diffusion of As(V) occurs in 2 stages. The first straight line is ascribed to the macropore and mesopore diffusion (phase I) and the second linear portion is attributed to micro-pore diffusion (phaseII).[10]The intraparticle diffusion constants for these 2 phases (K_{1id} and K_{2id}) and values of $R^2$are given in Table 8.1 which are higher than 0.9 for all adsorbents.Results indicate that the adsorption of As(V) ion on pure and doped HAP involves more than one process. In addition, the rate constants of the intra-particular diffusion on pure HAP and doped HAP are almost similar for both the stages and enhancement of rate is observed with doping of metal ions in pure HAP.

The parameters for kinetic adsorption data are summarized in Table 8.1.

Table 8.1 Parameters optimized from adsorption kinetic models for adsorption of As(V) using pure and doped HAP

Parameters optimized from adsorption kinetic models		HAP3	2%Cu-HAP1	2%Cu-HAP3	6%Cu-HAP3	2%Fe-HAP3	4%Fe-HAP3	6%Fe-HAP3
Experimental q_e, µgg^{-1}		36.89	62.93	32.14	63.24	65.2	18.82	40.74
Experimental C_0 µg L^{-1}		130.2	130.2	201.9	130.2	130.2	159.4	130.2
First -order kinetics	Rate constant, k_1 (min^{-1})	0.004	0.008	0.010	0.008	0.011	0.003	0.003
	Calculated C_0, µg L^{-1}	121.03	116.98	224.75	110.06	121.75	143.17	110.94
	R^2	0.966	0.994	0.904	0.985	0.934	0.850	0.903
Pseudo first - order kinetic model	Calculated q_e, µg g^{-1}	66.68	105.93	47.75	81.10	167.49	14.89	42.46
	Rate constant, k_1, (min^{-1}) (×10^{-2})	5.76	6.45	2.99	5.53	7.83	5.07	5.53
	R^2	0.833	0.856	0.848	0.982	0.987	0.843	0.967
Pseudo second - order	Calculated q_e, µg g^{-1}	58.82	90.91	27.03	90.91	142.86	25.64	52.63
	Rate constant, k_2 (g µg^{-1} min^{-1})	4.02×10^{-4}	3.6×10^{-4}	1.07×10^{-3}	4.31×10^{-4}	1.03×10^{-4}	2.00×10^{-3}	1.06×10^{-3}
	R^2	0.930	0.937	0.583	0.990	0.858	0.984	0.992
Elovich's equation	α, (µg g^{-1}min)	2.9562	7.2456	1.5795	5.8840	4.6299	2.5220	6.5430
	β, (g µg^{-1})	0.0790	0.0532	0.0618	0.0442	0.0336	0.1653	0.0867
	R^2	0.941	0.933	0.918	0.984	0.959	0.956	0.973
Intraparticle diffusion	K_{1id}, (µg g^{-1}min)	6.031	6.152	5.582	8.580	9.556	3.645	6.784
	K_{2id}, (µg g^{-1}min)	5.449	6.527	13.16	8.268	5.818	1.217	4.927
	Intercept C_1 , µg g^{-1}	-7.003	4.044	-15.72	-0.754	-12.83	-3.430	-3.183
	Intercept C_2 , µg g^{-1}	-7.985	10.55	-69.62	-0.344	20.13	9.455	2.717
	R_1^2	1	0.996	0.740	0.999	1	0.980	0.997
	R_2^2	0.985	0.953	0.998	0.925	0.996	0.982	0.995

8.4Conclusions

Elovich kinetic model and intraparticle diffusion model fit well with excellent correlation for all adsorbents.The correlation coefficients of adsorption data fitted to pseudo first-order model are slightly lower for pure HAP and both oven dried and thermally treated 2%Cu-HAP and also for thermally treated 4%Fe-HAP. Pseudo second-order kinetic model describes the adsorption process better than the pseudo first-order model. Moreover, the results are in good agreement with Elovich kinetic model, confirming chemical sorption nature of adsorption of As(V) ion on pure and doped HAP. First-order kinetic and pseudo second-order models well describe the adsorption kinetics and probably both physical and chemical adsorptions are involved in adsorption of As(V) ion.

References

1. Rashed M.N., El-Amin A.A, "Photocatalytic degradation of methylorange in aqueous TiO_2 under different solar irradiation sources", *Int. J. Phys. Sci.,***2007**, 2, 73-81.
2. Gupta V.K., Rastogi A, Nayak A,"Adsorption studies on theremoval ofhexavalent chromium from aqueous solution using alow cost fertilizerindustry waste material",*J. Colloid. Interf. Sci.,* **2010**, 342, 135–141.
3. McKay G., Ho Y.S., "Pseudo-second order model forsorptionprocesses",*Process Biochem.*,**1999**, 34, 451-465.
4. ChienS.H., Clayton W.R., "Application of Elovich equation to thekinetics of phosphate release and sorption on soils", *Soil Sci. Soc. Am.*, **1980**, 44, 265–268.
5. Rudzinski W., Panczyk T., "Kinetics of isothermaladsorption onenergetically heterogeneous solid surfaces:a new theoretical descriptionbased on the statistical ratetheory of interfacial transport", *J. Phys. Chem.*,**2000**, 104, 9149-9162.
6. Cheung C.W., Porter J.F., McKay G., "Sorption kineticanalysis for theremoval of cadmium ions from effluentsusing bone char", *Water Res.*,**2001**, 35, 605-612.
7. Sağ Y., Aktay Y., "Kinetic studies on sorption of Cr(VI)and Cu(II) ionsby

chitin,
chitosan and Rhizopus arrhizus", *Biochem. Eng. J.*,**2002**, 12, 143-153.

8. Weber W.J., Morris J.C.,"Kinetics of adsorption of carbon from solution", *J. Sanit. Eng. Div. Proc. Am. Soc. Civ. Eng.*, **1963**, 89, 31–59.
9. Asha H. Gedam, Rajendra S. D., "Adsorption characterization ofPb(II) ions ontoiodate doped chitosan composite: equilibrium andkinetic studies", *RSC Adv.*,**2015**,5, 54188-54201.
10. FierroaV.,Torne´-Ferna´ndezV., MontaneD., CelzardA., "Adsorptionof phenol onto activated carbons having differenttextural and surfaceproperties", *Microporous Mesoporous Mater.*, **2008**, 111, 276–284.

CHAPTER 9

Removal of priority toxic metals from real samples using HAPs

9.1 Introduction

An endeavor was made in this chapter to investigate the efficiency of the synthesized HAPs in removing or reducing arsenic, chromium and lead from the real waste water samples collected from different industrial units nearby Dhaka city.Successful applications of pure and doped HAPs to remove toxic metals from synthetic waste watersmotivated us to explore its application in case of real waste water samples. Accordingly, based on the high surface area and pore volume of HAP samplesa judicial selection was made in choosing the adsorbents. Hence, HAP3, 2%Fe-HAP3 and 6%Cu-HAP3 were selected as adsorbentswhile the experimental conditions were maintained consistent (Table 9.1) throughout the study.

Table 9.1 Experimental conditions for treatment of real waste water

Real waste water under investigation	**Adsorbent dose gL^{-1}**	**Contact time min**	**pH**	**Temperature °C**
Ground water (Arsenic contaminated)	5.0	60	Natural / measured	30
Tannery waste water (Chromium contaminated)		20		
Fertilizer extract (Lead contaminated)		30		

9.2 Arsenic in ground water

Arsenic contaminated ground water was collected from tube-wells placed at 100.0 and 130.0 ft depth under the ground which are located in Dohar, Dhaka. Measured pH of both the water samples were 7.1.Arsenic removal efficiency was investigated at thisnaturalpH keeping the others conditions fixed (as mentioned in Table 9.1).Experimental results are shown in Table 9.2.

Table 9.2Arsenic removal efficiency of HAPs from As contaminated ground water

Ground water from tube-well at depth, ft	Initial arsenic concentration, μgL^{-1}	Arsenic removal efficiency, %		
		HAP3	2%Fe-HAP3	6%Cu-HAP3
100	25.0	54.3	93.5	90.8
130	66.0	61.1	93.5	91.0

It is clearly evident from Table 9.2 that the efficiency of the selected adsorbents in removing arsenic fromground-water isconsiderably higher which prompt us to conclude that the method ispromising.Particularly both of the doped HAPs (i.e. Fe- and Cr-doped) showed more than 90% efficiency in removing arsenic from ground water. However, further work is deemed necessary to firmly establish such observation.

9.3 Chromium in tannery waste

Next approach was confined to remove chromium from tannery waste water collected from Hazaribagtannery area, Dhaka. Initial concentration of chromium in tannery waste water was 24.52 mgL^{-1}. Adsorption efficiency was measured atnatural pH (8.4) of thecollected samplesand the dataare shown in Figure 9.1. Surprisingly, in this case the adsorption efficiency of pure HAP is more than 75% while in removing arsenic from ground water the efficiency was 54–60%. On the other hand doped HAPs showed ~80% adsorption efficiency in removing chromium from tannery waste water and this value is slightly less than that of previous case (Section 9.1, where arsenic

removing efficiency ofdoped HAPs is more than 90%). Nevertheless, overall observation relating to adsorption efficiencyis encouraging.

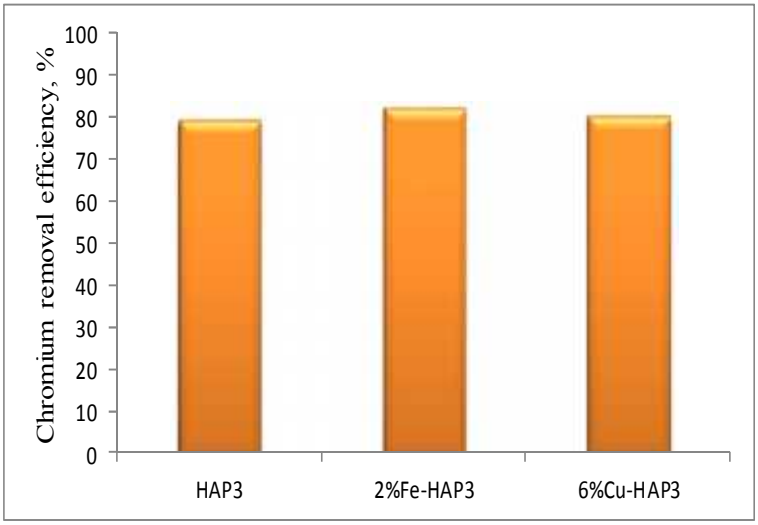

Figure 9.1 Chromium removal efficiency of HAPs from tannery waste water

9.4 Lead in fertilizer

Fertilizer extractgenerouslysupplied by Soil Research Division, BCSIR Laboratories Dhakawas used in this case. Initial concentration of lead was 60.0 mgL^{-1} in the supplied sample and the pH was 6.0. Adsorption experiment was conducted maintaining the conditions as in Table 9.1 and the results are shown in terms of bar diagram (Figure 9.2). The adsorption data in Figure 9.2 revealed that in this case the efficiency of HAP3 again decreased and came down to ~63%. On the other hand Fe-HAP3 showed an efficiency of ~71% while for Cu-HAP3 lead removal efficiency was more than 95%.

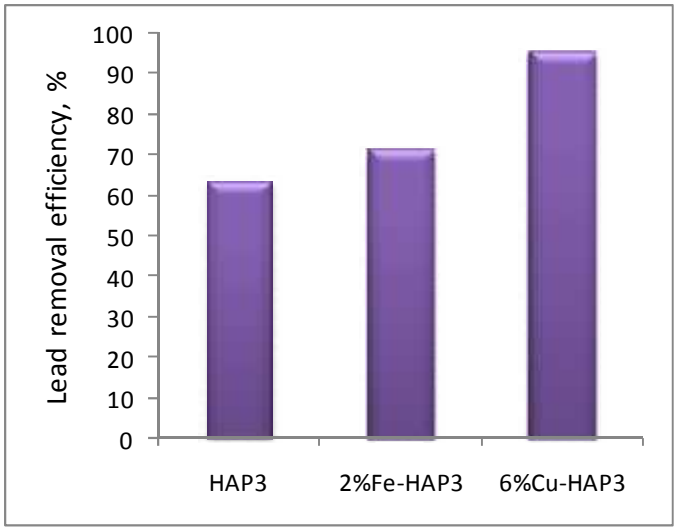

Figure 9.2 Lead removal efficiency of HAPs from fertilizer

9.5 Conclusions

The adsorption efficiency of HAP3, 2%Fe-HAP3 and 6%Cu-HAP3 revealed that even though all these adsorbents are capable insignificantly removing arsenic, chromium and lead in real samples, but their efficiency range differs depending on the nature of the sample which is rather expected. However, for a better understanding the factors which are controlling the adsorption efficiency, adsorption kinetics and adsorption isotherms must be systematically examined.

CHAPTER 10

Conclusions and recommendations

10.1 Conclusions

The primary objective of the present research was to use waste materials to generate value-added products, and subsequently apply those new materials for waste minimization. Pure HAP, Fe-HAP, Cu-HAP and nano HAP were prepared from bio-wastes (eggshells, prawnshells) and applied as promising adsorbents for the treatment of priority toxic heavy metals in aqueous medium. Hence, the research work can be categorically divided as follows:

(i) Synthesis and characterization of pure, Cu- and Fe-doped HAP and also nano- HAP.
(ii) Applications of the synthesized HAPs as adsorbents in treating synthetic waste water containing priority toxic heavy metals.
(iii) Applications of the synthesized HAPs as adsorbents in treating few real samples.

(i) Synthesis and characterization of HAPs

Synthesis of HAPs from waste materials

Waste materials eggshells and prawnshells were used as calcium sources in the synthesis of HAP and doped HAP following wet chemical precipitation method. Doping of Fe(III) and Cu(II) with different wt% of respective metal ion salts were also completed following same synthetic route. During the synthesis process $(NH_4)_2HPO_4$ was used as phosphate precursor solution and pH was strictly maintained at 9.0 with ammonia solution.The products were thermally treated at 100°, 300° and 600°C temperatures. Since the synthesized products have been utilized in remediation of aqueous environment, samples were not calcined at higher temperatures. As it is well-known that HAP samples started to crystallize at 600°C resulting in a decrease of surface area of the products. The most noticeable advancement of this work is the development of nano HAP where microemulsion method was applied for the first time to synthesize nano HAP using calcium precursorderived fromeggshells. A

quaternary reverse micelle system, tritonX-100(TX-100)/cyclohexane/*n*-pentanol/water, was used for the synthesis of nano HAP and ethanol was used to separate out the product from microemulsion. The nano HAP was subjected to thermal treatment at the same temperatures as in the case of pure and doped HAP.

Characterization of HAPs from waste materials

Characterization of the physical and chemical properties of pure, doped and nanoHAP powder synthesized from eggshells have been carried out using Fourier transform infrared spectroscopy (FT-IR), X-ray diffraction (XRD), scanning electron microscopy with energy dispersive X-ray analysis (SEM-EDX), DLS particle size analysis and surface area analysis from BET isotherms.FT-IR spectra and XRD patterns of all synthesized HAPsconfirmed the formation of single HAP phase.

Both eggshells and prawnshells were used as calcium sources to synthesize pure HAP.The yield of the products with eggshells is higher (93%) compared to prawnshells (15%), since eggshells contains higher % of calcium compared to prawnshells. Higher calcination temperature increased crystallinity of the products with subsequent decrease in surface area which was measured 66.80 and 22.40 m^2g^{-1} for HAP3 and HAP6 respectively. XRD pattern of HAP3 also confirmed the amorphous nature of the product.

The XRD analyses indicate that the crystallite size decreased from 34 nm for pure HAP to 14-16 nm for Fe-HAP and 15-12 nm for Cu-HAP. BET surface area of Fe and Cu doped HAP calcined at 300°C increased from 66.80 m^2g^{-1} for pure HAP to 122.29 and 153.39 m^2g^{-1} respectively. Surface area of Fe-HAP was significantly increased for 2 wt% Fe(III) doping (122.09m^2g^{-1}) followed by a decrease in the value (68.25m^2g^{-1}) for 6%Fe-HAP with an insignificant enhancement of the value for 4%Fe-HAP (122.29 m^2g^{-1}). Conversely, BET surface area of Cu-HAP gradually increased from 86.44 and 153.39 m^2g^{-1}in increase of Cu-content from 2.0 wt% and 6.0 wt% respectively.

Analysis of particle size by DLS technique of as prepared nano HAP was found to be 12 nm, which on thermal treatment at 100°C increased to 16 and 295 nm. SEM micrographs showed elongated spherical shape with particle size approximately 100 nm for nano HAP6. BET surface area of nano HAP6 increased to 79.23 m^2g^{-1} from

22.40 m^2g^{-1} for HAP6.Arsenic removal efficiency of nano HAP was tested at pH 7.0 and 9.0, which showed a significant increase in arsenic removal efficiency in comparison to synthesized HAP micro particles. Nano HAP shows a promising effect in removal of arsenic from aqueous system at pH 7.0, which would be helpful for the removal of arsenic from ground water as well.

(ii) Application of the synthesized HAPs as adsorbents in treating waste water

Removal of arsenic, chromium and lead from synthetic waste water

HAPs synthesized from eggshells were applied for the removal of heavy metals from aqueous systems, special attention was focused on removal of As(V) as this has been a major concern in Bangladesh. Selections of HAPs as potential adsorbents were made considering higher surface area and higher pore volume of the samples. It was observed that HAPs (pure, Fe- and Cu-doped and nano) calcined at 300°C temperature had higher surface area, and accordingly these HAPs were chosen as adsorbents. Adsorption study revealed that equilibrium was established in 60 min at pH 9.0 withAs(V) concentration of 100 μgL^{-1}. The experiment was carried out at room temperature of 30°C. As(V) removal efficiency was investigated in detail and it was observed that the efficiency of HAP increased from 22% to 48% and 50% upon doping with Cu(II) and Fe(III) respectively keeping the equilibrium conditions same. The adsorption capacity enhanced to 59% and 74% while adsorbent dosage of copper and iron were increased from 1.0gL^{-1} to 10.0 gL^{-1}. Moreover the results show that the arsenate removal efficiency for Fe-HAP and Cu-HAP is twofold higher than that for pure HAP. Arsenic removal efficiency of nano HAP was tested at pH 7.0 and 9.0, which showed a significant increase in arsenic removal efficiency as compared to synthesized HAP by wet chemical method.The equilibrium data fitted well with Langmuir model for 2% and 6%Fe-doped HAP while 4%Fe-HAP followed Freundlich isotherm. However, negative values for the constants of Langmuir, Freundlich and Temkin isotherms for As(V) adsorption for pure and Cu-doped HAP implied the inadequacy of the isotherm model to explain the adsorption process. First-order and Pseudo-second-order kinetic models well describe the adsorption kinetics and probably both physical and chemical adsorptions were involved in adsorption of As(V) ion by pure and doped HAP.

Experiments were conducted by varying the contact time and pH for adsorption of chromate ion from aqueous systems which were studied at equilibrium condition maintaining ambient temperature at 30°C and initial concentration of Cr(VI) was maintained at 100 $mgL^{-1}$with adsorbent dosage 1 gL^{-1}.Equilibrium was attained after 20 min for removal of Cr(VI) using HAP3 which showed its maximum value 35% at pH 9.0, while this value is 90% for 6%Cu-HAP3 at pH 6.0. Higher Cr(VI) removal efficiency of 6%Cu-HAP3 indicated the superiority of Cu-doped HAP over pure HAP sample as a promising adsorbent.

Pb(II) removal from aqueous systems was studied using pure and doped HAP calcined at 300°C, equilibrium condition was achieved at initial concentration of Pb(II) 5.0 mgL^{-1}, adsorbent dosage 1.0 gL^{-1} at 30°C room temperature. Adsorption equilibrium was reached in 30 min in removing Pb(II) from aqueous system.2%Fe-HAP3 showed highest Pb(II) removal efficiency 93% at pH 8.0.

Removal of arsenic, chromium and lead from real waste water

Inspired by the results of utilization of HAPs for the removal of above mentioned heavy metals from synthetic waste water, HAPs were further used as adsorbents in treating real waste water. Arsenic contaminated tube-well water samples were collected from Dohar, Dhaka. Tannery waste water was collected from Hazaribag area, Dhaka and a fertilizer sample was analyzed to check lead concentration.

Pure and Fe- and Cu-doped HAPs were used to remove heavy metals from the real samples and results were found quite promising.Arsenic removal efficiency of HAP3, 2%Fe-HAP3 and 6%Cu-HAP3 were calculated as 61, 94 and 88% respectively from ground water collected from Dohar, Dhaka. Chromium was also efficiently removed from tannery waste water, whose values were 79, 80 and 82% for HAP3, 6%Cu-HAP3 and 2%Fe-HAP3 respectively. Similarly, efficiency of lead removal from fertilizer sample was 64, 71 and 95% for HAP3, 2%Fe-HAP3 and 6%Cu-HAP3 respectively.

The efficiency of the pure, Cu- and Fe-doped and as well as nano HAP synthesized from eggshells was investigated to reveal a new dimension in waste management technology. This work is a significant step towards environmental remediation because it utilized waste eggshells from a local restaurant for the synthesis of value

added products, HAP Cu- and Fe- substituted as well as nano HAP which were successfully used as potential adsorbents for the removal of priority toxic heavy metals from aqueous medium.

10.2 Recommendations for future work

The results documented in this research are significant.However,I wish to add the following recommendations for further pursuing this research:

1. Further analyses of Fe-and Cu-doped HAP using NMR or ICP-AES to have better quantification of Fe and Cu content in HAP as well as understanding the structural changes after the substitution reactions.
2. Utilization of calcium from prawnshells yielded a by-product chitin which can form a composite with HAP to increase efficiency of HAP in various applications.This needs to be further investigated.
3. Doping of metal ions other than Fe and Cu in the structural moiety of HAP may be undertaken.Also, composites of HAP with other polymers can be prepared to enhance the adsorption efficiency of HAP.
4. Mechanism of removal of heavy metals is not yet clearly understood.Extensive study is required to reveal the mechanism involved in adsorption of heavy metals on Cu-HAP.
5. HAPs have to be explored more in the treatment of real waste water obtained from different industrial units.
6. Surfactant mediated preparation of nano HAP may be systematically undertaken. The microemulsion method for the preparation of nano HAP offer an excellent domain in HAP research and the applications of nano HAP may be further extended to biomedical fields as well as in environmental research.

Abstracts Published as Contribution in the Scientific Meetings

1. The 36th Annual Conference of Bangladesh Chemical Society, March 1, 2014, Dinajpur, Bangladesh, "Synthesis and characterization of hydroxyapatite and copper doped hydroxyapatite from eggshell", Jahan S.A., Mollah M.Y.A., Ahmed S., Susan M.A.B.H.

2. Seventh HOPE Meeting 2015, March 01-05, 2015, Tokyo, Japan, "Hydroxyapatite from waste materials for treatment of heavy metals in aqueous medium", Jahan S.A., Mollah M.Y.A., Ahmed S., Susan M.A.B.H.

Abstracts accepted for Scientific Meetings

3. 16th Asian Chemical Congress (16ACC), 18-21 November, 2015 Dhaka,Bangladesh, "Removal of arsenic from waste water using Fe(III) doped Hydroxyapatite synthesized from eggshell", Jahan S.A., Mollah M.Y.A., Ahmed S., Susan M.A.B.H.